Title	Accumulation mechanisms of trace metals into Arctic sea ice
Author(s)	Evans, La Kenya Elizabeth
Degree Grantor	北海道大学
Degree Name	博士(環境科学)
Dissertation Number	甲第13542号
Issue Date	2019-03-25
DOI	https://doi.org/10.14943/doctoral.k13542
Doc URL	https://hdl.handle.net/2115/84539
Type	doctoral thesis
File Information	LaKenya_ElizabethEvans.pdf

Accumulation mechanisms of trace metals into Arctic sea ice

北極海における海氷への微量金属蓄積メカニズムの解明

By

Evans La Kenya Elizabeth

Submitted in partial fulfillment of the requirements

for the degree of Doctor of Philosophy

Graduate School of Environmental Science,

Geochemistry Course,

Hokkaido University

2019

List of abbreviations

D   Dissolved (<0.22 μm)

TD   Total Dissolvable (Unfiltered)

LP   Labile Particulate (TD – D)

Fe   Iron

HDPE   High Density Polyethylene

LDPE   Low Density Polyethylene

NOBIAS   NOBIAS PA-1 M chelating resin

EDTA   Ethylenediaminetriacetic acid

IDA   Iminodiacetic acid

HAcO - NH$_4$AcO   Acetic Acid-Ammonium Acetate

RO   Reverse Osmosis

SD   Standard Deviation

DL   Detection Limit

GFAAS   Graphite Furnace Atomic Adsorption Spectrometer

IC-MS   Inductively Coupled Plasma Mass Spectrometry

Porosity %   % micropore analysis

MIZ   Marginal Ice Zone

Abstract

In the last 20 years the Arctic Ocean has experienced over 32% loss of summer sea ice. This loss can influence the cycling of biogeochemical materials, affecting seawater's biology and chemistry. Sea ice is important for the supply of biogeochemical materials (trace metals, nutrients, dissolved organic matter, suspended particulate matter, etc.) to the surface waters of the polar oceans, but its role is not clear. In this study we focus on trace metals. Understanding the accumulation and release mechanisms into Arctic sea ice will clarify the geochemical behaviour of trace metals. Both dissolved (D, <0.2 μm), and labile particulate (LP, Total Dissolvable - Dissolved) Fe, Mn, and Cd were examined in sea ice and seawater collected from the Chukchi Sea, Arctic Ocean. Samples were pre-concentrated utilizing the solid-phase extraction NOBIAS Chelate PA-1 resin (Hitachi High-Technologies Corporation) and analyzed on a Graphite Furnace Atomic Absorption Spectrometer. Chukchi seawater showed high percentages for DMn (71.5%) and DCd (66.3%) with a high percentage of LPFe (94.1%). In seawater, DCd was the only metal to correlate with phosphate ($R^2 = 0.78$) indicating a biogeochemical cycling source. Chukchi seawater concentrations of Fe and Mn may have been controlled through external sources. Sediments (shelf or river) supplied LPFe and LPMn. DFe and DMn were supplied by the Alaskan Coastal Current. Trace metal concentrations in Chukchi drifting ice were heterogeneous. Drifting ice showed high percentages for the LP fraction (99.2% Fe, 63.6% Mn and 71.2% Cd). This data indicated that, regardless of the trace metal behavior in Chukchi seawater, Chukchi drifting ice was observed to have a preference to accumulate or retain the LP trace metal fraction.

To examine possible trace metal accumulation processes utilized by Arctic sea ice, the association between trace metal concentrations and ice structure were observed in floe ice. The structure of sea ice reflects the process of ice formation, which may aid in the determination of accumulation processes. An Arctic sea ice core was examined. Using photographic analysis for the percentage of pore area and $\delta^{18}O$ analysis, sea ice structure in the core sample showed snow, granular, mixed (granular + columnar) and columnar ice. Salinity and nutrients were low, indicating brine drainage and multi-year ice. High trace metal concentrations in snow ice

indicated meteoric snow as a source. High concentrations of LPFe in granular ice indicated possible particulate trace metal scavenging by frazil ice. Concentrations of LPMn and LPCd were low compared to DMn and DCd in granular and snow ice. It is possible that reduction of LPFe and LPM after particle entrainment released DMn and DCd, indicating a chemical transformation process. Low dissolved and labile particulate trace metal concentrations in mixed and columnar ice indicated a release due to brine drainage.

The accumulation and retention of trace metals into Arctic sea ice may be influenced by the form of sea ice. Drifting sea ice can be a long-range transporter of LP metals. Floe ice can provide both D and LP metals to the local area. Therefore, sea ice form, processes of sea ice formation, chemical transformation and brine release, are important for the accumulation, retention and release of trace metals from sea ice.

Chapter 1

General introduction

1.1. Introduction

1.1.1. Loss of Arctic sea ice

Sea ice in the polar oceans is a vast, poorly understood ecosystem. During winter, sea ice covers up to 7% of the world's surface (Dieckmann and Hellmer, 2010). Sea ice is important for processes such as heat and gas exchange between the sea surface and atmosphere (Eicken et al., 1995), global climate circulation (Zwally et al., 1985) and the formation of bottom water (Comiso and Gordon, 1998) in the polar regions. Although sea ice is present in both the Antarctic and Arctic, these regions exhibit different characteristics. The Antarctic is a continent that is surrounded by the ocean. Within the ocean sea ice forms in a symmetric pattern, up to 2 meters, and have high drift speeds moving them to warmer waters where the sea ice then melts. Since the Antarctic is surrounded by ocean, humidity is high increasing snow precipitation. In contract, the Arctic is almost surrounded by land creating a calm semi-enclosed ocean. Arctic sea ice forms in an asymmetric pattern and is less mobile than Antarctic sea ice (NSIDC). In the Arctic region, the summer season is characterized by a persistent layer of perennial (multi-year, up to 5 meters) sea ice. Multi-year ice is of great importance to the Arctic Ocean. It is a buffer for solar radiation as well as a source of freshwater and trace metals to the underlying waters (Eicken et al., 1995). Yet increases of Arctic temperature have yielded decreases of sea ice extent (area with no less than 15% of ice present; NSIDC). This decline may be linked to global warming. The relationship between Arctic sea ice and the global climate was initiated with the 1956 Ewing-Donn theory. This theory states that the Ice Age, during the Pleistoncene, occurred when the North and South poles migrated to their current Arctic and Antarctic locations. The perceived fluctuations of ice-free to ice-covered areas mirrored that of glacial and interglacial climate fluctuations (Ewing and Donn, 1958). Currently, the Earth is in an interglacial period allowing for the effects of global climate change to be highly influential on Arctic sea ice.

Increases in Arctic temperatures have remained constant. In recent years, the Arctic has seen an increase in atmospheric temperatures by 1.6°C from October 2016 to September2017, over double the global average rate for mean temperatures (Overland et al., 2017). The most pronounced temperature increases are observed in the autumn and spring seasons of the Pacific and Canadian regions (Przybylak, 2007). Relating this to Arctic sea ice extent, a decreasing trend of -13.2% per decade was observed when compared to the sea ice extent averages of 1981 - 2010 (Perovich et al., 2017). Regarding multi-year ice, a decrease of 7 x 10^6 km^2 to 3.5 x 10^6 km^2 was observed from 1980 - 2017 (Comiso et al., 2017). The current observations for sea ice loss have increased the importance of sea ice studies and their role in biogeochemical cycling. The loss of Arctic sea ice, especially during the summer months, points to an ecosystem shift from multi-year to first-year ice. This can affect the Arctic by changing it from a calm system to a more dynamic environment, possibly changing the interactions between sea ice, ocean and the atmosphere.

1.1.2. Forms of sea ice

Sea ice is ice that is formed from frozen seawater. There are two major ice types: fast ice or pack ice. Fast ice is sea ice that is attached to the shore, or ice associated with land extending to the shore, usually forming around coastal areas. Pack ice is a broad term that can be used to describe any ice that is not fast ice (Toyota, 2018). The forms of ice that was observed in this study were of pack ice: floe ice and deformed drifting ice. Floe ice can be composed of either first-or multi-year ice, and reach thicknesses greater than 2 m (Toyota, 2018). In response to mechanical, current, or thermal stress, ice floe can travel westward, away from the coast into the Arctic (Maykut, 1985; Eicken et al., 2005). Floes can be over 10 km across (Toyota, 2018) and protected from wave stress in the interior of the floe. Therefore, the structure of sea ice can be determined as a result of formation processes. Drifting ice, for the purposes of this study, was used to describe free floating deformed sea ice (such as brash ice). Drifting ice can reside in a transition area between an ice floe and the open ocean (the marginal ice zone) where high energy creates a dynamic area (Smith, 1987; Maykut, 1985; McPhee et al., 1987). Drifting ice in the transition area is characteristically composed of smaller sizes (20 - 30 m diameter; Wadhams et

al., 1988). Strong influences from wind and wave stress (Häkkinen, 1986; Wadhams et al., 1986) can break up, or collide, drifting ice and advanced melting (McPhee et al., 1987) can further degrade the ice. This indicates that drifting ice may be more permeable than sea ice from a protected ice floe, inhibiting determination of the ice structure. If the overall decline in multi-year summer ice continues, is it possible that the Arctic may turn into an ice-free summer within this century (Massonnet et al., 2012). In response to this transition and the ultimate loss of sea ice, both regional and global biogeochemical cycling processes may be greatly impacted (Thomas and Dickmann, 2003; Vancoppenolle et al., 2010).

1.1.3. Biogeochemical cycling

Biogeochemical cycling is the interaction of chemical materials (i.e. iron (Fe), nitrate (NO_3^-), phosphate (PO_4), etc.) traveling via biological (i.e. phytoplankton) and geological (i.e. seawater, sea ice, etc.) processes (Hedges, 1992). In the Arctic Ocean, sea ice has a geochemical role as it can transport incorporated materials (trace metals, nutrients, dissolved organic matter, suspended organic matter, etc.) from areas of formation into new areas (Eicken et al., 2005; Masqué et al., 2007). As the loss of Arctic sea ice increases, its effect on the cycling of trace metals within the Arctic are unknown. Therefore, this study will focus on trace metals and how they are incorporated into sea ice. To accurately measure the chemical composition of sea ice, clean methods are needed. In recent years, chemical research on sea ice have aimed to create cleaner trace metal methods for sample collection, preparation and analysis. Unfortunately, these sampling techniques and measurements are varied (Miller et al., 2015). Efforts have been made to make more standardized approaches so that the intercomparison of data will be reliable (Miller et al., 2015) as biogeochemical sea ice studies become more frequent. This study follows trace metal clean methods that have been described by Takeda and Obata (1995), Nishioka et al. (2001) and Tsumune et al. (2005).

1.1.4. Trace metals of interest

The biogeochemical cycling of trace metals by sea ice is most noticeable during the spring melting season. In the Arctic, sea ice is a source of trace metals to the underlying surface waters. The concentrations of trace metals in sea ice have been reported to have elevated levels in

comparison to the underlying seawater (Hölemann et al., 1999; Aguila-Islas et al. 2008; Tovar-Sanchez et al. 2010; Kanna et al., 2014). When sea ice melts, it can release incorporated trace metals supplying them into the underlying waters (Grotti et al., 2005; Lannuzel et al., 2007, 2008). Aguilar-Islas et al. (2008) found increases of biomass in areas with ice present. In areas without ice, nutrient concentrations were high, but Fe and Chl *a* concentrations were low. They suggested that the addition of Fe from melting sea ice allowed phytoplankton to fully utilize the available nutrients, in the low salinity surface waters due to melting sea ice, which increased the biomass. Increases in biomass as a result of melting sea ice were also observed in the Antarctic showing that sea ice can be a source of trace metals to phytoplankton (Lannuzel et al., 2008). Therefore, it is important to understand the geochemical role of sea ice in the supply of trace metals. Most trace metals act as essential micro-nutrients that are necessary for phytoplankton growth, while some can be detrimental. In this study we focused on Fe, manganese (Mn) and cadmium (Cd). These three trace metals show different behaviors (REDOX potential, supply source, biochemically, etc.) in seawater. For example, Fe is a transition metal allowing for a range of oxidation-reduction properties. Iron is used in enzymes and proteins during photosynthetic and respiratory electron transport (Morel et al., 1991) that can increase the growth phytoplankton. It is a component of catalase, peroxidase and Fe-superoxide dismutase for oxygen cycling. Ferredoxin (Fe-sulfur (SO_4^-) protein) is used as an electron donor in SO_4^-, NO_3^- reduction and N_2 fixation. Iron can also have indirect roles such as regulation for cellular metabolism (Morel, 1983; Geider and Roche, 1994; Morel et al., 1991). The study of Fe as an essential micro-nutrient for phytoplankton increased after the introduction of the "Iron Hypothesis" by John Martin. The "Iron Hypothesis" states that dust derived Fe delivered to the Southern Ocean, during the glacial period, increased primary productivity resulting in a drawdown of atmospheric carbon dioxide (Martin, 1990; Martin et al., 1990). From this idea, studies have not only shown a limitation of phytoplankton growth by Fe but have expanded to understanding the role other trace metals as well.

As with Fe, Mn is a transition metal with extensive oxidation-reduction properties (Landing and Bruland, 1987; Morgan, 2005; Sunda et al., 1983). In seawater Fe and Mn have similar geochemistry (Landing and Bruland, 1987; Shiller, 1997) indicating that these two metals

are supplied through similar sources (Saager et al., 1989 and references within). Biologically Mn is an essential micro-nutrient used as an electron acceptor during water oxidation in photosystem II, the chemical breakdown of toxic superoxide radicles by activation of superoxide dismutase and can substitute for Fe(III) in some reactions (Peers and Price, 2004; Sunda, 1989). In contrast Cd is not a transition metal but a rare element that can be found in minute amounts within the ocean. As an essential element, Cd can increase carbonic anhydrase activity of phytoplankton and act as a substitute for other essential metals (Cullen et al., 1999; Morel and Price, 2003). At elevated concentrations, usually attributed to industrial pollution (Vallee and Ulmer, 1972), Cd can be detrimental to organisms. Increased Cd can alter the permeability of cellular membranes, disrupt electron transport, inhibit or activate enzymes, induce phytochelatins (thiol-containing peptides used for metal detoxification), limit or inhibit the uptake of macro-nutrients and cause oxidative stress (Miao and Wang, 2006; Smeets et al., 2005 and references within; Wang and Wang, 2009). Iron, Mn and Cd were chosen as the exhibit both similar and different geochemical behaviors within seawater as described above. These behaviors may influence how they are accumulated and retained into sea ice.

1.1.5. Trace metal size fractions

To gain a better understanding of the biogeochemical cycling of trace metals by sea ice, we must first understand the mechanisms for how trace metals accumulate into sea ice. A detailed study of trace metals by their size fractions will show the available processes utilized by sea ice. Fractionation is broadly defined as the classification of an analyte from a sample due to its physical (size, solubility, etc.) or chemical (i.e. redox potential) properties. This is different from speciation which is defined as the form of an element due to its isotopic composition, oxidation state, and/or molecular structure or complex (Templeton et al., 2000). Size fractionation is defined via the filtration of a sample through different pore sized membranes (Templeton et al., 2000 and references therein; Nishioka and Takeda, 2000). One of the major issues of filtration is contamination. The filter, filtration device and sample bottle must be acid-washed to avoid outside condemnation to the filtered sample (Nishioka and Takeda, 2000,2001). Filtration is usually done within a space that has continuous clean, filtered, air flowing in to

maintain a trace metal clean working space. Filtration of each sample must be done with an individual filter, and the filtration device cleaned between subsequent samples. This will decrease the chance of contamination to the filtered sample. If a lot of particulates are present in a sample, the filter must be changed during filtering in order to accurately catch the intended fractionated sample (Templeton et al., 2000). Separating trace metals by their size fractions allows us to better understand their chemical and physical behaviors in both sea ice and seawater. The particulate fraction (P, >0.2 μm or >0.4 μm) represents trace metals associated with particles and can be found resting on the filter. The D fraction (<0.2 μm) represents trace metals that pass through a filter and are found in the acidified filtrate. For the purposes of this study, both the colloidal (between 200 kDa and 0.2 μm) and soluble (<200 kDa) fractions (de Baar et al., 2005; Nishioka et al., 2005) are represented collectively in the D fraction. The total dissolvable fraction (TD, unfiltered) represents all metals (both metals associated with particulates and metals in the D faction) that were dissolved in an acidified matrix (Hurst and Bruland, 2007; Kuma et al., 1998; Nishioka et al., 2001). The LP fraction is calculated as the difference between the TD and D metals (Cid et al., 2011; Lannuzel et al., 2007). Subtracting out the D fraction from TD will leave the dissolvable particulate fraction of trace metals (LP). Figure 1.1, modified from Lannuzel et al. (2014), is a schematic of the D and P size fraction during filtration. This study focused on the dissolved (D) and labile particulate (LP) trace metal size fractions.

1.1.6. Study objectives

Previous studies have shown that the concentrations of trace metals in sea ice are higher than in underlying surface seawater (Grotti et al., 2005; Kanna et al., 2014; Lannuzel et al., 2007, 2008, 2011, 2015; van der Merwe et al., 2011). Most sea ice studies have occurred in the Antarctic Ocean (Grotti et al., 2005; Hendry et al., 2009; Lannuzel et al., 2007, 2008, 2010, 2011, 2014, 2016; van der Merwe et al., 2011). Whereas sea ice studies for the Arctic region are less (Aguilar-Islas et al., 2007, 2008; Hölemann et al., 1999; Kanna et al., 2014; Melnikov et al., 2002). The Arctic has mostly stable, thick characteristic multi-year ice. The addition of freshwater inputs (i.e. river and Pacific Ocean water inflow) encourages sea ice formation by decreasing the temperature of surface waters (Aagaard and Carmack, 1989; MacDonald et al., 1995). Thus,

Arctic sea ice maybe an important source of trace metals in the Arctic Ocean. Trace metal studies with sea ice observing trace metal size fractions have found variable concentrations. These differences may be due to trace metal accumulation processes. Yet the mechanisms behind trace metal accumulation into sea ice are unclear (Evans and Nishioka, 2018). Utilization of a tank experiment would allow for a trace metal clean, controlled observation of trace metal accumulation into sea ice (Janssens et al., 2018). Unfortunately, trace metal clean materials are needed. Therefore, the possible major mechanisms of accumulation and release were observed in two different forms of sea ice collected from a shelf and basin area.

The purpose of this study was to investigate trace metal accumulation mechanisms into Arctic sea ice. We first created a trace metal clean pre-concentration method utilizing the NOBIAS PA-1 resin with a manual system. This is described in Chapter 2. To gain an understanding of the role of sea ice in the geochemical cycling of trace metals we compared D and LP Fe, Mn, and Cd concentrations in free floating drifting sea ice with the surrounding surface seawater. This is described in Chapter 3. Based on the results from Chapter 3, we noticed differences in the size fractions of trace metals within sea ice but did not observe how they accumulated into sea ice. To gain more details on the accumulation processes for trace metals into sea ice we compared the D and LP concentrations of Fe, Mn and Cd to the structure of sea ice from an ice core samples collected from the interior of a sea ice floe. A trace metal clean method was created for the planing of sea ice in order to have reliable direct comparison of trace metals to ice structure. This is described in Chapters 4. Overall conclusions from these studies allowed us to elucidate on the role of different ice types in the geochemical cycling of trace metals in the Arctic Ocean. This is explained in Chapter 5.

1.2. Figures
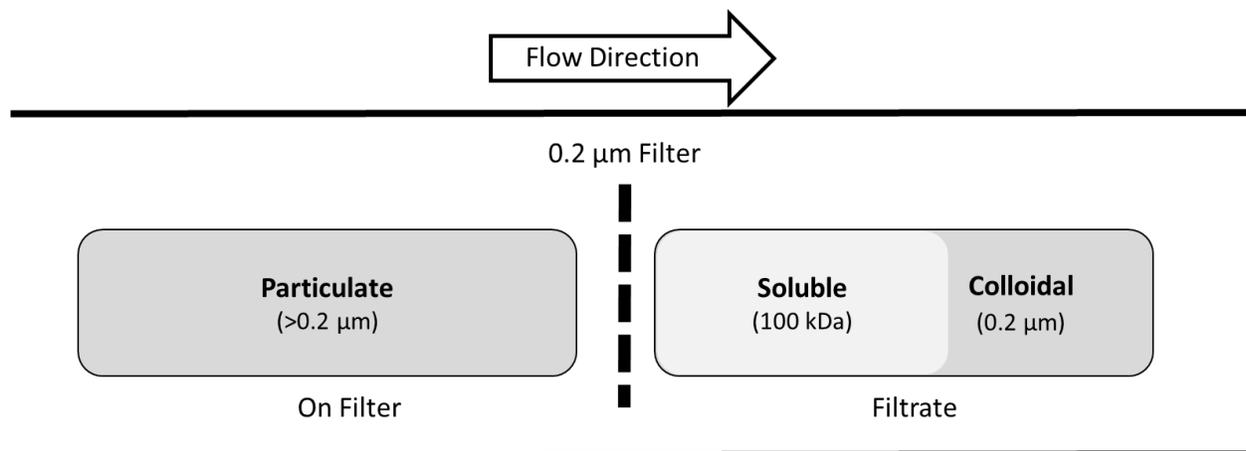
Figure 1.1. Size partitioning between the dissolved, <0.2 μm, (including soluble and colloidal size classes) and particulate, >0.2 μm, size fractionated trace metals (modified from Lannuzel et al., 2014).

Chapter 2

Construction and preparation for trace metal pre-concentration with the NOBIAS PA-1 resin

2.1.   Introduction

In the Arctic Ocean trace metals (i.e. Fe, Cd, etc.) concentrations are low, which prevents reliable direct analytical analysis. The size fractions of trace metals present another issue as D metals may have lower concentrations than the P fraction. Utilizing a pre-concentration method before analysis increases the concentrations of trace metals to detectable levels within a sample (Ueda et al., 2010). Pre-concentration can also allow for more reliable analysis as interferences resulting from seawater constituents (i.e. salts) are avoided (Sohrin et al., 2008). The resin column used for the pre-concentration of size fractionated trace metals from Arctic sea ice and seawater was the commercially available NOBIAS Chelate-PA-1 (NOBIAS) resin (150 mg, Hitachi High-Technologies Corporation). This resin holds some significant advantages over other resins making it a powerful tool. The NOBIAS resin is composed of three major components: 1) hydrophilic polyhydroxymethacrylate beads increases the accessibility of functional groups to metal ions. The beads improve the efficiency of metal adsorption and elution onto and from the resin (Persson et al., 2011). The use of a hydrophilic polymer stabilizes the resin, preventing the action of swelling or contracting during use (Mizutani et al., 2010). 2) Ethylenediaminetriacetic acid, an analogue to EDTA, allows the resin to form five coordinate bonds with metal ions (Minami et al., 2015; Sohrin and Bruland, 2011). 3) Iminodiacetic acid (IDA) can also prevent the resin from swelling during pre-concentration and further increase the resin's metal affinity (Sohrin and Bruland, 2011). The combination of EDTA and IDA allows for the NOBIAS resin to have a high enough affinity for trace metals to out compete natural ligands. The use of utilized isotopic dilution (Milne et al., 2010; Lee et al., 2011) or UV-oxidization (Biller and Bruland, 2012) can be avoided, due to the resin's high metal affinity. This will allow for multi-element quantitative analysis (including Mn and Co) from natural samples (Biller and Bruland, 2012). The NOBIAS can

also separate alkaline and alkali-earth metals from sample solutions (Ueda et al., 2010). Eliminating the presence of contaminates and interferences (i.e. seawater salts, particulates, etc.) during analytical analysis in the resulting eluent. Pre-concentration with the NOBIAS resin yields low blank values that can calculate low detection limits for each element of interest (Sohrin et al., 2008). Past studies have successfully used the NOBIAS resin to pre-concentrate rare earth metals (Hatje et al., 2014; Zhu et al., 2010), uranium from estuarine waters (Takata et al., 2011), thorium isotopes (Takata et al., 2011) and neodymium isotopes (Persson et al., 2011). Analysis after pre-concentration is usually done on an Inductively Coupled Plasma Mass Spectrometry (ICP-MS; Hatje et al., 2014; Lagerstrom et al., 2013; Persson et al., 2011; Takata et al., 2011; Sohrin et al., 2008; Zhu et al., 2010), or a Graphite Furnace Atomic Absorption Spectrometer (GFAAS; Ueda et al., 2010). For the purposes of this study a GFAAS was used.

2.2. Preparation

2.2.1. NOBIAS resin and materials preparation and cleaning

All reagents used for the pre-concentration of trace metals were of reagent, pure or ultra-pure chemical grade. Milli-Q water (Millipore Ltd.) was used to prepare all solutions. Standard solutions (Fe, Mn and Cd) were made in ultrapure nitric acid (HNO_3, 1 M final concentration, Tamapure-AA-100). Over time the standard curve slopes became unstable. In order to avoid sample value (after analysis) variability, each element's standard solution was made on the same day as analysis.

Materials used for trace metal pre-concentration were low- and high-density polyethylene (LDPE, HDPE, Nalgene Company, Limited) bottles, Teflon bottles, pipette tips, Teflon micro-tubing (OD 2-mm, 1-mm ID), and 25 ml plastic syringe (latex free, Henke Sass Wolf). Cleaning methods for materials followed documented procedures in Nishioka et al. (2001) and Takeda and Obata (1995). Briefly, all materials were submerged in a 5% Extran® (alkaline and phosphate-free liquid, Merck) bath for 48 hrs, 72 hrs for pipette tips. With the bottles, care was taken to avoid trapping air bubbles while submerged in the bath. Materials were then rinsed with reverse osmosis (RO) water and transported to an ultrapure hydrochloric acid (HCl, 4 N final concentration, Tamapure-AA-10, Tama Chemical) bath, located under a laminar fume hood in a

14

class 100 clean room, for 24 hrs. All materials were rinsed with Milli-Q water. New Teflon materials (bottles and valves) were placed into a 1 : 1 : 1 nitric : sulfuric : hypochlorous acid (ultrapure HNO_3 : H_2SO_4 : HClO, Tamapure-AA-100, Tamapure-AA-10) bath and heated to 80°C for 6 hrs. New Teflon micro-tubing were connected and a peristaltic pump was used to insert the 1 : 1 : 1 HNO_3 : H_2SO_4 : HClO solution before placing the micro-tubing in a 80°C water bath for 24 hrs. After heating, the 1 : 1 : 1 HNO_3 : H_2SO_4 : HClO solution was removed with a peristaltic pump into a waste container and Milli-Q water was flushed through the micro-tubes. All materials were then placed in a heated (80°C) ultrapure HCl (1 N final concentration) bath for 6 hrs. Separate baths were made for new and used bottles. Following the ultrapure HCl (4 N final concentration) bath, HDPE and LDPE bottles were filled with ultrapure HNO_3 (0.3 M final concentration), and heated to 80°C for 6 hrs. All materials were rinsed with Milli-Q water, placed in a Milli-Q water bath for 6 hrs before a final Milli-Q water rinse and air dried. GFAAS cups were cleaned in 5% Extran® for 72 hrs, rinsed with RO water, placed in an ultrapure HCl (4 N final concentration) bath for 48 hrs. The materials were then rinsed with Milli-Q water and air dried.

NOBIAS resins were individually cleaned following the methods outlined in Sohrin et al. (2008). An acid cleaned 25 mL syringe hand syringe was used to pass the following solutions through the resin, in succession, at 5 mL/min.: acetone (Wako Pure), methanol (Wako Pure), Milli-Q water, ultrapure $HCl-H_2O_2$ (1 M – 0.01 M final concentration, peroxide, Wako Pure), Milli-Q water, ultrapure NH_4 (0.5 M final concentration), and Milli-Q water. Cleaning the resin with $HCl-H_2O_2$ was necessary to lower the Fe blank values by reducing Fe^{3+} to Fe^{2+}. This process successfully removed all remaining Fe from the resin column (Minami et al., 2015). After the resin columns were cleaned, they were individually wrapped in clean plastic before use.

2.2.2. Pre-concentration manifold preparation and set-up

An acid cleaned in-line manual manifold, modified from Sohrin et al. (2008) and Kondo et al. (2016), was used for the pre-concentration of trace metals with the NOBIAS resin (Fig. 2.1). The manifold was set-up in a dust free, class 100, clean room below a HEPA filtered air vent. It consisted of three Teflon solution bottles (0.05 M HAcO-NH_4AcO buffer, Milli-Q water, and 1 M HNO_3). The sample line used the 125 mL LDPE bottles that the sample was collected and acidified

in. A 4-way valve connected the Teflon micro-tubings from the solution bottles directly to the bottom of the resin column. A separate micro-tube was connected to the top of the resin going towards the peristaltic pump. A waste line (Teflon micro-tube) ran from the resin column, through a peristaltic pump connected with Tygon tubing, into a waste container. To collect the eluent, the resin column was disconnected from the manifold and connected to an acid cleaned 25 mL in the opposite orientation of the sample flow direction.

After set-up, the manifold was cleaned following procedures described by Sohrin et al. (2008) before connecting the cleaned NOBIAS resin. 500 mL of ultrapure HCl : HNO_3 (1 M : 1 M) was passed through the manifold and allowed to sit in the Teflon micro-tubes for 24 hrs. The manifold was rinsed with Milli-Q water. 500 mL of 1 M HNO_3 (ultrapure) was passed through each line and held for 24 hrs. The manifold was rinsed again with Milli-Q water and the cleaned resin column was connected. 1 M HNO_3 (ultrapure) was passed through the manifold with the resin column attached and held for another 24 hrs. The manifold, with the resin column attached, were then rinsed with Milli-Q water. This last step with 1 M HNO_3 (ultrapure) was repeated four times with no contamination to the manifold. After each 1 M HNO_3 (ultrapure) pass, the manifold was rinsed with Milli-Q water. Milli-Q water was held in the Teflon micro-tubes flow lines once the manifold was cleaned.

2.3. Methods

2.3.1. NOBIAS pre-concentration methods

The buffer solution used for the pre-concentration of trace metals was acetic acid-ammonium acetate (HAcO-NH_4AcO). A 3.6 M HAcO-NH_4AcO buffer was made following the methods outlined in Minami et al. (2015): 30 g of Acetic Acid, Glacial (Optima Acid, Fisherchemical Fisher Scientific; Optima buffer), 70 g Milli-Q water and 50 g 20% NH_4OH (ultrapure, Tamapure-AA-10) in Teflon bottles. A 0.05 M HAcO-NH_4AcO buffer was prepared by diluting 3.6 M HAcO-NH_4AcO with Milli-Q water than double purifying it with the NOBIAS resin before storing the diluted buffer in acid clean Teflon bottles. The 0.05 M HAcO-NH_4AcO buffer was used to condition the resin column to pH 6 and removed alkali, alkaline earth metals and any remaining sea salts that remained in the column (Minami et al., 2015; Sohrin et al., 2008).

After the manifold was set-up, Milli-Q water procedural blanks were made to check for contamination from: the manifold materials, pre-concentration solutions and the pre-concentration method (Table 2.1). The pre-concentration method was modified from Sohrin et al. (2008; Fig. 2.2). Before each sample was pre-concentrated, the manifold was cleaned with 15 mL of 1 M acidic acid (HNO_3, ultrapure, Tamapure-AA-100, 1 mL/min.) then conditioned with 30 mL Milli-Q water (3 mL/min.) and 40 mL of 0.05 M HAcO-NH_4AcO (3 mL/min.). During this step, a Milli-Q water procedural blank was prepared. 125 g of Milli-Q water was measured on a precision scale in an acid cleaned 125 mL LDPE bottle. 1.8 µL of 3.6 M HAcO-NH_4AcO buffer was added via pipette and the pH was adjusted to 6.0 ± 0.05 with 20% NH_4OH (ultrapure). A pH sensor (AsOne Compact pH meter, Laquatwin) was used to check the pH of the sample. During measurement a small amount of the procedural blank was poured directly on the sensor (accuracy ± 0.1). This allowed for the procedural blank to stay clean and limit the chance for contamination and misreading. After the pH adjustment step, the procedural blank was loaded at 3 mL/min. and 40 mL of 0.05 M buffer at 3 mL/min. followed the sample. To collect the eluent, the column was moved to an acid clean hand syringe, in the opposite direction of the flow from the solutions, and back-eluted with 10 mL of 1 M HNO_3 (ultrapure, 1 mL/min.) into an acid clean polyethylene collection tube. The resin was then re-connected to the manifold. A stop watch was used to time all solutions. For subsequent samples, the procedure was repeated from the beginning cleaning step (1 M HNO_3 (ultrapure) at 1 mL/min.) to ensure no cross contamination between samples. The concentration factor was individually calculated by dividing the weights of the elution and samples. After the samples were analyzed on a GFAAS, their values were divided by their concentration factor to determine the original concentration of each sample before pre-concentration.

Sea ice and seawater (D and TD) samples in chapters 3 and 4 followed the pre-concentration procedure as described above. In chapter 3 particles were observed in the total dissolvable sea ice samples, therefore, a new line was made with acid cleaned filters so that the sample was filtered (0.22 µm, Durapore, Millipore Ltd.) before loading onto the column followed by 40 mL of the diluted buffer. This filtration step allowed for the flow lines to remain clean during pre-concentration.

2.3.2. GFAAS measurement methods

For all samples the % absorbance of Fe, Mn and Cd were analysed individually on a GFAAS. A standard curve and three analytical blank samples (1 M HNO_3, ultrapure) were measured before the experimental samples for each element's run. The analytical blank samples were used to calculate the analytical detection limit of the GFAAS for each element. This was determined by calculating the standard deviation of all analytical blanks and multiplying this by three. An analytical blank was then measured between every 10 samples to ensure no cross contamination in the GFAAS sampler between samples. Two analytical blanks were put as the last samples to ensure that the GFAAS sampler was cleaned after all samples were ran.

Each individual sample was measured 5 times, the first measurement was dropped to ensure there was no interference from the previous sample's measurement. The average, standard deviation and relative standard deviation (RSD) absorbance values were then corrected for by subtracting out the average absorbance value from the analytical blank. This was done to account for analytical noise of the GFAAS. To calculate the standard curve, the standards average values were graphed by absorbance (%) verses standard (parts per billion, ppb). If the standard curve was non-linear, a polynomial trendline was used for the absorbance equation. The absorbance equation was used to calculate the sample data in ppb. The sample data was then calculated to nano molar (nM) by dividing the ppb value with the desired element's molecular weight and multiplying it by 1000. If the raw calculated data values were below the analytical detection limit, the data was considered non-detectable. All raw data was considered reliable if the RSD was below 0.5%.

2.3.3. NOBIAS pre-concentration recovery tests methods

To measure the recovery of trace metals by the NOBIAS resin, 120 mL of Milli-Q water was spiked with known concentrations of Fe, Mn, and Cd (10.03 nM, 1.73 nM and 1.33 nM, respectively) from individual 50 ppb stock solutions. All recovery blanks were pre-concentrated with the NOBIAS resin and analysed via GFAAS.

2.3.4. NOBIAS pre-concentration validation tests methods

Seawater reference material for trace metals (NASS-6, salinity of 33.5, National Research Council Canada) was used to validate the NOBIAS pre-concentration procedure. 30 - 50 g of NASS-6 (n = 8) was measured via precision scale and placed in acid cleaned LDPE 125 ml bottles. Samples were pre-concentrated and analysed via GFAAS for Fe, Mn, and Cd.

2.4. Results

2.4.1. Procedural blank, recovery test and reference materials

Milli-Q water procedural blanks were pre-concentrated for Fe, Mn and Cd. The pre-concentration detection limit (DL), after the pre-concentration step and analysis on the GFAAS, was determined for each element by multiplying the standard deviation (SD) of the Milli-Q procedural blanks, by three. This DL was used for the sea ice and seawater samples in chapters 3 and 4. After the samples were pre-concentrated, their measured values were compared to the DL. If the samples were above the DL, then their measured values were calculated with the concentration factor and reported. The final *in situ* DL of our method varied depending on the pre-concentration factor used for each sample type but resulted in the following averages: 0.3 nM for Fe, 0.06 nM for Mn and 0.0002 nM for Cd (Table 2.1). Recovery of Fe, Mn and Cd from spiked Milli-Q water blanks after pre-concentration was 102.1 ± 5.6%, 100.3 ± 1.8%, and 106.3 ± 5.1% respectively (Table 2.2).

Recovery for each metal agreed with Sohrin et al. (2008) and Minami et al. (2015) published data. Three samples, from this study, were used to represent the recovery data as these samples were the most stable and repeatable. Values of NASS-6 seawater reference materials (n = 8) measured in this study after pre-concentration showed: 9.5 ± 1.3 nM Fe, 11.2 ± 1.4 nM Mn and 0.3 ± 0.1 nM Cd. Measured seawater reference values were comparable to the certified values (National Council of Canada; Fig. 2.3).

2.5. Summary

The analysis of trace metals in Arctic sea ice and seawater is problematic as concentrations are typically low. One way to overcome this is with the use of a concentration step, of the samples in question, before analysis. The NOIBAS PA-1 chelating resin was chosen

for its high affinity towards trace metals and its ability to separate out seawater constituents during pre-concentration. The manifold used for this study was an in-line manual system. The manifold consisted of Teflon bottles and tubing with Tygon tubing to minimize contamination. To ensure the eluent of the Milli-Q water procedural blanks were not contaminated, the NOBIAS resin was back hand eluted with acid cleaned 25 mL hand syringes. To minimize contamination during the pre-concentration step, an Optima Glacial Acid buffer was made in Teflon bottles. Milli-Q water procedural blanks had low trace metal values with low detection limits. These methods were implemented in the NOBIAS pre-concentration method for trace metal analysis in this study (Chapters 3 and 4). The recovery for all interested metals (Fe, Mn, and Cd) with spiked Milli-Q recovery blanks agreed with published data. The validation of the NOBIAS pre-concentration method with NASS-6 reference seawater yielded data that were within range of certified values from the Nation Research Council Canada. Based on the results of this study, metal pre-concentration utilizing the NOBIAS PA-1 resin on an acid cleaned in-line manual manifold is trustable and reliable for the determination of low trace metal concentrations in Arctic sea ice and seawater.

2.6. Figures
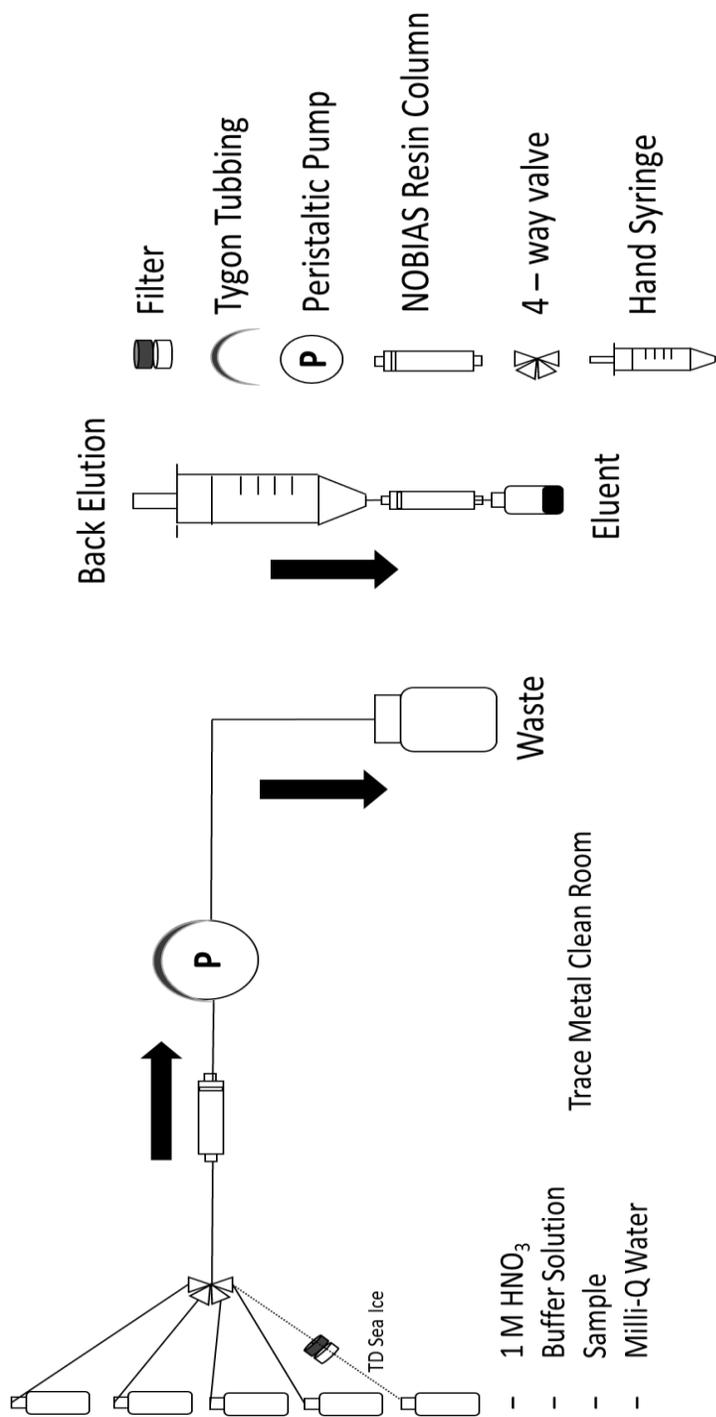
Figure 2.1. Diagram of the NOBIAS pre-concentration in-line manual manifold modified from Sohrin et al. (2008) and Kondo et al. (2016) . Arrows indicate the direction of flow for solutions and samples. All solutions but the sample were held in Teflon bottles. The acidified sample was held in the original LDPE sample bottle. Tygon tubing was used to connect the Teflon tube around the peristaltic pump. A waste line went directly to a waste container. During elution, the resin column was removed and back eluted with an acid-cleaned 25 ml hand syringe.

Step 1
Column Conditioning

15 mL 1 M HNO$_3$

1 mL/min.

30 mL MQW

3 mL/min.

40 mL 0.05 M
HAcO-NH$_4$AcO

3 mL/min.

Waste

Step 2
Sample Preparation

1) Acidified Sample

2) 3.6 M HAcO-NH$_4$AcO

3) pH to 6.0 (± 0.1) via 20% NH$_4$OH

Step 3
Sample Loading

Load Sample

3 mL/min.

40 mL 0.05 M
HAcO-NH$_4$AcO

3 mL/min.

Waste

Step 4
Sample Elution

Back Hand Eluted

10 mL 1 M HNO$_3$

1 mL/min.

Eluent

NOBIAS Resin Column

Solution Flow Direction

Hand Syringe

Figure 2.2. NOBIAS pre-concentration procedure for sea ice, seawater and blank samples. For subsequent sampling, the procedure repeated from the beginning 1 M HNO$_3$ (15 mL/min.) step to avoid cross contamination between samples. Sample pre-concentration was done in a class 100 trace metal clean room.
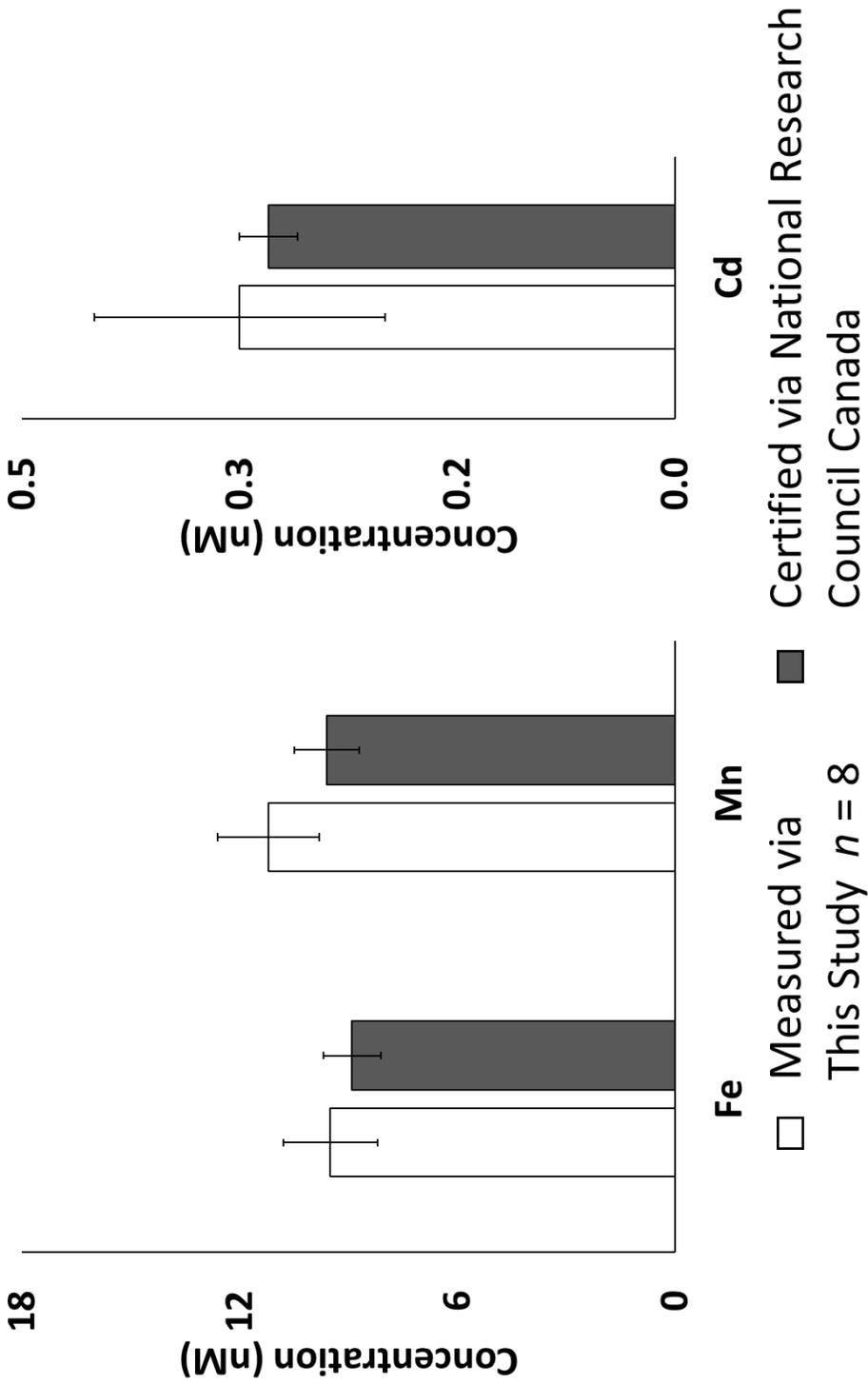
Figure 2.3. Recovery data for seawater reference materials (NASS-6) utilizing the NOBIAS resin pre-concentration method (*n* = 8, white) verses certified values from the National Research Council Canada (grey). Error bars represent standard deviation.

Table 2.1. Detection limit for Fe, Mn and Cd determined from multiplying the standard deviation of the 125 mL Milli-Q water procedural blank by three. The detection limit was calculated after the pre-concentration step and analysis with the GFAAS. The final *in situ* detection limits were lower as they were calculated with the pre-concentration factor.

Element	*n*	avg ± SD (nM)	Detection Limit [a] (nM)	*in situ* Detection Limit [b] (nM)
Fe	6	3.3 ± 1.3	3.9	0.3
Mn	6	0.57 ± 0.24	0.7	0.06
Cd	6	0.007 ± 0.0006	0.002	0.0002

[a] 3*SD of Procedural Blank

[b] 3*SD of the procedural blank after calculation with the pre-concentration factor

Table 2.2. Recovery of Fe, Mn, and Cd from spiked Milli-Q water. Samples were pre-concentrated with the NOBIAS resin.

Element	n	Added (nM)	This Study Recovery (%) avg ± SD	Sohrin et al. (2008) avg ± SD	Minami et al. (2015) avg ± SD
Fe	3	10.03	102.1 ± 5.6	77 ± 11	92.9 ± 9.2
Mn	3	1.73	100.3 ± 1.8	100 ± 3	106 ± 4
Cd	3	1.33	106.3 ± 5.1	101 ± 9	105 ± 6

Chapter 3

Quantitative analysis of Fe, Mn and Cd from sea ice and seawater in the Chukchi Sea, Arctic Ocean

3.1. Introduction

In the Arctic Ocean, the decline of sea ice has become more evident in recent years. This can have great impacts on the underlying water's physical and chemical structures and productivity (Eicken and Lange, 1989; Fritsen et al., 1994; Macdonald et al., 1999). Currently, trace metal profiles in sea ice are very limited. A study done on Fe in the marginal, Sea of Okhotsk showed that snow and sea ice TDFe and DFe concentrations were higher than those observed in seawater under the sea ice (Kanna et al., 2014). Tovar-Sanchez et al. (2010) observed that multi-year ice in the Greenland current and Fram Strait were more enriched with trace metals when compared to the underlying seawater. These studies indicate that sea ice in the Arctic Ocean may be a potential source of trace metals.

In the Antarctic region, sea ice has been observed to accumulate Fe up to two orders of magnitude higher than the underlying surface waters (Grotti et al., 2005). Within sea ice, the distribution and concentrations of trace metal size fractions have been observed for and compared to seawater (Lannuzel et al., 2010, 2011a, 2011b, 2014). In addition, observations of Antarctic sea ice brine have been shown to influence nutrient and trace metal interactions, along with possible retention or release from the ice interface (Hendry et al., 2009; Lannuzel et al., 2007, 2008; van der Merwe et al., 2011). Within the Arctic region, the study of trace metals in sea ice are not as extensive as for the Antarctic (Aguilar-Islas et al., 2007, 2008; Hölemann et al., 1999; Kanna et al., 2014; Melnikov et al., 2002). Although studies from both the Arctic and Antarctic regions have shown that sea ice is able to accumulate trace metals, the mechanism behind trace metal accumulation into sea ice remains unclear. It is possible that trace metals accumulate during ice formation and sediment entrainment processes and are then transported as ice is exported from the area of formation into new areas (Eicken et al., 2005; Masqué et al.,

2007; Nürnberg et al., 1994; Pfirman et al., 1995, 1997). This gives sea ice a geochemical role as a transporter of incorporated materials. Eicken et al. (2005) observed a westward export of sediment-laden sea ice in the Chukchi and Beaufort Seas. This suggests that sea ice can be a potential source of trace metals in the Arctic Ocean as they are released along with entrained sediments during ice melt.

Understanding the processes of how trace metals accumulate into sea ice is very important to gain a clearer understanding of the role for trace metals geochemical cycling in the polar oceans. In this chapter, the concentrations of Fe, Mn and Cd in Chukchi drifting sea ice were compared to Chukchi seawater. Dissolved (<0.2 µm), and LP concentrations of Fe, Mn and Cd were observed. Labile particulate represents the dissolvable particulate metal size fraction and was determined by taking the difference between TD (unfiltered) and the D size fractions (Lannuzel et al., 2007; Cid et al., 2011). Iron, Mn and Cd have different characteristics of source, sink, cycle and redox potential in seawater. Thus, they were used to investigate the trace metal accumulation features of Arctic sea ice.

3.2. Materials and methods

3.2.1. Sampling location and sample collection

All materials used for the sampling and analysis of sea ice and seawater followed trace metal clean sample collection and preparation methods. LDPE bottles, Teflon bottles and devices were acid cleaned as described in chapter 2.

Sea ice was collected during the Oshoro-Maru cruise in July 2013. Three individual free floating sea ice (drifting ice) pieces were collected in the Chukchi Sea, about 8 - 16 km downwind from the sea ice edge. The ship approached the drifting ice from the downwind direction, to avoid the ship's exhaust, at three different locations: Ice 1) 70˚58' N, −165˚24' W; Ice 2) 71˚3' N, −164˚28' W; and Ice 3) 70˚48' N, −164˚9' W (Fig. 3.1). The three drifting ice pieces were within the size range of 0.5 m^3 to 2.25 m^3. Drifting ice was collected using a 1.8 m x 1.8 m nylon sling mounted on a vinyl coated stainless frame. The sling was hung from the ship's crane from the

bow. Once the ice was collected it was placed upon a clean tarp on the ship's deck. During collection care was taken to avoid touching any of the drifting ice surface, with non-acid cleaned materials, to avoid contamination. Once on the tarp, each drifting ice sample was individually separated into several block pieces using a titanium ice pick. The inside of the ice block was then immediately shaved with an acid cleaned ceramic knife and small chips (samples, Ice 1 n = 4, Ice 2 n = 4, Ice 3 n = 14) of ice were collected into separate acid cleaned polyethylene buckets, double wrapped with clean plastic bags, then stored at −20°C. In an on-shore clean area, each sample bucket was placed in an incubator, with double plastic bags, and melted at 20°C. This decreased the chances of sample contamination. Once melted, the sample buckets were transferred to a class 100 clean room. The outer bag was removed from each bucket in the clean room; and half of the sample's meltwater was immediately filtered by acid cleaned 0.22 μm filters (Durapore, Millipore Ltd.) using acid cleaned Teflon filter holder and acid cleaned Teflon micro-tubing connected to a peristaltic pump with Viton Tubing (Cole-Parmer Instrument Company). The Viton Tubing was in contact with the waste solution only. For sample filtration, one half of the sea ice meltwater was filtered. First a 25 mL wash of meltwater was used to clean the filter and tubing. The sea ice meltwater sample was then filtered allowing the filtrate (D) to be collected into acid clean 125 mL LDPE bottes. All samples were acidified to pH 1.8 with 0.05 M hydrochloric acid (HCL, ultrapure, Tamapure-AA-10, Tama Chemical). After sample filtration of each sample, the system was cleaned with Milli-Q water, held for one hour with 0.1 N HCl (ultrapure), then rinsed with 0.1 n HCl (ultrapure) and Milli-Q wash before subsequent sampling. The other half of the sample meltwater (TD) was immediately placed into acid clean 125 mL LDPE bottes and acidified to pH 1.8. Both the TD and D samples for each of the drifting ice pieces were stored for three years, at room temperature, before analysis for this study.

Chukchi surface seawater (~3 m) was collected from off the coast of Barrow Canyon (hereafter the Barrow Canyon samples; 70°34' N, −160°50' W to 70°57' N, −161°48' W) and off the coast of Point Lay (hereafter the Point Lay samples; 70°44' N, −164°36' W to 71°2' N, −164°28' W, and 69°32' N, −166°34' W to 70°23' N, −165°33' W; Fig. 3.1). Seawater was collected near the sea ice sampling sites (described above). Sampling was done following the methods outlined in Tsumune et al. (2005). Briefly samples were collected via a towed-fish, metal free sampling

system with Teflon tubing (ID 12 mm) covered by polyvinyl chloride (PVC). The tubing opened from the towed-fish's front and water was carried, by air driven Teflon pump, to a clean-air space (clean booth, air filtered with a HEPA filter) built into the ship's laboratory. Sample tubing was split into two and surface seawater samples were collected every 30 minutes to 2 hours with speeds up to 10 knots. One tube collected surface seawater into acid cleaned 125 mL LDPE bottles and the samples were immediately acidified (TD sample, 0.05 M ultrapure HCl, pH 1.8). The other tube collected surface water though a 0.22 µm filter (Millipak 100, Millipore Ltd.) into acid cleaned 125 mL LDPE bottles and were immediately acidified (D sample). Both the TD and D samples were also stored at room temperature after acidification for three years before analysis for this study.

3.3. Trace metal analytical methods

3.3.1. DFe in seawater samples by flow injection analysis

Comprehensive observation of surface seawater from the Bering Sea to the Chukchi Sea was conducted to measure DFe (Nishioka et al., Unpublished results). The seawater samples from Point Lay and Barrow Canyon used in this study are part of the comprehensive data set from the Bering Sea to the Chukchi Sea (Nishioka et al., Unpublished results); and were used to compare with one another. In an on-shore clean room DFe was initially analyzed, in all seawater samples 3 – 6 months after sampling, with the chemiluminescence and flow injection method (detailed in Obata et al., 1993). Once analyzed, the seawater samples were stored for three years at <pH 1.8. After this time period, seawater samples from Point Lay and Barrow Canyon were re-analyzed for the current study by pre-concentration via the NOBIAS chelating resin and analyzed for total dissolvable and DFe, Mn, and Cd on a GFAAS. Pre-concentration of the sea ice and seawater samples were performed as explained in detail in chapter 2.

3.4. Results

3.4.1. Physical properties in Chukchi seawater

Temperature, salinity and nutrients were measured in the seawater samples as part of a comprehensive observation from the Bering Sea to Chukchi Sea (Nishioka et al., Unpublished results). In the Point Lay samples observed in this study, temperature ranged from 2.2 to 9.5°C and in the Barrow Canyon samples the temperature ranged from 0.5 to 2.2°C (Fig. 3.2a). Salinity ranged from 26.9 to 30.7 in the Point Lay samples and 29.7 to 32.4 in the Barrow Canyon samples (Fig. 3.2b).

The nutrient data, given in detail in Nishioka et al. (Unpublished results), was used to calculate N** for both the Point Lay and Barrow Canyon samples (Fig. 3.2c). N** was calculated as shown in equation 1:

$$N** = 0.87(N - 16P) + 2.90 \; \mu mol / kg \hspace{2cm} (1)$$

N** ranged from -2.5 to 2.0 μmol / kg in the Point Lay samples and -10.8 to -1.9 μmol / kg in the Barrow Canyon samples.

3.4.2. Dissolved metals from Chukchi sea ice and seawater

The concentration factor is presented in ranges for sea ice (4.2 – 8.6 times) and seawater (4.2 – 8.6 times) due to sample volume variability. Dissolved Fe in drifting ice samples ranged from 0.9 – 10.8 nM. Ice 1 held significantly higher concentrations (avg. 6.08 ± 3.3 nM, Fig. 3.3a, $p < 0.05$, n = 4) when compared to Ice 2 and 3. The trend of DFe concentration showed Ice 2 to have lower concentrations (avg. 1.2 ± 0.2 nM, n = 4) than observed in Ice 3 (avg. 2.4 ± 1.4 nM, n = 14). Dissolved Fe in seawater ranged from 2.3 – 10.7 nM. Concentrations of the Point Lay samples (avg. 5.1 ± 2.4 nM, n = 16) were similar to the Barrow Canyon samples (avg. 4.5 ± 0.6 nM, n = 8).

Dissolved Mn in drifting ice samples ranged from 1.4 – 35.9 nM. As seen with DFe, Ice 1 held significantly higher concentrations of DMn (avg. 19.9 ± 10.1 nM, Fig. 3.3b, $p < 0.05$, n = 4) when compared with Ice 2 and 3 (5.5 ± 1.3 nM, n = 4 and 5.0 ± 2.2 nM, n = 14, respectively). Dissolved Mn in seawater ranged from 13.9 – 109.7 nM and was observed to have significantly higher concentrations than found in sea ice ($p < 0.05$). Dissolved Mn concentrations observed in the Point Lay samples had significantly higher concentrations (avg. 46.6 ± 30.0 nM, $p < 0.05$, n = 8) than the concentrations observed in Barrow Canyon samples (avg. 18.3 ± 2.9 nM, n = 16).

Dissolved Cd concentrations were very low (Fig. 3.3c). In drifting ice samples they ranged from <DL − 0.2 nM. Dissolved Cd did not have any discernible differences between the three sea ice samples. In seawater DCd concentrations ranged from <DL − 0.5 nM. The Barrow Canyon samples were significantly higher (avg. 0.23 ± 0.1, $p < 0.05$, n = 8) when compared to the Point Lay samples (avg. 0.1 ± 0.05, n = 16).

3.4.3. Labile particulate metals from Chukchi sea ice and seawater

The LP fraction was calculated as the difference between the TD and D metals as explained in Cid et al. (2011) and used to represent dissolvable particulate metals (Lannuzel et al., 2007). Labile particulate Fe in drifting ice ranged from 75.9 − 2278.9 nM (Fig. 3.4a). Ice 1 showed significantly higher concentrations (avg. 1447.8 ± 678.9 nM, $p < 0.05$, n = 4) when compared to Ice 2 and 3 (avg. 389.5 ± 132.4 nM and 372.4 ± 283.1 nM respectively). Labile particulate Fe in seawater ranged from 12.7 − 702.9 nM. Barrow Canyon samples had significantly higher concentrations (avg. 421.8 ± 99.2 nM, $p < 0.05$, n = 8) when compared to the Point Lay samples (avg. 205.2 ± 200.0 nM, n = 16).

Labile particulate Mn in drifting ice ranged from <DL − 1650.2 nM (Fig. 3.4b). Ice 1 had significantly higher concentrations (avg. 781.9 ± 712.0 nM, $p < 0.05$) when compared to Ice 2 and Ice 3 (avg. 6.8 ± 2.5 nM and 10.4 ± 7.1 nM respectively). In seawater, LPMn ranged from <DL − 25.8 nM. Significantly higher concentrations were observed for the Barrow Canyon samples (avg. 19.5 ± 7.9 nM, $p < 0.05$, n = 8) when compared to the Point Lay samples (avg. 8.7 ± 5.0 nM, n = 16).

Labile particulate Cd in drifting ice and seawater was low (Fig. 3.4c). Drifting ice ranged from <DL − 1.0 nM, but no discernible differences were observed among the samples. Labile particulate Cd in seawater ranged from <DL − 0.2 nM. Barrow Canyon samples were observed to have significantly higher concentrations (avg. 0.1 ± 0.06 nM, $p < 0.05$, n = 8) when compared to the Point Lay samples (avg. 0.04 ± 0.03 nM, n = 16).

3.4.4. Percent contribution of dissolved vs labile particulate metals in Chukchi sea ice and seawater

The distribution of sized fractioned trace metals (D or LP) within a medium (sea ice or seawater) can be determined by analysing the amount (%) of each size fraction within the medium (Lannuzel et al., 2014). This percent contribution was calculated by dividing a size fraction (i.e. D) by the sum of the size fractions (i.e. D + LP) and multiplying it by 100. In Chukchi sea ice the percent contributions for each trace metal are as follows (Table 3.1; % ± SD): 0.8 ± 0.7% DFe and 99.2 ± 0.7% LPFe, 36.4 ± 22.1% DMn and 63.6 ± 22.1% LPMn, 28.8 ± 28.3% DCd and 71.2 ± 28.3% LPCd. Sea ice yielded high concentrations of LP metals. For Chukchi seawater, the percent contributions for each trace metal are as follows (Table 3.1; % ± SD): 5.9 ± 11.9% DFe and 94.1 ± 11.9% LPFe, 71.5 ± 20.8% DMn and 28.5 ± 20.8% LPMn, 66.3 ± 25.2% DCd and 33.7 ± 25.2% LPCd. Seawater was observed to have high percentages of LPFe with high DMn and DCd.

3.5. Discussion

3.5.1. DFe comparison of NOBIAS resin pre-concentration method vs flow injection analysis

Acidified (<pH 1.8) seawater samples (from the Bering Sea to Chukchi Sea) were initially analyzed in 2013 for DFe (Nishioka et al., Unpublished results) using flow injection after pre-concentration with the 8-HQ chelating resin and luminol-hydrogen peroxide chemiluminescence detection methods (Obata et al., 1997). Samples were re-acidified to <pH 1.8 and held at room temperature in a clean room for 3 years before a portion of the samples (Barrow Canyon and Point Lay samples) were pre-concentrated via the NOBIAS resin at pH 6 for the dissolved and total dissolvable size fractions in this study. Comparing the DFe data collected with the NOBIAS resin pre-concentration method to the flow injection method, the NOBIAS resin data were 1.3 ± 0.4 (n = 24) times higher than the flow injection data. Both methods for the determination of DFe were applied successfully and validated by certified reference materials (NASS-6 reference seawater, see chapter 2). A previous study also compared DFe in the same Chukchi seawater samples analyzed through flow injection (Hioki et al., 2014) and the NOBIAS resin pre-concentration method (Kondo et al., 2016). The DFe concentrations observed in Kondo et al. (2016) were 1.6 ± 0.5 times higher than those observed in Hioki et al. (2014). One reasoning for this is the acidification level in the samples. Seawater acidification allows for the disassociation

32

of metals that are bound to colloids or ligands, thus increasing the concentration of D metals that can be analyzed (Bruland and Rue, 2001). Over the course of a couple of years, DFe in the low pH seawater samples had a longer time to disassociate with any substrates they were still bound to after the initial analysis. It is possible that this allowed for the samples to have higher concentrations of DFe that was reflected when pre-concentrated with the NOBIAS resin. Both methods are able to give oceanographically correct measurements of DFe that represents the chemically-labile dissolvable fraction of Fe in seawater.

3.5.2. Trace metal trends for Chukchi seawater

3.5.2.1. Internal source of trace metals

Previous studies have stated that the composition of trace metals in Chukchi seawater showed high concentrations of LPMn, LPFe, LPCo and LPPb; and high concentrations of DNi, DCu, DZn and DCd (Cid et al., 2012; Kondo et al., 2016). Comparisons of observed surface (3 m) values for D and LP Fe, Mn and Cd, with the exception of DMn, in the current study were within range of Cid et al. (2012; ≤20 m; Table 3.2). Comparisons of the current studies data with Kondo et al. (2016; ≤20 m; Table 3.2) surface values yielded higher concentrations, indicating possible annual variations in trace metal availability. The trace metal composition of Chukchi seawater from this study yielded the percent contributions of DFe (5.9%) DMn (71.5%) and DCd (66.3%; Table 3.1). It is possible that the actions of each individual trace metal (Fe, Mn and Cd) within seawater may influence their concentrations. To examine the behavior of Fe, Mn and Cd in seawater, their relationship with surface phosphate data collected from the towed-fish observation (Bering Strait to Barrow Canyon; Nishioka et al. Unpublished results) was examined. A relationship would indicate that any biogeochemical cycling processes controlling the removal of nutrients would also influence the trace metal (Boyle et al., 1981; Matsunaga and Abe, 1985). Out of the three metals, Cd was the only metal that showed a relationship with phosphate (Fig. 3.5c). Dissolved Cd and PO_4 showed moderately strong correlations (r = 0.88) with a regression of:

[DCd nM] = 0.24 [PO_4 µmol / kg] + 0.042

R^2 = 0.78, n = 24

Cid et al. (2012) was also able to observe a relationship between Cd and phosphate in the Chukchi and Beaufort Seas. In seawater Cd exhibits a nutrient-type depth profile, low surface concentrations resulting from the uptake via phytoplankton and high depth concentrations resulting from release by remineralization of biological materials (Boyle et al., 1976; de Baar et al., 1994). This allows Cd to mirror phosphate during its cycling in the ocean (Boyle et al., 1976; Bruland et al., 1978; Knauer and Martin, 1981) giving it an internal source though biogeochemical cycling process.

3.5.2.2. External sources of trace metals

Iron and Mn did not show any relationships with phosphate (Fig. 3.5a,b). This indicates that Fe and Mn may be controlled through external sources within Chukchi seawater. One possible source is river inputs. Shelf sediments can also supply trace metals as they are released into the water column (Cid et al., 2012; Kondo et al., 2016). It is possible that the observed high concentrations of LPFe and LPMn (Fig. 3.4a,b) from this study indicated that sediments maybe a major source to Chukchi seawater. To understand this relationship N** from both sampling sites (off the coast of Barrow Canyon and off the coast of Point Lay) were calculated. N** is used to trace the variability of nitrogen resulting from denitrification and nitrogen fixation processes (Deutsch et al., 2001; Gruber and Sarmiento, 1997). N** is different from N* because N** requires N to represent total NO_3^- (nitrates, nitrites and ammonia; Nishino et al., 2005). The Chukchi Sea has significant ammonia concentrations due to high primary productivity during bloom season (Cooper et al., 1997) and both nitrates and nitrites are used during the decomposition of organic matter. If N** values are high, equation 1 is reflecting the P signal indicating nitrogen fixation occurring within the water column. Low values of N** reflect the N signal indicating denitrification within the sediment pore water has occurred (Deutsch et al., 2001). Therefore, total dissolved inorganic nitrogen (DIN) should be used instead of NO_3^- for N to accurately account for nitrogen replete or deficient conditions in the Chukchi Sea (N**; Nishino et al., 2005; Kondo et al., 2016).

Observations of the N** showed low values in the Barrow Canyon sampling site of the current study (Fig. 3.2c). This indicates denitrification within the sediment pore water and

subsequent release into the water column for this area. It is possible that vertical mixing and westward movement of seawater displaced bottom shelf water towards the surface (Weingartner et al., 1998; Eicken et al., 2005). Nishino et al. (2005) showed that Chukchi Shelf bottom water spread from the Barrow Canyon westward to the outer shelf area by using N** minimum values. Kondo et al. (2016) also suggested that high NH_4^+ with the Chukchi Sea shelf region was due to sedimentary input as opposed to organic matter degradation. Therefore, sediments are highly influential in this area.

The LP fraction represents the dissolvable particulate metals within a sample. Therefore, they may be supplied through a sedimentary source. High concentrations of LPFe, and relatively high LPMn, were observed in the Barrow Canyon samples (Fig. 3.2i,j). These observations were supported by TD/D metal ratios for Fe and Mn (Fig. 3.2d,e). Since the TD fraction represents a combination of D and dissolvable particulate metals in a sample; ratio analysis can indicate which form is more dominate in a sample. The TDFe/DFe ratios were high, with relatively high TDMn/DMn ratios, in the Barrow Canyon samples. This indicates a supply of particulate metals for this area. Klunder et al. (2012) observed that high TDFe/DFe ratios indicated a supply of LPFe by sediment, river, or sea ice sources. Upon comparison of the low N** values (Fig. 3.2c), high TD/D ratios and high LP metal concentrations in the Barrow Canyon samples, the supply of LPFe and LPMn was sourced through shelf sediments.

Elevated DFe and DMn concentrations were observed in the Point Lay samples (Fig. 3.2f,g). This indicates that a separate external source supplied this trace metal fraction. In the Chukchi Sea different currents can be defined by their salinities and temperatures. From the Bering Strait two currents enter the Chukchi Sea from the Pacific Ocean: the Bering Shelf-Anadyr waters (salinity from 32 - 33) and Alaskan Coastal Current (ACC, salinity below 32; Coachman et al., 1975; Roach et al., 1995; Woodgate et al., 2005). Salinity measured in the Point Lay samples in this study, away from the ice edges (samples PL 6 - PL 16), yielded a range of 26.8 - 30.7 (Fig. 3.2b). Temperature measured in these samples ranged from 8.4 to 9.5°C (Fig. 3.2a). These values indicate that the ACC supply waters to samples PL 6 -PL 16. Comparisons of temperature and salinity (Fig. 3.2a,b) and the D metal concentrations (Fig. 3.2f,g) indicate that the ACC supplies

DFe and DMn to the Point Lay samples. The ACC is a yearly, coastal current originating from the Gulf of Alaska (Royer, 1998; Weingartner et al. 2005). As it flows through the Bering Strait, it is freshened from the Yukon river (about 200 km^3/yr), contributing up to 200 - 450 km^3/yr to the Chukchi Sea (Woodgate and Aagaard, 2005). The high river influence in the ACC indicate a river water supply of D metals to the Chukchi Sea (Macdonald et al., 1998; Cid et al., 2012).

In Chukchi seawater DMn concentrations were higher than LPMn concentrations (Fig. 3.2 g,j, 3.6). High DMn was also observed in the shelf area of the Bering Sea and decreased towards the Green Belt area (Hurst et al., 2010). The distributions of Fe and Mn in the ocean are dependent on the chemical characteristics of their oxidation states and the ocean's chemistry, physics and biology (Balistrieri et al., 1992). A possible reason for high DMn and high LPFe in the water column of the Chukchi Sea may result from chemical reactions between the water column and shelf sediments. Reduction in sediment pore water supplies the water column with Fe(II) and Mn(II) where they are oxygenated to insoluble Fe(III) and Mn(IV) respectively (Balistrieri et al., 1992; Mortimer, 1941; Sunda et al., 1983). Iron oxidation from Fe(II) to Fe(III) is faster than for Mn. After oxidation Fe can yield colloidal forms that can pass through filters and be analyzed as DFe (Stumm and Morgan, 1981), quickly bind with organic ligands (99%; Sunda, 2001; Wu and Luther, 1995) or precipitate as Fe(III) oxyhydroxides that can create particulate Fe (Hurst et al., 2010; Lohan and Bruland, 2008). This in turn can decrease the detectable amount of DFe in samples.

Manganese oxidation is slower than observed for Fe, resulting in DMn to remain in the water column longer. Oxidation rates can increase in the presence of bacterial processes (Nealson, 1978; Stumm and Morgan, 1981) but are significantly reduced in the presence of light (Sunda et al., 1983). Removal processes such as phytoplankton uptake, scavenging of suspended and sinking particles (Landing and Bruland, 1987; Sedwick et al., 2000) can also control the size fraction concentrations of Fe and Mn in the water column. Although these processes are important for the concentration of D and LP Fe and Mn, sediment reductive processes and shelf sediments may play a stronger role in the behavior of Fe and Mn within the Chukchi Sea (Cid et al., 2012; Kondo et al., 2016).

3.5.3. Trace metal trends for Chukchi drifting sea ice

Iron, Mn and Cd concentrations observed in each of the sea ice samples were heterogeneous. It is possible that this is due to the accumulation and release processes in sea ice. It was observed that the behavior of Fe, Mn and Cd differed in Chukchi seawater. Iron and Mn had external sources (sediments for LPFe and LPMn, and ACC for DFe and DMn) and Cd an internal source (biogeochemical cycling processes). The contribution of trace metal in Chukchi drifting ice showed high LPFe (99.2%), LPMn (63.6%) and LPCd (71.2%; Fig. 3.4, Table 3.1). When comparing Chukchi seawater trace metal concentrations to Chukchi drifting ice trace metal concentrations, drifting ice was observed to have higher LP concentrations (Fig. 3.6, Table 3.3). This indicates that Chukchi drifting ice has a preference to accumulate or retain the LP fraction of Fe, Mn and Cd. A possible explanation for the high concentrations of LP metals (representative of dissolvable particulate metals) in Chukchi drifting ice may be due to sediment sources (shelf or river; Cid et al., 2012; Kondo et al., 2016). In the Arctic Ocean, the Chukchi shelf provides sediments (fine particles such as silt and clays) and a shallow environment (~50 m) where scavenging can occur (Nürnberg et al., 1994) during frazil ice formation (Reimnitz et al., 1993; Smedsrud, 2001). River inputs add additional particles into the shelf areas (Cid et al., 2012; Kondo et al., 2016). During winter storm events, the water is mixed downward, re-suspending shelf sediments upward within the shallow shelf waters or polynyas (Eicken et al., 2005; Reimnitz et al., 1992). At the same time frazil crystals form, and rise, to the seawater surface. With the combination of re-suspending sediments and frazil crystals rising, the frazil crystals combine into a solid matrix where it can trap, nucleate or adhere to particulate matter of terrigenous or biogenic origin (Eicken et al., 2005; Ito et al., 2017; Reimnitz et al., 1993). This scavenging or suspension freezing of particles can allow for particulate trace metals to accumulate into the ice (Campbell and Collin, 1958; Reimnitz et al., 1993). Sediment-laden sea ice from the Chukchi and Beaufort Seas were associated with frazil ice growth formed in a well-mixed nearshore environment (Eicken et al., 2005). In the Antarctic region, high concentrations of PFe (biogenic or lithogenic) observed in land-fast ice were determined to be due to coastal shelf sediment re-suspension (Grotti et al., 2005; Lannuzel et al., 2008, 2010). Within the shelf areas wind speeds, up to 25 m s^{-1}, and current speeds, up to 1.5 m s^{-1}, can allow for re-suspended, trace metal bound,

sediments to entrain into forming frazil ice (Ito et al., 2017; Eicken et al., 2005). Sediment-laden sea ice has been observed to be heterogeneous (Eicken et al., 2005) which can translate to the heterogeneity observed in the trace metals concentrations from the Chukchi sea ice. Once ice is formed into floes, enrichment of particulate trace metals may occur through wave propagation on the consolidated ice (Ito et al., 2017; Spindler, 1994).

Below the ice floe, brine channels are a possible avenue for the release or introduction of trace metals. Chukchi drifting ice showed low concentrations of the D fraction for Fe, Mn and Cd (Fig. 3.3, 3.6). It may be that sea ice released the D metals during brine drainage. As ice forms, seawater salts precipitate out into the brine system. Brine that are trapped in the sea ice are released into the underlying water due to density differentials when the permeability of sea ice increases (Untersteiner, 1968; Maykut, 1985). Through this process, sea ice can release 60 – 70% of incorporated dissolved matter (i.e. salts, metals. etc) into the underlying seawater (Giannelli et al., 2001). A temporal decoupling showed that particulate Fe (PFe, metals on 0.2 µm filters and digested; Lannuzel et al., 2011a) was enriched in Antarctic sea ice. Whereas, DFe was observed to be enriched in the brine (Lannuzel et al., 2014; van der Merwe et al., 2011) indicating DFe release from sea ice. Particulate metals can be locked into the ice from frazil entrainment or attached to brine channels, as observed in Antarctic sea ice, allowing this fraction to be released during advanced ice melt (Lannuzel et al., 2007, 2008). It is possible that, due to the late season when Chukchi drifting ice was collected and its subsequent high permeability, the observed low concentrations of the D metals (Fe, Mn and Cd) is due to brine release. This would allow for the LP (dissolvable particulate fraction) to be preferentially retained in the Chukchi drifting ice. This indicates that this temporal partitioning of trace metals observed in the Antarctic may occur in Arctic sea ice. It is possible that atmospheric deposition (wet or dry) add trace metals to sea ice (Fischer et al., 2007; Maenhaut et al., 1996; Wagenbach et al., 1998). Yet the current study did not measure snow or identify different ice types before analysis. To clarify the source of trace metals and the processes utilized by sea ice to accumulate trace metal, it is necessary to compare the concentrations of trace metals to sea ice structure. Therefore, more studies are needed to understand the mechanisms for trace metal accumulation into Arctic sea ice.

3.6. Summary

Sea ice plays an important role in the biogeochemical cycling of trace metals in the Arctic Ocean. Therefore, it is important to understand the mechanisms of trace metal accumulation into sea ice. Dissolved and LP Fe, Mn and Cd was observed in Chukchi seawater and drifting ice to understand the form and concentrations of trace metal in Arctic sea ice. In Chukchi seawater, Fe, Mn and Cd behaved differently. Fe and Mn were controlled by external sources: sedimentary inputs for the labile particulate fraction and the ACC for the dissolved fraction, where Cd was controlled though internal sources: biogeochemical cycling of phosphate. The metal composition of Chukchi seawater showed high percentages for LPFe, DMn and DCd. Comparing the concentrations of Chukchi seawater to drifting ice, Chukchi drifting ice had high concentrations for LPFe, LPMn and LPCd. The low concentrations of D metals observed in Chukchi drifting ice could be due to a temporal partitioning of trace metals from the sea ice (D fraction released with the brine; van der Merwe et al., 2011; and the particulate fraction retained until advanced melting; Lannuzel et al., 2008) as observed with Antarctic sea ice. Entrainment of sediments during frazil formation, in underwater polynyas or leads, can add LP metals to the sea ice (Ackley et al., 1987; Reimnitz et al., 1993; Weissenberger and Grossmann, 1998) as well as atmospheric deposition onto sea ice (Maenhaut et al., 1996). Based on the results of this study, Chukchi drifting ice was observed to have preference to accumulate or retain the LP metals. Future studies should focus on collecting drifting sea ice from different locations and seasons then compare the sized fractioned trace metal concentrations to the surface seawater. This will help expand our understanding of the geochemical behavior of trace metals within sea ice.

3.7. Figures
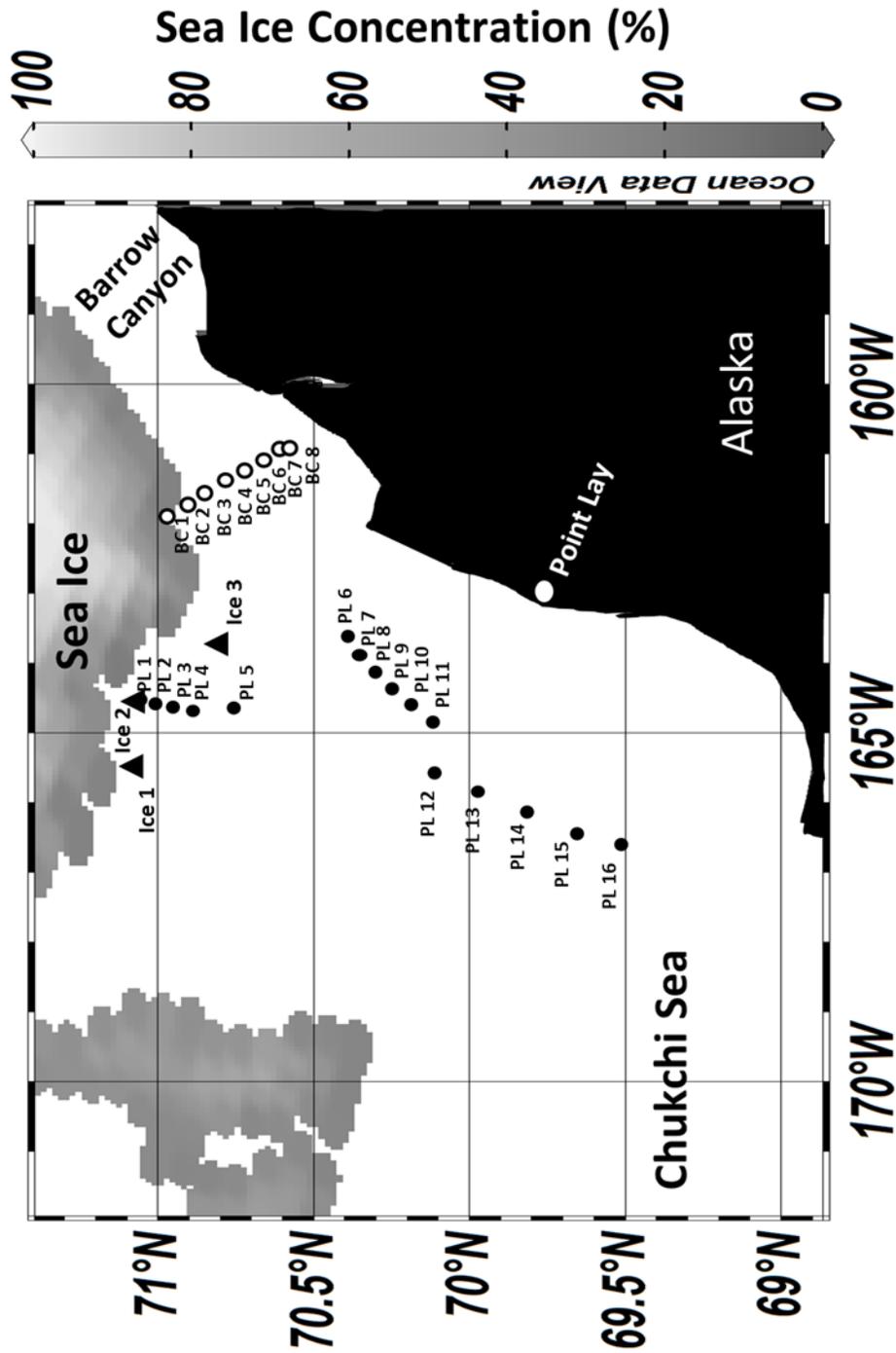
Figure 3.1. Sampling locations for sea ice (black triangles) and seawater off the coast of Barrow Canyon (BC, white circles) and off the coast of Point Lay (PL, black circles) in the Chukchi Sea. Each sampling site can be located by the sampling ID.
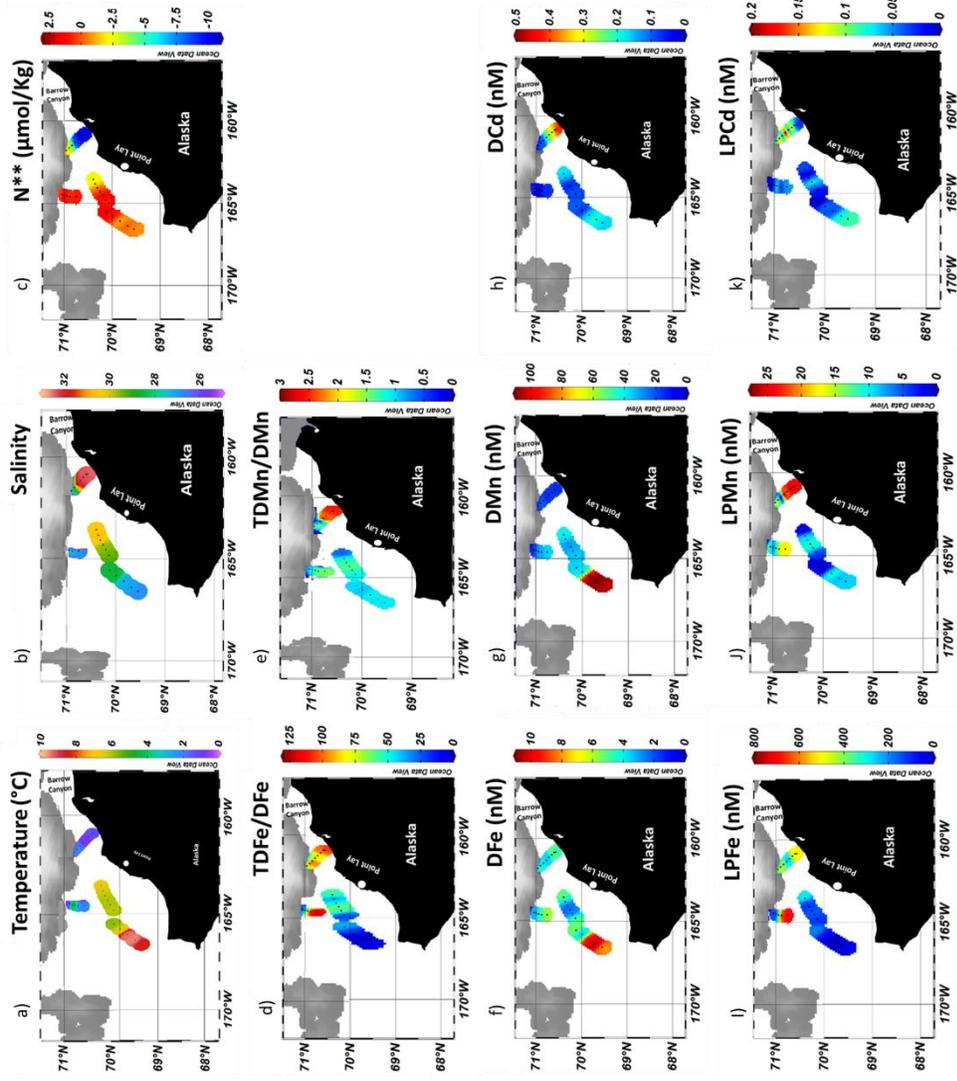
Figure 3.2. Concentrations of a) N** , b) TDFe/DFe ratios, c) DFe, d) LPFe, e) TDMn/DMn, f) DMn, g) LPMn plotted in a horizontal orientation of the seawater samples from off the coast of Barrow Canyon and off the coast of Point Lay.

41
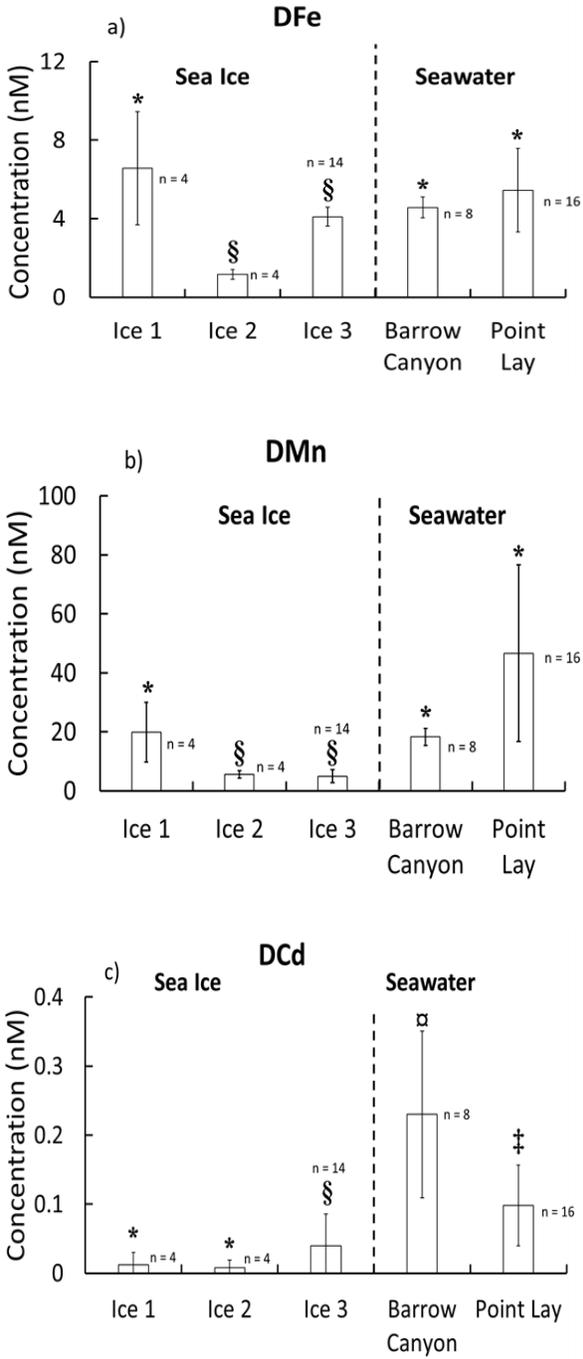
Figure 3.3. Concentration of dissolved metals from the three sea ice samples (concentration factor range of 4.2 – 8.6 times), and seawater from below Barrow Canyon and off the coast of Point Lay (concentration factor range of 2.7 – 3.2 times). Different symbols next to each data bar indicate the statistical difference between samples. a) DFe, b) DMn, c) DCd.
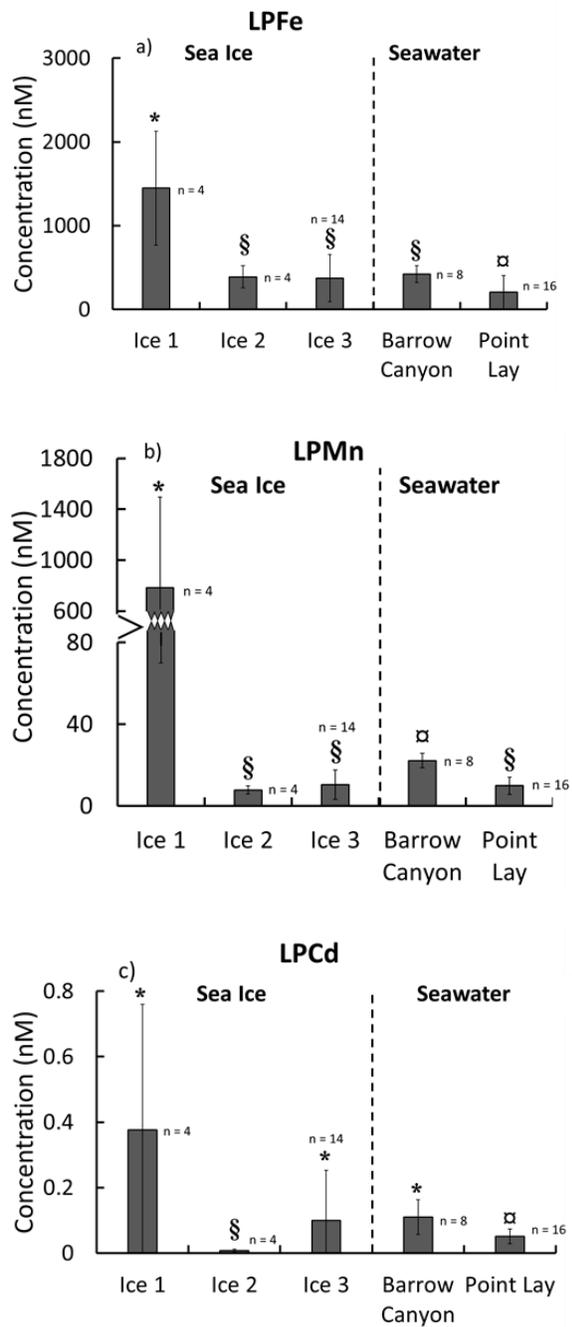
Figure 3.4. Concentration of liable particulate metals from the three sea ice samples (concentration factor range of 4.2 – 8.6 times), and seawater from off the coast of Barrow Canyon and off the coast of Point Lay (concentration factor range of 2.7 – 3.2 times). Different symbols next to each data bar indicate the statistical difference between samples. a) LPFe, b) LPMn, c) LPCd.
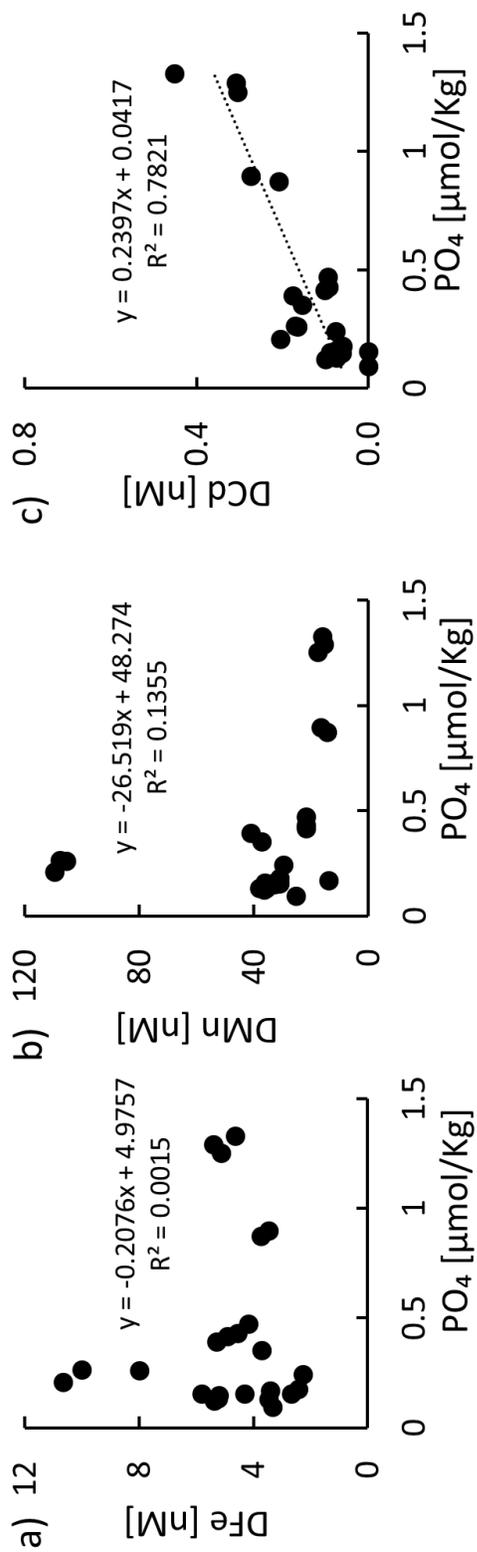
Figure 3.5. Seawater regression analysis of dissolved metals with phosphate. a) DFe, b) DMn, c) DCd.
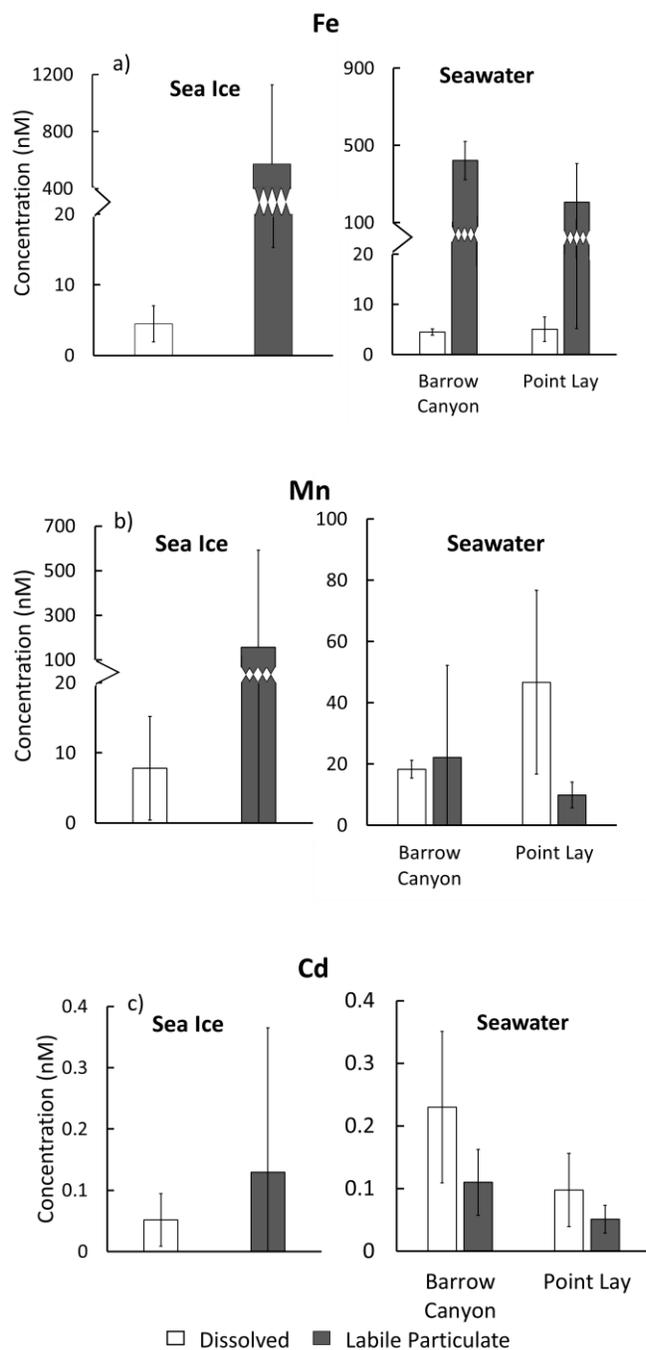
Figure 3.6. Concentrations of dissolved and labile particulate a) Fe, b) Mn and c) Cd in sea ice and seawater. Concentration factors varied between sea ice (4.2 – 8.6 times) and seawater (4.2 – 8.6 times) due to sample volume variability. Seawater was collected below Barrow Canyon and off the shore of Point Lay. Dissolved concentrations are represented in white and labile particulate concentrations are in grey.

Table 3.1. Mean percent contribution of dissolved and liable particulate trace metals in Chukchi sea ice and Chukchi seawater. a) Fe, b) Mn and c) Cd.

a)	DFe	LPFe
	(% ± SD)	(% ± SD)
Sea Ice	0.8 ± 0.7	99.2 ± 0.7
Seawater	5.9 ± 11.9	94.1 ± 11.9

b)	DMn	LPMn
	(% ± SD)	(% ± SD)
Sea Ice	36.4 ± 22.1	63.6 ± 22.1
Seawater	71.5 ± 20.8	28.5 ± 20.8

c)	DCd	LPCd
	(% ± SD)	(% ± SD)
Sea Ice	28.8 ± 28.3	71.2 ± 28.3
Seawater	66.3 ± 25.2	33.7 ± 25.2

Table 3.2. Comparison of minimum and maximum surface seawater (≤20 m). Dissolved and labile particulate Fe, Mn and Cd concentrations from the Chukchi Sea Shelf to the Canada Basin were compared to published studies with the current study.

Element		This Study (nM)	Cid et al. (2012) (nmol/kg)	Kondo et al. (2016) (nM)
Fe	D	2.3 – 10.7	1.4 – 10.4	1.1 – 2.7
	LP	12.7 – 702.9	24.1 – 9300.4	2.7 – 33.4
Mn	D	13.9 – 109.7	0.3 – 26.3	8.2 – 15.0
	LP	<DL – 25.8	3.8 – 193.9	1.2 – 22.8
Cd	D	<DL – 0.5	0.2 – 0.5	0.1 – 0.4
	LP	<DL – 0.2	<DL – 0.09	<DL – 0.2

Table 3.3. Raw data from a) sea ice and b) seawater samples. D - dissolved and LP - labile particulate. Sea ice pre-concentration factor ranged from 4.2 – 8.6 times and the seawater pre-concentration factor ranged from 2.7 – 3.2 times.

a)			Sea Ice			
Sample	DFe (nM)	LPFe (nM)	DMn (nM)	LPMn (nM)	DCd (nM)	LPCd (nM)
1	2.7	1947.6	12.3	33.5	0.04	0.1
1	3.2	2278.9	10.2	1316.1	<DL	0.1
1	10.8	875.3	21.3	127.6	<DL	1.0
1	7.6	689.4	35.9	1650.2	<DL	0.3
2	0.9	297.2	3.5	5.8	<DL	0.01
2	1.4	611.0	6.9	10.4	<DL	0.01
2	1.0	370.5	5.9	7.3	<DL	0.01
2	1.5	279.2	5.8	3.6	0.03	<DL
3	1.3	518.5	5.0	17.1	0.02	0.05
3	2.1	344.2	6.5	10.0	<DL	0.1
3	2.4	714.0	8.5	15.1	0.02	0.04
3	2.7	75.9	5.0	<DL	0.2	<DL
3	1.4	81.5	5.1	2.7	<DL	0.02
3	5.5	647.8	1.4	21.2	0.05	0.1
3	1.6	223.2	2.9	12.6	<DL	0.04
3	4.0	560.2	7.9	15.4	0.1	0.6
3	1.1	101.3	3.6	2.9	0.02	0.04
3	0.9	88.6	3.7	3.4	<DL	0.03
3	5.0	888.9	9.3	17.5	0.03	0.1
3	3.3	729.3	4.5	19.2	0.08	0.06
3	1.2	150.8	2.6	5.9	0.03	0.03
3	1.5	89.4	3.9	1.6	0.03	0.01

b) | | | | **Seawater** | | |

Sample	DFe (nM)	LPFe (nM)	DMn (nM)	LPMn (nM)	DCd (nM)	LPCd (nM)
Barrow Canyon 1	4.9	459.5	21.9	18.5	0.1	0.09
Barrow Canyon 2	4.5	451.4	21.8	15.7	0.09	0.2
Barrow Canyon 3	4.2	426.7	21.9	<DL	0.09	0.05
Barrow Canyon 4	3.7	272.4	14.4	25.8	0.2	0.2
Barrow Canyon 5	3.5	245.7	16.6	20.9	0.3	0.04
Barrow Canyon 6	5.1	506.1	17.9	25.1	0.3	0.1
Barrow Canyon 7	5.4	477.2	15.7	25.1	0.3	0.1
Barrow Canyon 8	4.6	535.5	16.0	24.3	0.5	<DL
Point Lay 1	3.4	148.8	13.9	12.0	0.07	<DL
Point Lay 2	3.3	121.0	25.4	5.6	<DL	0.04
Point Lay 3	4.3	330.1	31.1	10.2	<DL	0.08
Point Lay 4	5.2	668.4	32.8	16.7	0.06	0.03
Point Lay 5	5.8	702.9	36.2	17.7	0.07	0.05
Point Lay 6	5.3	298.4	41.2	<DL	0.2	0.04
Point Lay 7	3.7	132.1	37.4	9.9	0.2	<DL
Point Lay 8	2.3	116.2	29.7	9.4	0.08	0.03
Point Lay 9	2.4	152.2	31.0	12.0	0.06	0.08
Point Lay 10	2.7	155.8	33.9	10.5	0.09	0.05
Point Lay 11	5.2	119.5	35.7	4.4	0.09	0.02
Point Lay 12	5.4	197.1	36.6	0.9	0.1	<DL
Point Lay 13	3.4	68.2	38.2	<DL	0.07	0.04
Point Lay 14	10.0	13.5	107.9	10.9	0.2	0.04
Point Lay 15	10.7	12.7	109.7	8.6	0.2	0.08
Point Lay 16	8.0	46.9	105.6	9.2	0.2	0.09

Chapter 4

Accumulation processes of trace metals into Arctic sea ice: Distribution of Fe, Mn and Cd associated with ice structure

4.1. Introduction

Comparison of D and LP Fe, Mn and Cd in Chukchi drifting ice yielded high concentrations of the LP fraction. These concentrations eclipse those observed in the underlying seawater. Seawater trace metal composition also differed from that of drifting ice in that higher concentrations of D Mn and Cd were observed. Yet the accumulation and release processes of trace metals utilized by drifting ice were not clearly observed. In order to understand the biogeochemical cycling of trace metals by Arctic sea ice, it is important to identify the mechanisms of how sea ice interacts with trace metals. Therefore, the size fractions of trace metals were examined in relation to sea ice structure.

Ice structure is an indication of the formation processes utilized by sea ice. Sea ice initially forms when seawater is supercooled (-1.86°C) creating thermohaline mixing by the convection of heat from the warmer water at depth to the now cooler surface water. With the aid of wind and wave energy frazil ice will form (Eicken, 2003). Frazil ice crystals (3 to 4 mm) form under rough conditions (strong winds or rough currents) at the water's surface, within the water column, or along shelf areas (Kempema et al., 1989; Maykut, 1985; Weeks and Ackley, 1986). As frazil ice float to the surface they mix with seawater and freshwater (snow or river) to create a slush layer that can reduce thermohaline mixing and wind stress (Eicken, 2003; Maykut, 1985; Toyota, 2018). Continual freezing and ice condensing forms grease ice that can solidify up to 10 cm depth (granular ice; Maykut, 1985) creating calm conditions under the ice. As seawater congeals downward in calm conditions it forms vertically elongated, prismatic crystal structures known as columnar ice (Eicken et al., 1995; Maykut, 1985). The composition of sea ice is a complex, porous matrix. As sea ice forms, salts concentrate into interstitial dense liquid brine. Some of this brine is released from the ice to ultimately form dense bottom water (Weingartner et al., 1998), while

some can be trapped in ice pockets (brine channels) until ice permeability increases (Golden et al., 1998). As brine is retained in sea ice, it can affect the sea ice's nutrient and trace metal composition (Lannuzel et al., 2008; van der Merwe et al., 2011). The rapid decline of multi-year ice in the Arctic may affect the biogeochemical cycling of trace metals, hindering the supply of these metals to the underlying seawater.

Observations of ice structure can allow for the detection of the formation process of sea ice. It is possible that, as sea ice forms, it may incorporate trace metals into the ice. Trace metals may also accumulate into ice after it is established. The processes by which trace metals are retained or released from the ice are varied and not clear. In seawater, Fe, Mn and Cd exhibit different chemical sensitivity and behavioral (i.e. oxidation-reduction reactions) properties. Manganese displays a scavenging-type distribution where it has interactions with particles and shelf sediments. Cadmium is an example of a nutrient-type distribution. This metal is influenced by biological processes (i.e. phosphate cycle) and organic particulate matter. Iron shows more of a scavenging-type distribution and can also display nutrient-type behavior (Bruland et al., 1994; Bruland and Lohan, 2006). Comparisons of Fe and Mn yield different reduction potentials (Landing and Bruland, 1987; Saager et al., 1989) which may influence the concentrations of their size fractions (Evans and Nishioka, 2018). The purpose for this study was to compare the concentrations of trace metals to the observed sea ice structure, from a single Arctic core sample, to aid in revealing mechanisms behind trace metal accumulation.

4.2. Materials and methods

4.2.1. Materials trace metal cleaning process

Ceramic knifes used during the cleaning (planing) step for sea ice were cleaned in an onshore clean room by the following procedure: knives were placed in 5% Extran® (alkaline and phosphate-free liquid, Merck) for one day, rinsed with reverse osmosis (RO) water then placed in ultrapure hydrochloric acid (0.1 M HCl, Tamapure-AA-10, Tama Chemical Ltd.) for one day. The knives were rinsed with Milli-Q water (Millipore Ltd.) and air dried on a laminar flow clean bench before use.

An acrylic ice holder (Fig. 4.1) was used in the ice planing step to keep the ice core sample stable during planing. The ice holder was cleaned by a 5% Extran® bath for one day, rinsed with RO water and air dried. Ice samples were prepared by planing in a 137 L freezer (cold tub, Panasonic; Fig. 4.1) located in a dust free clean room. The cold tub was covered with clean plastic, allowing it to maintain the preset temperature (-20˚C). 24 hrs before ice planing, the cold tub was turned on and all planing materials (ceramic knifes, gloves, collection buckets, etc.) were double bagged and placed in the cold tub as the tub cooled down to -20˚C. For each subsequent sample that was planed, the cold tub was cleaned of previous ice waste generated during planing and air dried in the clean room.

4.2.2. Sea ice sampling

Sea ice was collected from the Beaufort Sea on August 2013 at ice station 76˚56′N, 138˚38′W during the JIOS cruise aboard the *CCGS Louis S. St-Laurent* (Fig. 4.2). Sea ice was sampled with a 9 cm diameter corer and the core length was immediately measured with a tape measure (Fig. 4.3a). The core sample was then cut in half (50 cm and 53 cm respectively), individually placed in coolers and transported to an onboard cold room (-15˚C) before being transported to an onshore cold room (-15˚C). The sample was held for 4 years before analysis.

4.2.3. Milli-Q ice contamination test

The corer used to collect the sea ice was made of metal. Unfortunately, this process can contaminate the outer layers of the sea ice sample for trace metal analysis. To account for this contamination, sea ice is usually cleaned through planing a couple of centimeters off the outer ice layers with acid cleaned ceramic knives. The cleaned inner core of the ice is then analyzed for trace metals. To determine the amount of contamination contributed by ice planing materials (ceramic knifes, plastics and collection buckets), the coring process and the planing procedure, a contamination test was performed on Milli-Q ice. All samples were handled with clean plastic gloves and plastic wrap. In an onshore class 100 clean room, two Milli-Q ice samples were prepared by freezing Milli-Q water in acid cleaned 500 mL HDPE bottles (tops cut off). The resulting ice formed as a cylinder (Milli-Q ice). One day before planing, one of the Milli-Q ice samples was removed from the 500 mL bottle and wrapped in aluminum foil (Foil ice). It was

placed in the cold tub to mimic contamination resulting from the coring process during sample collection. The other Milli-Q ice was left untouched in the freezer before the planing step (Milli-Q Clean ice). Each Milli-Q ice was planed separately.

Before ice planing, the ice holder was wrapped in clean plastic and placed in the cold tub (-20˚C). For the Foil ice, the aluminum foil was removed before planing. For the Milli-Q Clean ice, the ice sample was removed from the bottle and immediately planed to minimize handling. For each ice sample two layers (1 cm each) was planed using acid cleaned ceramic knifes. A new, clean knife was used to plane each side as evenly as possible. All ice pieces that were in contact with the planing materials were collected into acid cleaned 325 mL HDPE jars. The planed ice core was collected in acid cleaned HDPE buckets and all samples were melted at room temperature in a dust free clean room. Melted samples were immediately acidified by ultrapure HCl (final concentration 0.05 M with <pH 2.0, Tamapure-AA-10) and pre-concentrated via the NOBIAS resin before analysis on a GFAAS (for pre-concentration methods see chapter 2). The Milli-Q ice contamination test results are shown in Figure 4.4 (pre-concentration factor ranging from 4.6 - 8.7 times, avg. 7.5 times). Planing 2 cm of ice off the outer core sample was enough for trace metal analysis as the ice planing materials and procedure did not contribute contamination to the ice sample.

4.2.4. Sea ice planing and preparation

When the sea ice core sample was planed, a blank sample (Milli-Q water) was frozen (Milli-Q blank) in a 325 mL LDPE jar and set in the cold tub. The Milli-Q blank was used to check that the planing conditions were clear of contamination. The planing of sea ice followed the methods outlined above. Once 2 cm of the outer ice core was planed, the sample was visually observed and separated based on sea ice structure. Pictures of each section were taken with a digital camera to aid with the sea ice structure determination. Pictures were transformed to black and white and overlaid with a filter to detect the outline of the pore microstructure captured in the pictures (GNU Image Manipulation Program, GIMP). The % white area in the transformed pictures, the area that represents the outline of the pore microstructure (hereafter porosity %), was calculated using R analysis package (R Core Team 2013; Jeroen, 2018; Mouselimis, 2018).

This analysis allowed for an objective discrimination between granular and columnar ice, and the identification of mixed (granular plus columnar) ice to a certain extent. All planed samples, and the Milli-Q blank, were placed in acid clean HDPE buckets and melted at room temperature in a clean room.

Immediately after melting, samples were separated for trace metal analysis, salinity, $\delta^{18}O$, and nutrients. Nutrient samples were re-frozen immediately after melting and stored before analysis. To prepare for trace metal analysis, a portion of the meltwater was separated into acid cleaned 125 mL LDPE bottles for total dissolvable samples and immediately acidified with ultrapure HCl (final concentration 0.05 M with <pH 2.0, Tamapure-AA-10). Another portion of meltwater (dissolved) was immediately filtered by 0.22 μm Durapore filters (Milipore) with a peristaltic pump (Cole-Parmer Instrument Company), Teflon micro-tubing and a Teflon filter holder into acid cleaned 125 mL LDPE bottles. The filtrate was immediately acidified with ultrapure HCl (final concentration 0.05 M with <pH 2.0, Tamapure-AA-10). All samples were held for 3 weeks in a clean room before analysis.

4.3.   Analytical methods

4.3.1. NOBIAS pre-concentration method

The procedure for pre-concentration with the NOBIAS resin (TD and D sea ice samples) is explained in detail in chapter 2. All pre-concentrated samples were analyzed on a GFAAS. After pre-concentration and analysis with GFAAS, ice core sample data was compared to the pre-concentrated DL (Table 2.1, chapter 2). Comparison with the pre-concentrated DL allowed for accurate detection of the lowest concentrations of elements (Fe, Mn or Cd) within a sample. Pre-concentrated ice core sample data that was above the DL was calculated with the concentration factor (range 2.3 - 3.0 times) and presented within this study.

4.3.2. Analysis of salinity, $\delta^{18}O$, and nutrients

For salinity measurements, a portion of the sea ice meltwater was measured for chloride ions using a chloride analyzer (Model SAT-500, Towa Electronic Industry, repeatability: <0.5%). A lab standard regression curve (paired salinity and chloride; AUTOSAL 8400B salinometer, Ocean

Scientific International Ltd.) was used to determine the salinity of the meltwater from the measured chloride values. Oxygen isotopes for sea ice were determined by an isotope water analyzer (Picarro, Inc.) with an analytical precision of ± 0.3%. For the nutrient analysis a portion of sea ice meltwater that was frozen was re-melted at room temperature in an onshore class 100 clean room. Samples were analyzed on a continuous flow system autoanalyzer (QuAArto, BL TEC, Inc.). Standard solutions were made in Milli-Q water to match the low salinity of the sea ice samples.

4.4. Results

4.4.1. Physical and chemical properties in sea ice

Immediately after the ice sample was collected, the sea ice core length was measured to 103 cm and photographed (Fig. 4.3a). The sea ice structure was determined by visual inspection using the terms defined by Petrich and Eicken (2010). Usually thick (5 mm) and thin (0.5 mm) ice sections illuminated by polarized light are used to observe the crystallographic structure (textural variability, boundary layers, etc.; Toyota et al., 2004) of sea ice. These sections are cut with a metal saw, contaminating the ice samples for trace metal analysis. To avoid adding contamination during the ice structure analysis, visual observations, photographic image analysis and porosity % analysis were performed on planed ice samples in this study.

The ice structures of the planed ice core were analyzed in six sections: 0 - 24 cm, 24 - 41 cm, 41 - 58 cm, 58 - 75 cm, 75 - 91 cm and 91 - 103 cm (Fig. 4.3b). Each section was homogenized before separation for salinity, $\delta^{18}O$, nutrients and trace metal analysis. Sections were large to account for the volume necessary for the NOBIAS pre-concentration before trace metal analysis. The 0 - 24 cm section showed snow/slush-like ice that was in the transition of turning more solid. The porosity % (Fig. 4.3c) of this section show 1.9, indicating highly porous ice. A piece of solid ice (below 9 cm; Fig. 4.3b) may represent snow that was melted and re-frozen, hinting at multi-year ice. Sections 24 - 75 cm showed ice with disconnected pore microstructure that was more apparent than in the 0 - 24 cm section. The porosity % for each section (0.7%, 1.3%, and 0.6%, respectively, Fig. 4.3c) were lower than seen from 0 - 24 cm. From 75 - 91 cm the porosity % (0.5) was similar to the 58 - 75 cm section, but lacked obvious pore microstructure. Instead the

structure represented solid ice intermixed with ice that had disconnected pore microstructures. From 91 - 103 cm solid ice (porosity 0.04%) was observed.

Sea ice salinity was observed to be low (1.3 to 2.1, Fig. 4.5a). In first-year ice, typical salinity profiles exhibit a C-type profile (Cox and Weeks, 1988) with salinities around 5 - 15 (Eicken et al., 1995). As sea ice ages and thickens, desalination processes decrease the salinity to below 4 characterizing multi-year ice (Cox and Weeks, 1974; Eicken et al., 1995). Therefore, the observed salinity for this study indicates multi-year ice. It is possible that brine may have been artificially released during the coring process, lowering salinity, nutrient and trace metal concentrations within the ice core sample. After coring an adjacent ice core was tested for salinity. High salinity values would indicate that brine was present in the adjacent sea ice core after coring. If brine was released in the sea ice, before coring, salinity values would be low in the adjacent ice core. The concentrations from the adjacent ice core matched the concentrations within the ice core sample after a 3 year holding period. Therefore, it is unlikely that the brine was artificially released in the sea ice site by coring during sampling. Nutrient concentrations in the ice core were below the DL (0.02 µmol/L NO_3 + NO_2, 0.02 µmol/L PO_4, and 0.1 µmol/L SiO_2). It is possible that the nutrients, along with the salinity, were released from the sea ice during desalination before coring. Measured $\delta^{18}O$ values are shown in Figure 4.5b and were used to identify source water to sea ice. As seawater freezes to form sea ice, it induces the fractionation of oxygen isotopes (Toyota et al., 2004; Ukita et al., 2000). This allows for the comparison of $\delta^{18}O$ with sea ice to determine the water source (freshwater or seawater). During the JIOS cruise, an average surface seawater (<50 m) $\delta^{18}O$ value for the area near the sampling site was observed at -3.38‰ (Yamamoto-Kawai personal comm.). It is possible that sea ice melt, Pacific origin water and river water mixed with the surface seawater, to decrease the $\delta^{18}O$ value (Yamamoto-Kawai et al., 2008). A freshwater sample was collected from snow-like ice observed on the surface of the ice sample. The $\delta^{18}O$ was observed to be -4.1‰ (Surface; Fig. 4.5b), indicating a meteoric snow source. Although there was a strong freshwater influence on the seawater in this study, the seawater $\delta^{18}O$ values was higher than that for the surface snow value allowing for the distinction between freshwater and seawater sources during sea ice formation. The sea ice section from 0 - 24 cm had a $\delta^{18}O$ value of -2.6‰. This section may represent a mixture of both freshwater and

seawater sources. Sea ice sections from 24 - 103 cm had $\delta^{18}O$ values ranging from -1.2 to -0.8‰. This indicates that these sections were sourced from seawater (see discussion). The ice structure was then determined by comparing the $\delta^{18}O$ values with the picture analysis and porosity % analysis from each section. Snow ice was dominate for section 0 - 24 cm, granular ice for section 24 - 75 cm, mixed ice for section 75 - 91 cm and columnar ice for section 91 - 103 cm. The ice structures determined from these analyses will be used for the remainder of this study.

4.4.2. Trace metals

4.4.2.1.   Dissolved metals in sea ice

Sea ice concentrations for DFe ranged from 1.1 to 4.8 nM (Fig. 4.6a). Snow (3.1 nM) and granular ice (3.6 ± 0.8 nM, n = 3) showed higher concentrations when compared to mixed ice (1.1 nM) and columnar ice (1.3 nM). Dissolved Mn in sea ice ranged from 1.4 to 11.0 nM (Fig. 4.6c). The snow and granular ice showed higher concentrations (5.5 nM and 8.5 ± 3.5 nM, respectively) than mixed (1.5 nM) and columnar (1.4 nM) ice. Dissolved Cd in sea ice was low and ranged from <DL to 0.2 nM (Fig. 4.6e). Dissolved Cd was only observed in snow (0.1 nM) and granular (0.1 ± 0.06 nM) ice. Within this sea ice sample the snow and granular ice structures held the highest trace metal concentrations.

4.4.2.2.   Labile particulate metals in sea ice

Concentrations of LP metals seemed to be dependent on the trace metal. Labile particulate Fe in sea ice ranged from 2.2 to 475.6 nM (Fig. 4.6b). The snow (92.3 nM) and granular (232.9 ± 172 nM, n = 3) ice had higher LPFe concentrations when compared to the mixed (7.6 nM) and columnar (2.2 nM) ice. Labile particulate Mn was low in sea ice and ranged from <DL to 0.5 nM (Fig. 4.6d). Labile particulate Mn was detected in snow (0.5 nM), granular (0.1 nM) and mixed (0.08 nM) ice. Labile particulate Cd was also low in sea ice ranging from <DL to 0.08 nM (Fig. 4.6f) and only detected in granular ice (0.03 ± 0.03 nM, n = 3). The LP fraction for trace metals were high in the snow and granular ice structures as observed with the D fraction. For both fractions, concentrations of trace metals were dependent on the metal.

4.5.   Discussion

4.5.1. Sea ice stratigraphy and formation processes

The formation processes are reflected in the ice structures that are created and manifested in distinct vertical sections of an ice core. In the snow ice section, the observed $\delta^{18}O$ showed a mixture of freshwater (meteoric snow) and seawater and freezes (Fig. 4.5b). Snow ice formation may have occurred through a flood-freeze cycle (Ackley et al., 1990). Generally meteoric snow will collect and accumulate onto the surface of sea ice. As more snow is added, the weight can compress sea ice below the water's surface. Snow ice can then form as accumulated meteoric snow mixes with incoming seawater (Fritsen et al., 1998; Hudier et al., 1995). At the bottom part of the snow ice section, slush-like ice was observed (Fig. 4.3b, above 24 cm). Slush ice is created by seawater mixing with snow, further indicating that the flood-freeze cycle process may have occurred.

A large portion of the sea ice sample was composed of granular ice (Fig. 4.3c). Granular ice has two genetic classifications: snow-granular and frazil-granular that can be identified through grain (via thick, 5 mm, or thin, 0.5 mm, sections) and $\delta^{18}O$ analysis (Toyota et al., 2004; Ukita et al., 2000). Since it was not possible to make trace metal clean thick or thin sections for grain analysis to classify ice stratigraphy, $\delta^{18}O$ was used to differentiate between the two genetic classifications. Frazil-granular ice usually has higher $\delta^{18}O$ values (seawater) than observed for snow-granular ice (freshwater). The $\delta^{18}O$ in granular ice for this study yielded high values (-0.8 to -1.1‰) due to isotopic fractionation from a seawater source (Fig. 4.5b; Lange et al., 1990; Toyota et al., 2004; Ukita et al., 2000). Therefore, the granular ice section was composed of frazil ice. The mixed ice section (75 - 91 cm) yielded similar porosity % (0.5) values as observed in the granular ice. The photo analysis of the thick section indicated that this structure was not fully granular ice but a mixture of granular and columnar ice (Fig. 4.3b,c). Mixed ice may be an indication, along with frazil ice, of dynamic growth processes (Toyota et al., 2007). Mixed ice can form during rough currents and high winds which can allow for: 1) the formation of new frazil ice over established/deformed ice regardless of ice texture, 2) the overlapping of ice sheets, and 3) frazil ice formation in between floe gaps caused by rafting/ridging event (Hopkins et al., 1999; Lange and Eicken, 1991; Lange et al., 1989). The observed columnar ice within this sample was

created through the congelation of seawater in calm conditions (Toyota et al., 2004). This is supported by observations of the ice structure from photo analysis (Fig. 4.3b), and low porosity % value (Fig. 4.3c). It should be noted that sea ice within a single ice floe is heterogeneous allowing for the ice stratigraphy within a floe to be variable. The heterogeneity of sea ice may be due to different wind conditions during ice growth (Eicken and Lange, 1989). Therefore, the use of one ice core sample represents only a subset of the trace metal accumulation and release mechanisms that can affect the composition of Arctic sea ice.

4.5.2. Sources and accumulation processes of trace metals into sea ice

Ice structure explains the formation processes utilized by sea ice. Comparing ice structure to trace metal concentrations within a single core sample allows the determination of trace metal sources. In addition, the determination of possible mechanisms behind trace metal accumulation in, and release from, sea ice become clearer. In this study the snow ice showed high concentrations of D for all metals and high concentrations of LP for Fe and Mn (Fig. 4.6). This indicates that one mechanism for trace metal accumulation into sea ice is snow ice formation through the flood-freeze cycle (Ackley et al., 1990).

Polar snow is mostly composed of water (99.99%), with less than 1% composed of particulate dust and sea salt aerosols (Barrie, 1986; Planchon et al., 2004). The amount of contaminates within Arctic snow can fluctuate depending on anthropogenic activities from Eurasia and North America, with higher particulate dust available in winter than in summer (Krachler et al., 2005). Trace metals, bound to particulate dust, are then deposited onto sea ice during snow fall. As snow ice forms, these trace metals can become trapped within the ice crystals. Increases in Arctic temperatures have increased water vapor which, along with increased anthropogenic emission, has yielded higher precipitation in the Arctic Ocean (Tovar-Sanchez et al., 2010). Therefore, the high concentrations of LPFe observed in this study may be due to meteoric snow. Lannuzel et al. (2007) observed that TDFe and DFe in snow were lower than the concentration observed in sea ice from the Antarctic region. This indicates that atmospheric deposition was a minor source of trace metals to the snow ice fraction of sea ice when compared to seawater influences. The range of DFe (3.1 nM, Fig. 4.6a) from snow ice in

this study was comparable to that of Antarctic snow (1.0 - 6.5 nM). Total dissolvable Fe from snow ice in this study (92.3 nM Fig. 4.6b) was observed to be higher than in Antarctic snow (1.8 - 23.7 nM). This indicates that atmospheric deposition may be a source of trace metals to Arctic sea ice. Snow ice from the sub-polar marginal Sea of Okhotsk was also observed as comparable concentrations of DFe (3.7 ± 1.3 nM DFe) with that of snow ice from this study. Although the comparison for the different size fraction of Fe concentrations were variable depending on location, the trace metal trend further supports meteoric snow as a source of trace metals to snow ice. Another possible mechanism for trace metal accumulation from meteoric snow may be the influence of snow meltwater during snow ice formation (Granskog and Kaartokallio, 2004; Marsay et al. 2018). In the current study, results from the $\delta^{18}O$ analysis yielded the snow ice section source water as a mixture of both freshwater and seawater (Fig. 4.5b). Although the percent contribution from the two water sources was not quantified; it is possible that meteoric snow was a source of trace metals to snow ice.

The concentration of trace metals was higher in granular ice than observed in snow ice, indicating another mechanism for trace metal accumulation into Arctic sea ice. As discussed above, the granular ice structure was composed of frazil ice indicating that the high concentrations of LPFe (Fig. 4.6b) can be explained by particle entrainment. In the Arctic Ocean, frazil ice can form in shallow (<50 m) shelf areas (Dethleff et al., 1998; Eicken et al., 2005; Reimnitz et al., 1994). Turbulence in the water column, due to fall storms, can re-suspend shelf sediments and smaller particles in the water column. Frazil ice can interlock with these suspended particles through suspension freezing and rise together to the water surface (Campbell and Collin, 1958; Nürnberg et al., 1994; Osterkamp and Gosink, 1984; Reimnitz et al., 1992). As frazil ice thickens (from slush ice to floe ice), particles are entrained into the granular ice structure (Dethleff, 2005). Ito et al. (2017) used Acoustic Doppler Current Profiler backscatter data to observe the entrainment of sediments by frazil ice. They found that at a wind speed of 15 - 19 m s^{-1} and a current speed of 1.0 - 1.5 m s^{-1} sediments were re-suspended into the water column where they interlocked with the frazil ice. Through this process, trace metal bound sediments and smaller particles are also suspension frozen by frazil ice and finally entrained into granular ice (Hölemann et al., 1997; Ito et al., 2017; Lannuzel et al., 2010, 2017), increasing the concentrations of

sediment/particle associated metals in the sea ice. Lannuzel et al. (2007) reported that the Fe concentrations in sea ice, made from seawater, were also due to sediment entrainment. Sea ice formed in the southeastern Chukchi and western Beaufort shelf areas is characteristically sediment-laden (Eicken et al., 2005). This sea ice can follow the Beaufort Gyre moving westward further into the Arctic Ocean. Sea ice collected for this study may have formed in the shelf areas of the Beaufort Sea. As the sea ice aged and travelled following the Beaufort Gyre flow, trace metals may have been added during ridging events or frazil formation in the leads between floes (Lange et al., 1989; Lange and Eicken, 1991; Toyota et al., 2004). Based on the visual observations of sea ice melt in the lab, sediments were not detected in this sample. Labile particulate Fe showed a trend of higher concentrations in granular ice (232.9 ± 172 nM) when compared to mixed and columnar ice (7.6 nM and 2.2 nM respectively; Fig. 4.6). Particulates derived from fine-grained sediment or organic matter origins (Dethleff, 2005; Kempema et al., 1989; Nürnberg et al., 1994) can be influential to trace metals. Comparing the trace metal concentrations from snow ice to granular ice yields higher concentrations in the granular ice (with the exception of LPMn; Fig. 4.6). In addition, the sea ice sourced from seawater in the current study's ice sample yielded more volume than observed for the snow sourced ice. It is possible that a sediment source from a seawater medium is more influential than from atmospheric deposition (Granskog and Kaartokallio, 2004). Thus, particle scavenging during the dynamic growth processes used to form frazil ice allowed trace metals to entrain and accumulate into the granular structure of sea ice.

The process of trace metal accumulation by particle entrainment is further supported by the concentrations of D and LP Cd observed in granular ice (Fig. 4.6e,f). Cadmium is associated with clay materials (Pardue et al., 1992) and with Fe/Mn oxides in oxic sediments (Guo et al., 1997). As sediments entrain into sea ice, fine silts or clays are effectively retained in the ice crystals (Nürnberg et al., 1994). It is possible that the observed concentrations of Cd in granular ice further indicates the presence of fine particles, possibly sourced from sediments, in this ice structure. Dissolved and LP metal concentrations in granular ice were also observed to be vertically heterogeneous (Fig. 4.6). The dynamic environment where frazil ice forms and its non-uniformity (such as shelf seas), have yielded patchy sediment-laden ice within Arctic sea ice (Eicken et al., 2005; Garrison et al., 1983). Patchy entrainment of sediments into sea ice can then

translate to heterogeneous concentrations of trace metals observed in sea ice (Evans and Nishioka, 2018). Based on the observations from this and previous studies (Campbell and Collin, 1958; Dethleff, 2005; Hölemann et al., 1997; Ito et al., 2017; Lannuzel et al., 2007, 2010, 2017; Nürnberg et al., 1994; Reimnitz et al., 1992), the accumulation of trace metals into granular ice may be due to frazil ice formation and particle entrainment.

4.5.3. Release processes of trace metals from sea ice

Mixed and columnar ice structures in Arctic sea ice yielded trace metal concentrations that were low or below the detection limit (Fig. 4.6). This indicates a trace metal release mechanism resulting from brine drainage. In the early stages of sea ice formation during fall, most of the seawater salts are released from the ice crystal lattice. In sea ice around 0.05 m thickness, bulk salinity is about 25. As sea ice thickens (1.5 m) the percent bulk salinity can decrease to 5 (Kovacs, 1996). The interstitial salts remaining in the sea ice will concentrate into liquid brine (Kingery and Goodnow, 1963; Untersteiner, 1968). Brine drainage occurs when dense brine convects through permeable ice from cold (top of the ice) to warm (bottom of the ice; Jardon et al., 2013) temperatures. As the ice strives for thermodynamic equilibrium, the movement of brine widens brine channels (Petrich and Eicken, 2010) through the ice lattice increasing the potential for fluid percolation. Relating the ability of brine drainage with sea ice structure, the columnar structure maybe more efficient in releasing brine when compared to the granular structure (Lannuzel et al., 2007). Columnar ice structure can form more slowly (approximately factor of 2) than granular ice structure (Eicken and Lange, 1989; Weeks and Ackley, 1986). The formation of different ice structures dictates the orientation of brine channels (Spindler, 1994; Weissenberger et al., 1992). In granular ice the branching of brine channels retains the liquid brine until they widen. In the columnar ice structure brine channels have a laminar orientation (Petrich and Eicken, 2010). This can allow brine to be rejected more efficiently (Janssens et al., 2016; Weissenberger and Grossmann, 1998). In sea ice, nutrients have a decreasing linear trend with bulk salinity (Thomas et al., 2010). Therefore, the presence of brine can be detected by its salinity and nutrient concentrations. In this study, the nutrient concentrations analyzed in sea ice were below the detection limit. This indicates that brine, along

with the trace metals, was released from the sea ice. Brine has been shown to retain high concentrations of trace metals. In the Antarctic region, concentrations of TDFe and DFe from brine sack-holes were two orders of magnitude higher than the surrounding seawater (Lannuzel et al., 2007). When compared to sea ice, brine concentrations of DFe were elevated (van der Merwe et al., 2011). Dissolved trace metals in brine can thus be influenced by brine release, decreasing their concentrations within sea ice (Lannuzel et al., 2007; van der Merwe et al., 2011). In contrast, PFe concentrations in Antarctic brine have been observed to be low. This indicates that PFe may bind to the brine channel walls or organic matter (Lannuzel et al., 2010). A robust community of phytoplankton and bacteria has been observed in the brine channels of the sea ice interior (Ackley et al., 1979; Horner et al., 1992) and at the sea ice-seawater interface (Spindler, 1994). Ice algae and bacteria create exopolymeric (i.e. exopolysaccharides) gel like substances. They are composed of uronic acids and sulphates allowing them to act as organic ligands for both D and LP fractions within sea ice (Krembs et al., 2002; Lannuzel et al., 2015). Trace metals can bind to these ligands, increasing the dissolved concentrations, and bind to brine channels walls (Lannuzel et al., 2007, 2015). Phytoplankton were not observed in this ice sample, but they may have been present in the brine allowing for some of the dissolved metals to bind to the channel walls before collection. Regardless of the sorption properties of brine channel walls, the decreasing trend for the trace metals along the virtual profile of the sea ice sample indicates that the release of liquid brine can drive trace metal concentrations in the mixed and columnar ice structures.

4.5.4. Chemical transformation of trace metals in sea ice

The concentrations of trace metal size fractions were variable within sea ice. For example, high concentrations of LPFe, DMn and DCd were observed in the granular ice structure (Fig. 4.6). The presence of high LPFe in granular ice indicated that suspended particles, possibly from sediments, was a major source of LPFe. During turbulent conditions Fe(III) and Fe(II) are released into the overlying water column as sediments are re-suspended (Lohan and Bruland, 2008). Once in the oxic environment Fe(II) is quickly oxidized (Landing and Bruland, 1987) creating particulate Fe oxides. This reaction was estimated to occur within hours in the bottom waters of the Bering

Sea (Lohan and Bruland, 2008). As water temperatures cool (-1.86°C) and turbulent conditions persist, this newly available pool of Fe oxides along with re-suspended sediments containing Fe can accumulate as a result of suspension freezing by frazil ice (Ito et al., 2017).

Granular ice also showed high concentrations of DFe and low concentrations of LPMn (Fig. 4.6b,c,d). As discussed above, particle entrainment allowed for the accumulation of LPFe into granular ice. Due to their similar behaviors, LPMn concentrations should mimic LPFe, but LPMn concentrations were observed to be low (Fig. 4.6d). Therefore, the resulting high DMn observed in granular ice can be explained by chemical transformation. The concentration of oxygen in sea ice is low, where brine is supersaturated in oxygen (Glud et al., 2002; Rysgaard and Glud, 2004). Oxygen concentrations in sea ice can further decrease due to organic matter decomposition from bacteria (Rysgaard et al., 2008) or from limited access to wind generated waves (Ackley and Sullivan, 1994; Huang et al., 2017). The nutrient concentrations within the sea ice sample were low (<DL), therefore, brine release had a greater influence on the oxygen concentration. As sediments are re-suspended during turbulent conditions, both Fe and Mn oxides are released into the water column. The oxides are then entrained into frazil ice through suspension freezing. Manganese has a higher reduction potential than Fe (Froelich et al., 1979; Hatta et al., 2013) allowing elevated concentrations of DMn to be represented in the ice structure. Sea ice and snow also have the potential to allow for the photochemical transformation of Mn (LPMn to Mn^{2+}) within its matrixes (Granskog and Kaartokallio, 2004). Another indication for the chemical transformation to D metals in sea ice is its effect on DCd concentrations in granular ice (Fig. 4.6e,f). At the sediment-water column interface and in surface sediments, Cd is adsorbed onto the surfaces of Fe and Mn oxides. Therefore, the increase in DCd concentrations observed in this sea ice sample is mainly due to release from Fe and Mn oxides during the reduction process (Yu et al., 2000; Huang et al., 2017). This process can also occur in the suboixc areas of sea ice, making chemical transformations another mechanism that can control the concentrations of DMn and DCd.

4.6. Summary

In the Arctic Ocean, sea ice is an important player in the biogeochemical cycling of trace metals. However, the processes by which trace metals accumulate into sea ice are not well known. Comparing sea ice structure to trace metal concentrations gives a clearer understanding of these processes. To determine the structure of sea ice, photographic images, porosity % and $\delta^{18}O$ analyses were used. The structures observed in sea ice, from top to bottom, are as follows: snow ice, granular ice, mixed ice and columnar ice. Analysis of the sized fractionated (D, and LP) trace metals (Fe, Mn and Cd) showed that their concentrations differed depending on ice structure. The sea ice used in this study had low salinity indicating a multi-year ice sample. In addition, brine was determined to be released from the sea ice as both nutrients and salinity were observed to be low. Low trace metal concentrations in mixed and columnar ice were also determined to be due to the brine release process. The concentration of Fe, Mn and Cd differed among sea ice structures, indicating that accumulation processes for trace metals are reliant on sea ice formation processes. The observed differences within trace metal size fraction concentrations indicated that there are additional controls through external sources: meteoric snow, particle entrainment, and reductive processes.

Figure 4.7a represents a schematic of the possible accumulation and release processes, and Figure 4.7b represents the chemical transformation process observed for Mn oxides in granular ice. As Fe and Mn oxides have similar behaviors, Figure 4.7b will hold true for Fe oxides as well. High concentrations in snow ice indicated that snow ice formation, through the mixing of meteoric snow and seawater, can add atmospheric trace metals. High and heterogeneous concentrations of LPFe in granular ice indicate particle (possible hydroxide and clay particles) entrainment by frazil ice scavenging. During frazil ice formation, sea ice can entrain suspended trace metal bound particles (Fe and Mn) that are reflected in granular ice. Once LPFe and LPMn (oxides) accumulates into sea ice, it can undergo reduction to release DFe, DMn and (adsorbed) DCd in granular ice. This chemical transformation process within sea ice can increase the bioavailability of trace metals. Low trace metal concentrations observed in mixed and columnar ice show that these structures are unable to retain metals following brine drainage. The differences observed in trace metals within sea ice structure show that sea ice formation, chemical reduction, and brine release were the processes behind trace metal accumulation and

65

release in this Arctic sea ice. Although the results from this study are promising, this study was limited to one ice sample. Therefore, future studies should look to validate the trace metal clean sea ice structure analysis by preforming the picture and Porosity % analysis followed by a 5 mm and 1 mm thick section analysis. In addition, more studies are needed to compare a larger array of sized fractionated trace metal concentrations to sea ice structure for a fuller understanding on the mechanisms behind trace metal accumulation in, and release from, sea ice.

4.7. Figures
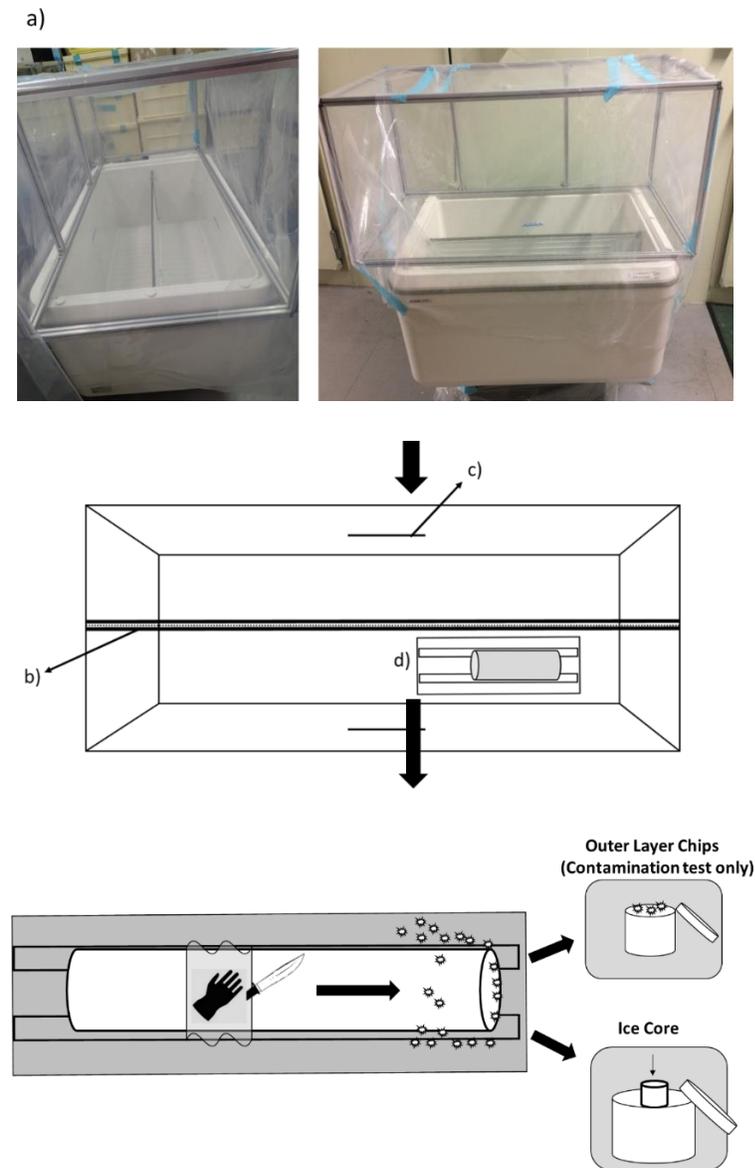
Figure 4.1. Picture and schematic of cold tub used during the ice core planing step. Cold tub was cooled to -20°C by cooling coils located inside the tub's chamber. The temperature inside the chamber remained consistent below a temperature limit line. Above this line the temperatures significantly increased. a) Picture of cold tub, b) cooling coils, c) pre-set temperature limit line, and d) ice planing step.
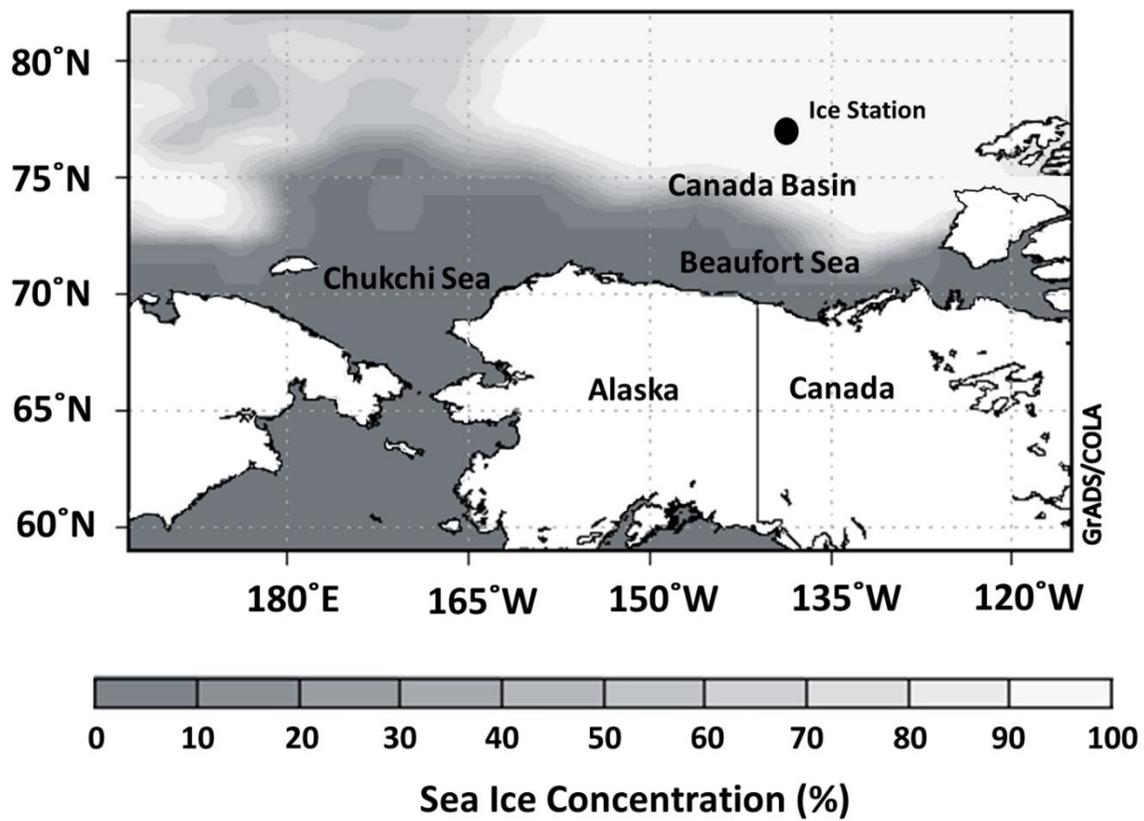
Figure 4.2. Location of sea ice sampling site. Sea ice concentration on August 24, 2013 (24 hr average) from ECMWF metadata. Black dot – Location of the ice station where sea ice was collected.
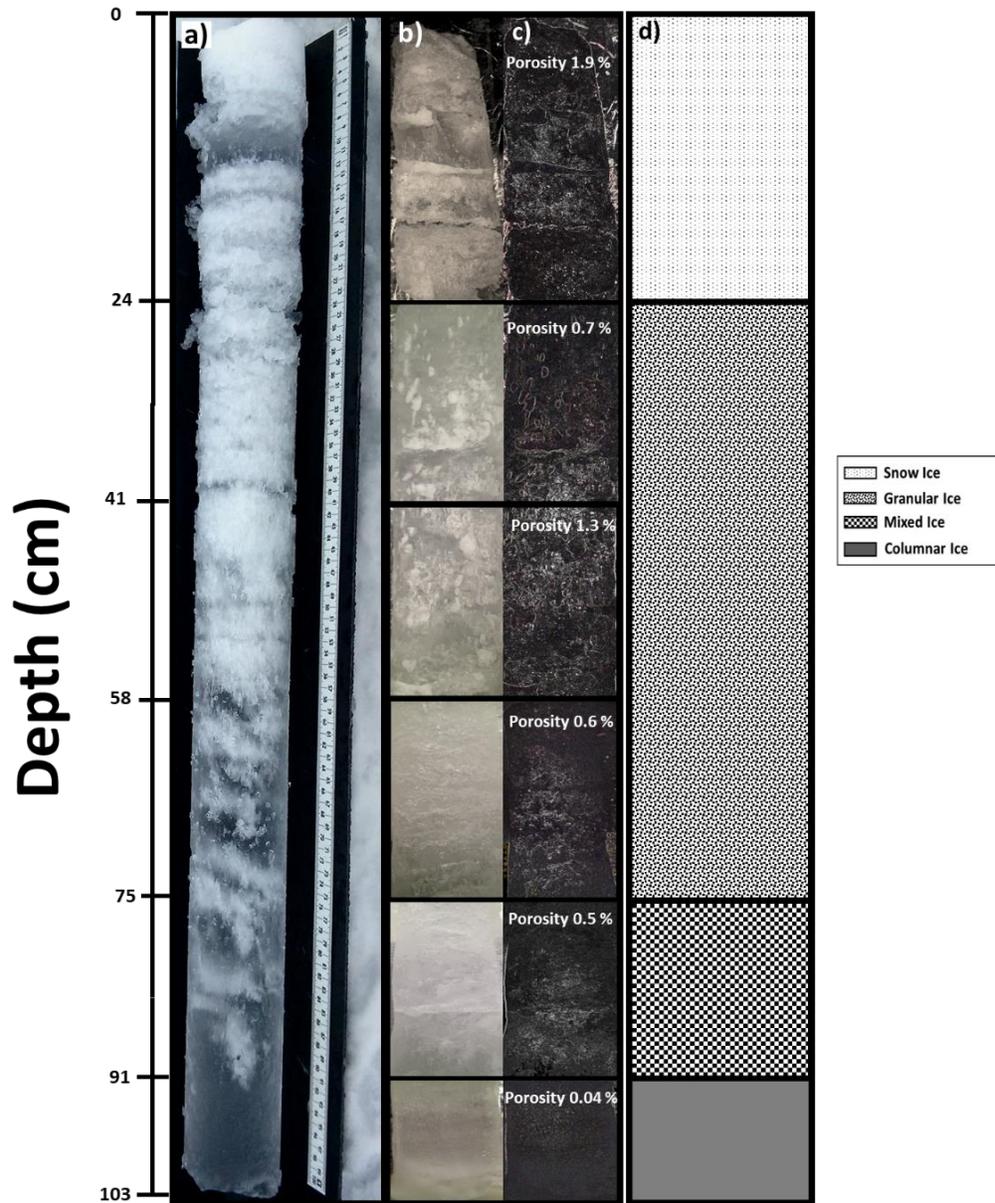
Figure 4.3. Photo and schematic of ice core structure. a) Photo of ice core taken after collection from coring with the depth representing the length of the core, b) photos taken after planing (2 cm), c) transformed planed photo to black and white, with a filter overlaid, to represent the outline of the micropores (porosity %), d) schematic of observed sea ice structure. 0 - 24 cm snow ice, 24 - 75 cm granular ice, 75 - 91 cm mixed ice and 91 - 103 cm columnar ice.
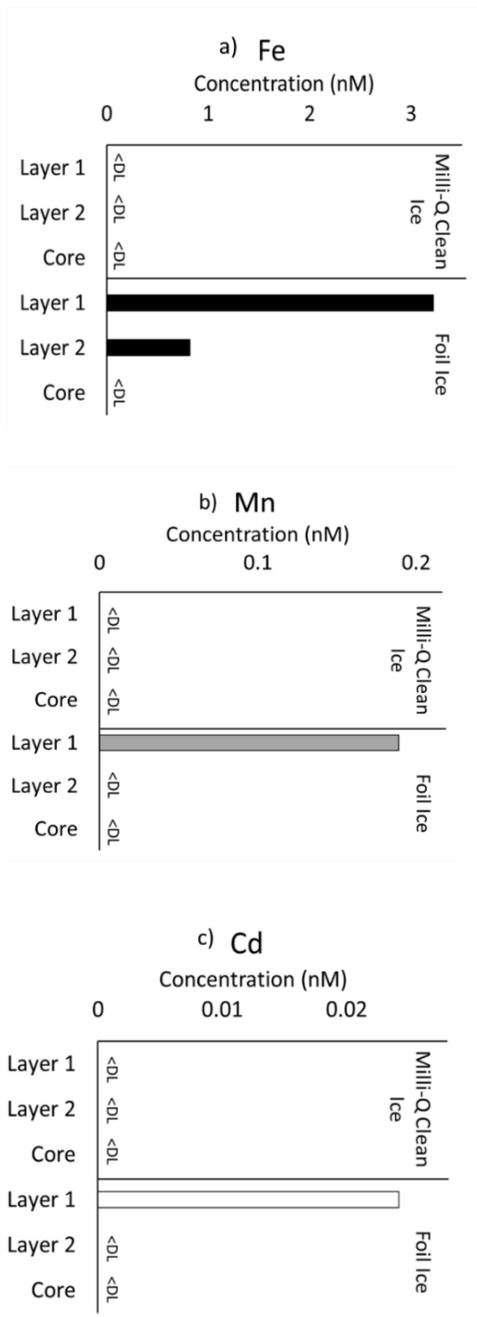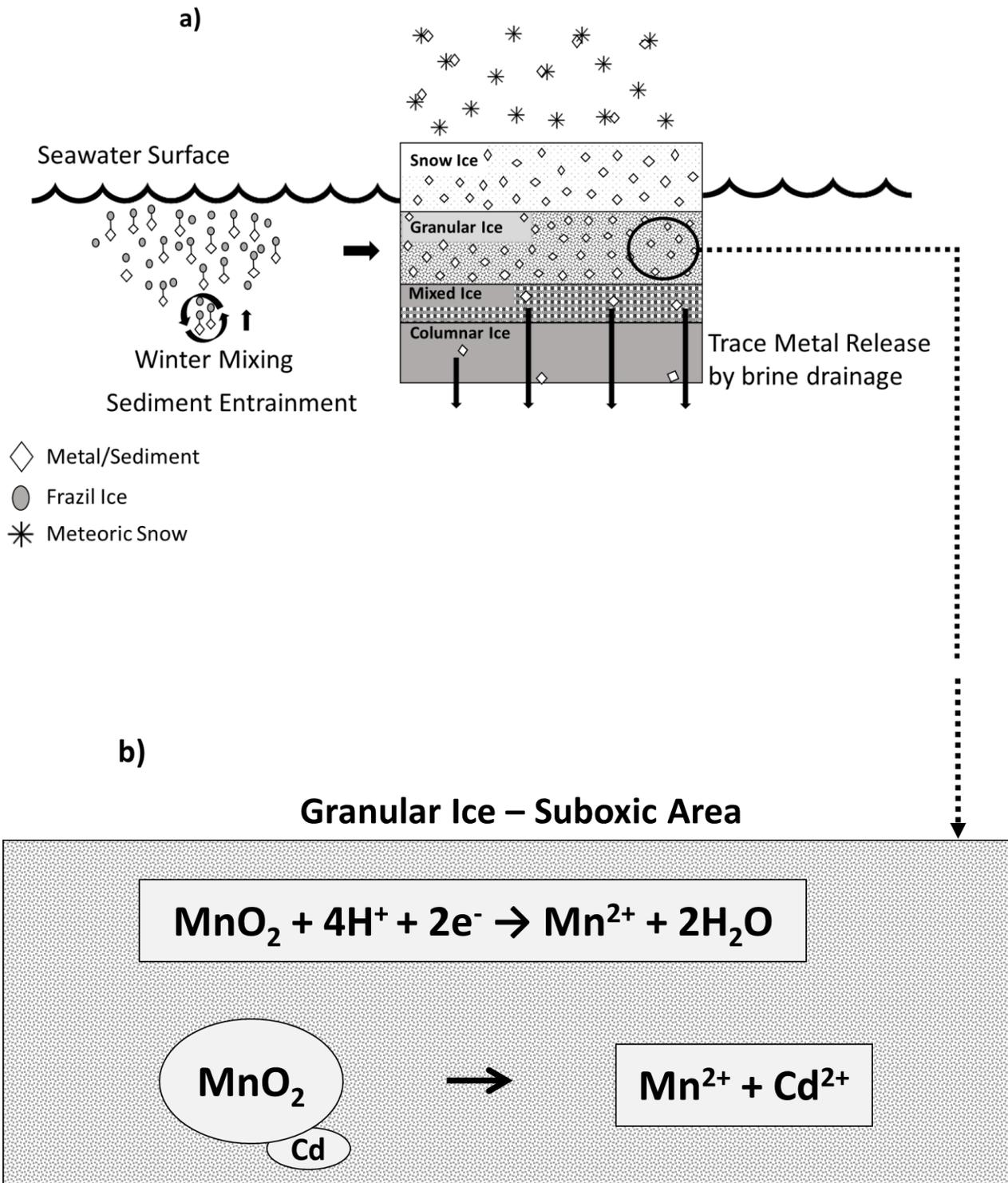
Figure 4.4. Milli-Q Ice Contamination Test. Concentrations of a) Fe, b) Mn, and c) Cd in Milli-Q ice without foil (Milli-Q Clean Ice) and Milli-Q ice wrapped in aluminum foil (Foil Ice). Samples were planed up to 2 cm and each layer (Layer 1 – Outer 1 cm of ice, Layer 2 – Inner 1 cm of Ice, Core – Cleaned ice) was pre-concentrated with the NOBIAS resin. Presented values were above the pre-concentrated DL and then calculated with the pre-concentration factor (4.5 - 8.6 times). The pre-concentration factor was determined by the sample weights before pre-concentration and the eluent weights after pre-concentration.
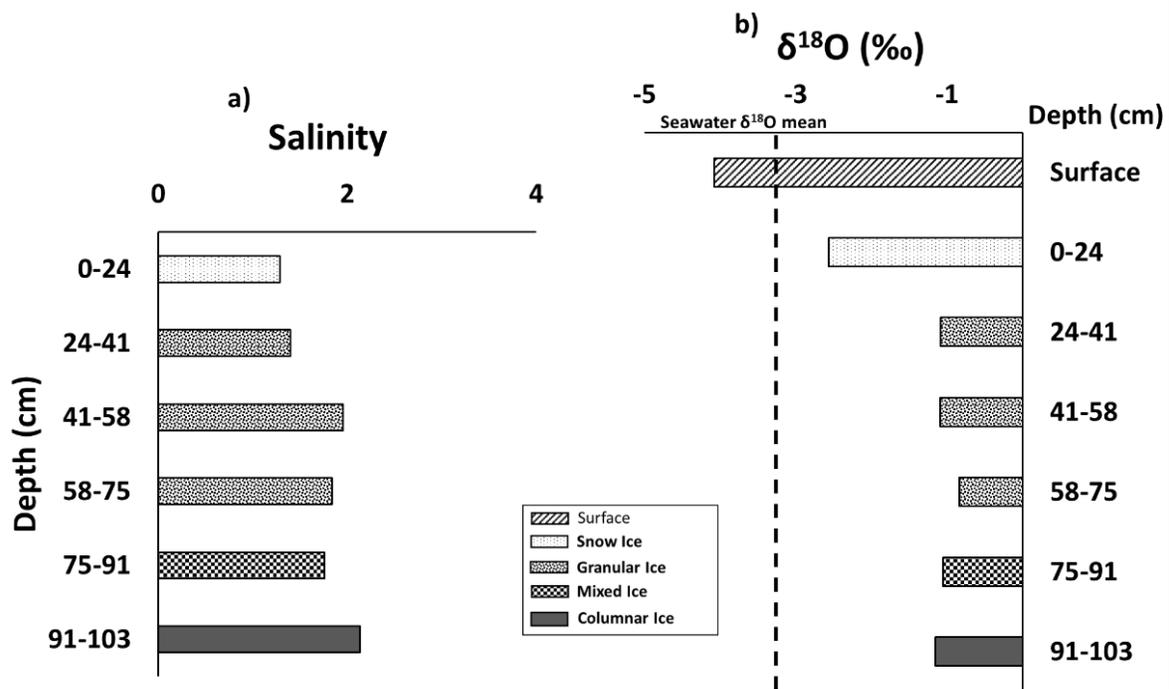
Figure 4.5. Salinity and $\delta^{18}O$ for each ice structure. a) Salinity, b) $\delta^{18}O$, dotted line represents $\delta^{18}O$ values from the surrounding surface seawater (<50 m; Yamamoto-Kawaii personal comm.).
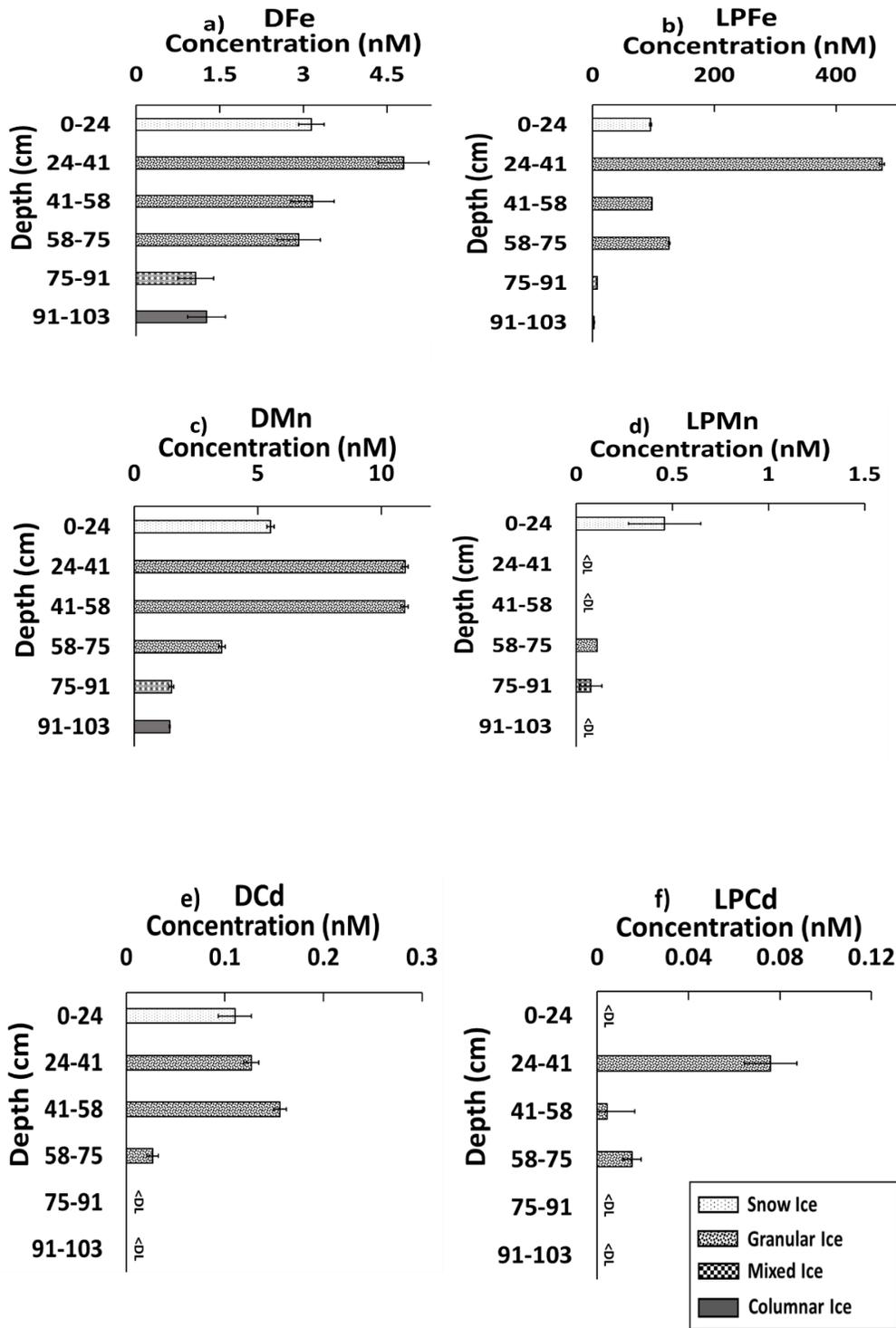
Figure 4.6. Concentrations of dissolved and labile particulate metals for snow ice, granular ice, mixed ice and columnar ice. The ice core depth is represented on the y-axis. Error bars are SD from GFAAS measurement data. a) DFe, b) LPFe, c) DMn, d) LPMn, e) DCd, f) LPCd.

a)

Seawater Surface

Winter Mixing

Sediment Entrainment

◇ Metal/Sediment
● Frazil Ice
✳ Meteoric Snow

Snow Ice

Granular Ice

Mixed Ice

Columnar Ice

Trace Metal Release
by brine drainage

b)

Granular Ice – Suboxic Area

$$MnO_2 + 4H^+ + 2e^- \rightarrow Mn^{2+} + 2H_2O$$

MnO_2
Cd

$\rightarrow$

$Mn^{2+} + Cd^{2+}$

Figure 4.7. a) Schematic of trace metal accumulation and release processes in multi-year Arctic sea ice, and b) schematic of chemical reduction process for multi-year Arctic sea ice.

Chapter 5

Overall conclusions

5.1   Summarized conclusions of each chapter

The increase in Arctic temperatures has resulted in the decrease of summer, multi-year, Arctic sea ice. The decreased presence of sea ice may adversely affect the cycling and biogeochemistry of trace metals in the Arctic Ocean. To gain better insights on the relationship between sea ice and trace metals; we must understand how sea ice acquire and retains trace metals. Therefore, the goal of this study was to investigate the mechanisms behind trace metal accumulation into, and release from, Arctic sea ice.

The concentrations of dissolved (D) and labile particulate (LP) Fe, Mn and Cd were observed in Arctic sea ice (drifting and interior floe ice) and seawater. The differences in geochemical behavior among Fe, Mn and Cd will allow for a better understanding of how sea ice acquire trace metals. All samples were prepared, in a class 100 clean room, by a trace metal clean pre-concentration method utilizing the NOBIAS PA-1 chelating resin (NOBIAS, chapter 2). This ensured that trace metal concentrations at low levels in sea ice or seawater samples were elevated to detectable levels when analyzed on a Graphite Furnace Atomic Absorption Spectrometer (GFAAS). The pre-concentration step before analysis also prevented analytical interferences from the salts that may have been present in the sea ice or seawater matrices. Dissolved Fe in Chukchi seawater was analyzed by two different methods: flow injection method and the NOBIAS pre-concentration method (Chapter 3). Comparisons of the two methods, with the same samples, showed that analysis with the NOBIAS pre-concentration method was 1.3 ± 0.4 times higher than the flow injection method due to a longer sampling storage time. Although the two methods were different, they were oceanographically correct and represent the chemically-labile dissolvable fraction of DFe in seawater. In addition, the comparison of these two methods further supports the accuracy of the NOBIAS pre-concentration method.

Trace metals in Chukchi seawater were supplied through internal and external sources (chapter 3). Cadmium had an internal source though the biogeochemical cycling of phosphate. Labile particulate Fe and LPMn were externally sourced through sediments (shelf or river). Dissolved Fe and DMn had a separate external source via the Alaskan Coastal Current. In seawater, DMn concentrations were higher than DFe. This may have been a result of reduction processes within the sediments followed by supply to the water column. Manganese oxidizes slower than Fe, allowing for DMn to have a longer residence time in the water column. In Chukchi Sea drifting ice, both the D and LP trace metal concentrations were heterogeneous. The LP fraction for all observed trace metals was high. The low trace metal concentrations in the D fraction resulted from brine release or wave propagation. Therefore, drifting ice had a preference to accumulate or retain the LP trace metal fraction. To understand how trace metals accumulate into sea ice, D and LP Fe, Mn and Cd were observed in relation to the sea ice structure of individual interior floe ice samples.

Multi-year sea ice was collected from the interior of an ice floe from the Canada Basin (chapter 4). Sea ice samples yielded low salinity and nutrients indicating multi-year ice and a release of brine. Sea ice was measured to 103 cm upon collection. In order to make a trace metal clean analysis of the sea ice structure, a combination of picture analysis (taken after ice planing (2 cm)), % micropore analysis (porosity %; calculation of the % white area of a black and white photo that was overlaid with a filter by R software) and $\delta^{18}O$ were utilized. Sea ice structure was determined to be snow, granular, mixed (granular + columnar) and columnar ice. Based on high D and LP concentrations in snow ice, trace metal accumulation occurred during snow ice formation. High LPFe concentrations in granular ice indicated trace metal accumulation occurred during suspension freezing by forming frazil ice followed be entrainment during granular ice formation. Chemical transformation process increased D metal concentrations. High DMn and DCd in snow ice was due to photochemical reduction. In granular ice, the high concentrations of DMn and DCd were due to the reduction of Fe and Mn oxides after entrainment. The low concentrations observed in mixed and columnar ice structures were due to brine release.

The two different sea ice forms, degraded drifting and floe ice collected from the interior of the ice zone, used for the observation of trace metals in this study expressed different trends

in the concentrations of D and LP trace metals. It is possible that the environment surrounding the sea ice may influence trace metal concentrations in sea ice. If this is correct, then it is important to understand the conditions of sea ice and its surrounding area, to clearly elucidate the trace metal accumulation mechanisms.

5.2   Retention of trace metals in drifting ice vs sea ice from the interior of an ice floe

In the Arctic Ocean, drifting ice and sea ice from the interior of the ice zone (floe ice) exhibit different physical characteristics. For example, the age and ice structure were identified for the ice floe sample. This was not possible with the drifting ice samples as they were more degraded. Drifting ice was highly influenced by seawater waves, which can give the ice oxic conditions and allow it to be more mobile than floe ice. Whereas, floe ice was more stable, had limited interactions with seawater waves creating a more suboxic environment (Table 5.1). It is possible that physical and environmental differences between the two ice forms observe in this study can influence the internal concentrations of trace metals. Therefore, the concentrations of D and LP Fe, Mn and Cd were compared between the drifting and interior floe ice. For the D metal concentrations, significant differences were not observed between drifting and floe ice (Fig. 5.1). It is possible that brine drainage maybe a driving factor for the release of D trace metal concentrations, especially in floe ice. In contrast, drift ice is heavily influenced by constant wave flushing. Thus, wave propagation may have also released D metals from the drifting ice. Floe ice is protected from wave influence as drifting ice or the outside edge of the floe dampens wave energy (Ackley and Sullivan, 1994). This can restrict oxic seawater (waves)-sea ice interactions to the interior of the ice floe. Restricted seawater interaction and the process of brine drainage can create suboxic areas in sea ice (Glud et al., 2002). Within these areas the reduction of accumulated metal oxides increases the concentration of bioavailable D metals, even after brine has been released, over time. In addition, accumulated LP metals in snow ice can be reduced through photochemical reduction (Granskog and Kaartokallio, 2004). Adding to the overall concentrations of D metals in floe ice over time. Whereas, the consistent influence of waves on drifting ice can force the more immediate release of D metals from the drifting ice. Leaving the

LP fraction of metals to be retained in the sea ice until release during the advanced melting stage (van der Merwe et al., 2011).

Comparing the concentrations of LP metals in the two ice forms showed that drifting ice held elevated concentration for all three LP metals compared to floe ice (Fig. 5.2). This was a result of LP metal addition by seawater waves to drifting ice. As current and wind speeds increase at the seawater surface, Langmuir circulation allows for disturbed bottom sediments and particles to vertically rise towards the water surface (Dethleff et al., 2009). Vertical mixing allows the particles to remain in the water column and, through wave propagation, can introduce LP trace metals into the drifting ice. This was observed in Arctic slush ice where sediment concentrations were similar to those in the surrounding seawater (Kempema et al., 1989). Although floe ice held lower concentrations of LP metals, high concentrations of LPFe was observed (snow and granular ice structures). The mechanisms for the elevated LPFe concentrations in sea ice from this study was 1) snow ice formation and 2) particle scavenging in floe ice, and 3) wave filtration that can supply LP fraction of all metals in drifting ice. Both LPMn and LPCd concentrations were low in floe ice. This was driven by chemical transformation (reduction) in the snow and granular ice structures.

5.3   Biogeochemical cycling of trace metals by sea ice

This study was able to determine that the accumulation of trace metals into sea ice, and the release or supply of trace metals to surface waters was dependent on the form of sea ice. Comparing the trace metal concentrations, along with the observed accumulation or release mechanisms, among the two ice forms (Table 5.2) showed that brine drainage is a mechanism for trace metal release. As sea ice initially forms frazil ice crystals, suspension freezing of suspended particles from the water column occurs. As sea ice thickens, forming a granular ice structure, the release of brine decreases the oxygen concentrations in the formed floe ice. This can initiate the reduction of entrained Fe and Mn oxides, increasing the concentrations of D metals over time. Further thickening of sea ice forms mixed and columnar ice structures. Where, due in part to the slow formation process and the brine channel structure (increased permeability leading to brine drainage, further widening the brine channels), trace metals (D or LP) are not

retained. Above the granular ice, atmospheric derived LP metals will accumulate via snow ice formation. As the snow ice absorbs UV-light, accumulated LPMn can be reduced, increasing DMn and DCd (as it is released from the oxide) over time. Since wave action on floe ice is restricted, floe ice can be stable. This gives floe ice the ability to be a long-term local storage and/or source of D and LP metals. When the floe ice deforms, constant wave action can flush out the D metals from the ice and add LP metals that are available in the surface waters. The continual flushing of seawater introduces oxygen into the ice matrix, eliminating the chance for D metals to increase through oxide reduction. The retention of LP metals and the high mobility of the more deformed drifting ice can allow it to be a long-range transporter of LP metals (Fig. 5.3). Drifting ice can travel further into the Arctic where it will melt during the spring season in trace metal limited surface waters. As LP metals are released, they may become bioavailable to phytoplankton (Hurst and Bruland, 2007; Hurst et al., 2010; Kanna and Nishioka, 2016). Thus, the transport of potentially bioavailable LP metals by drifting ice may increase productivity in the Arctic Ocean. It is unclear if a shift from a multi-year to a first-year ice summer sea ice environment will hinder the supply of bioavailable trace metals in the Arctic Ocean. If climate change eliminates the presence of Arctic summer sea ice, the supply of trace metals to surface seawaters will come from external sources (shelf sediments, rivers, glacier melt). These sources do not have the ability of winter storage, which can affect primary productivity, especially during the spring season (Lannuzel et al., 2016). The role in the remineralization of trace metals by animals that rely of the sea ice habitats will also be affected (Tovar-Sanchez et al., 2007; Lannuzel et al., 2016). Therefore, more studies are needed to understand the affects the loss of sea ice will have on the biogeochemical cycling of trace metals in the Arctic Ocean.

One of the major limitations of this study is the low number of samples for each chapter. More study is needed using samples from: 1) different sampling locations and 2) different seasons. Different sampling locations should include different areas of the Arctic Ocean and different locations within a single ice floe. Observing samples collected in different seasons may show different processes that occur in sea ice. This may hold true for the mixed and columnar ice structures. In winter the sea ice temperature will be lower, restricting brine drainage. It is possible that this in turn will affect trace metal concentrations. During brine drainage, brine will exchange

with underlying seawater within the brine channels which can supply trace metals. This study, using samples collected in the summer, did not observe upward flooding of seawater. In addition, different forms of ice should be observed for trace metal concentrations. Ridging or rafting, that occurs when seawater has rough conditions, may influence trace metal concentrations but these processes were not observed in this study. Decaying ice at different stages can also reflect differences in trace metal concentrations that will aid in the understanding of accumulation or release mechanisms.

5.4 Future Directions

From this thesis study, some of the available trace metal accumulation and release processes were determined within drifting ice, collected from the marginal ice zone located in a shallow shelf area, and a single ice core sample, collected from the interior of the ice zone in an ice floe. In order to directly observe these processes that are utilized by sea ice, a trace metal clean tank experiment should be performed. Tank experiments can allow for processes to be observed under a controlled environment. In previous studies, ice formation (frazil, grease, pancake, etc.; Martin and Kauffman, 1981, Wadhams et al., 1988; Newyear and Martin, 1997; Weissenberger and Grossmann, 1998; de la Rosa and Maus, 2012; Toyota and Koda, 2016), scavenging followed by entrainment (Reimnitz et al., 1993; Smedsrud, 2001), gas exchange (Tison et al., 2002; Nomura et al., 2006) organic and inorganic nutrient accumulation (Giannelli et al., 2001; Janssens et al., 2016) processes has been observed. As trace metal clean conditions have become more prevalent in sea ice studies, tank experiments for trace metal (i.e. Fe) incorporation (Janssens et al., 2018) have become necessary.

A tank experiment observing the accumulation process, particle scavenging for granular ice, and the release process, brine drainage for columnar ice, should be performed. Toyota and Koda (2016) were able to successfully create granular and columnar ice structures in order to observe ice production rates under turbulent and calm conditions. Janssens et al. (2018) was able to observe that growing columnar ice preferentially accumulated biogenic PFe (from sea ice algae) when compared to lithogenic PFe (from dust). This points to the importance of sea ice algae for the retention of trace metals within the ice matrix. Based on the results of this thesis study,

granular ice held higher concentrations of trace metals (either biogenic or inorganic) than columnar ice. The high concentrations were due to particle scavenging by forming frazil crystals. As columnar ice forms, brine drainage occurs. Since trace metals were released with the brine, it is possible that forming columnar ice will not retain the amount of available trace metals when compared to granular ice. The use of tank experiment will allow for the observation of sized fraction (D, TD, LP, etc.) trace metals (biogenic or inorganic) accumulation and/or release as granular or columnar ice forms.

In chapter 4, the objective determination of sea ice structure used a combination of picture analysis, Porosity % analysis and $\delta^{18}O$ analysis. Although this analysis is novel, it allows for trace metal clean processes to be observed. To validate this process, a second study is needed. Sea ice is highly heterogenous. To avoid any difference due to this a single core should be collected from the interior of the ice zone. To determine sea ice structure, the core will first follow the methods detailed in Ch. 4, planed up to 2 cm and photographed. Then the planed core will follow the methods outlined in Toyota et al. (2004) where a 5 mm to 1 mm thick section is cut. The cut sections will be placed on polarized light or observe the crystallographic structure. The remaining core will be cute into sections based on the observed ice structure and the $\delta^{18}O$ will be analyzed. This study should be performed on multiple cores collected from different sites. This will ensure and/or validate that the methods suggested in Ch. 4 will work on sea ice with different ice structures.

5.5　Figures
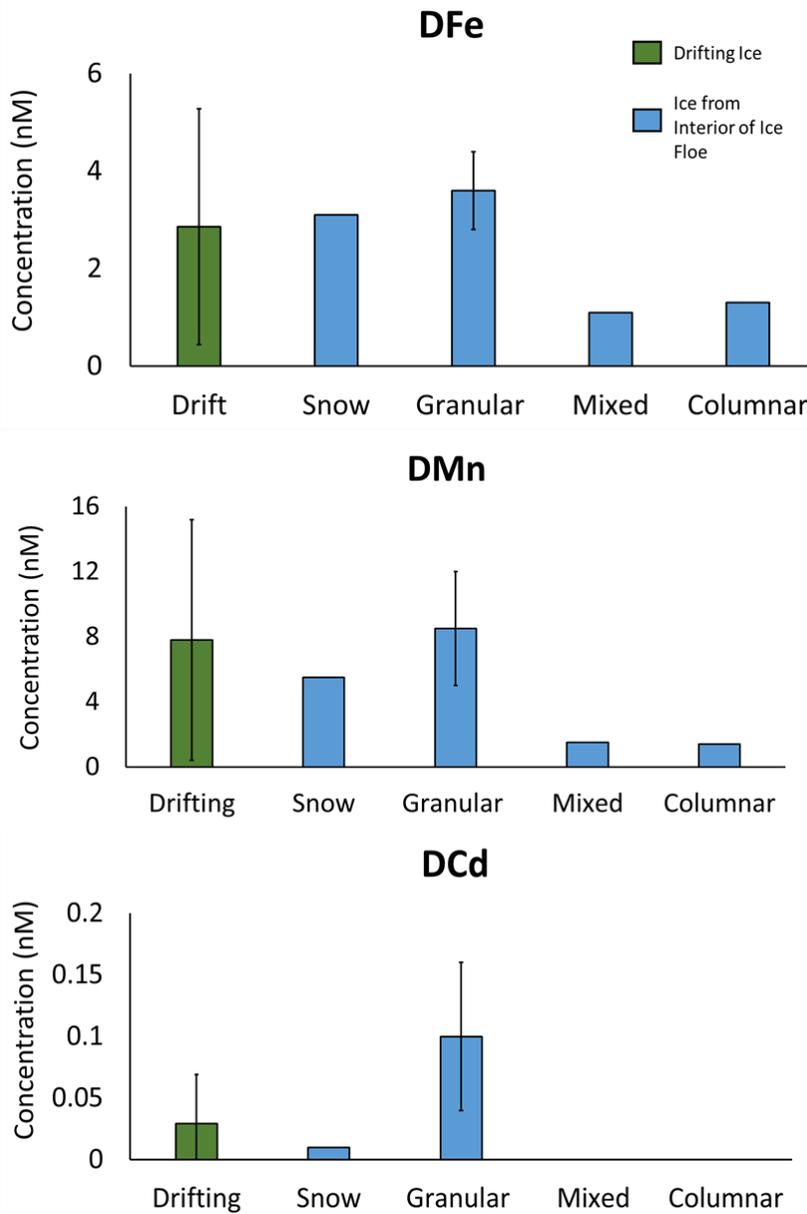
Figure 5.1. Trace metal concentrations of dissolved Fe, Mn and Cd in drifting ice from the Chukchi Sea (in green) and sea ice from the interior of an ice floe in the Canada Basin (in blue). Trace metal concentrations from the inner floe ice samples are represented by the determined sea ice structure and compared to the drifting ice. Error bars are representative of the standard divination.
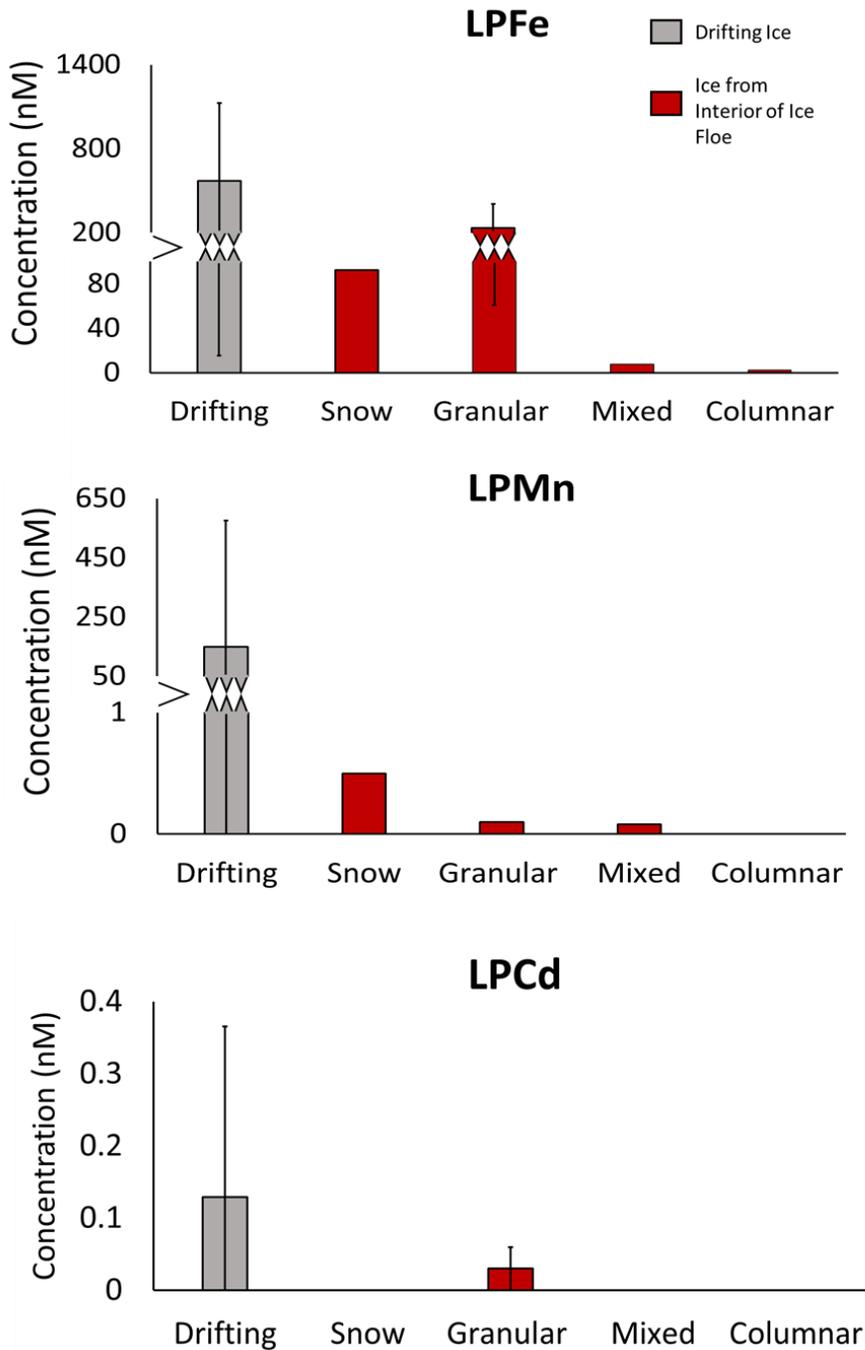
Figure 5.2. Trace metal concentrations of labile particulate Fe, Mn and Cd in drifting ice from the Chukchi Sea (in grey) and sea ice from the interior of an ice floe in the Canada Basin (in red). Trace metal concentrations from the inner floe ice samples are represented by the determined sea ice structure and compared to the drifting ice. Error bars are representative of the standard divination.
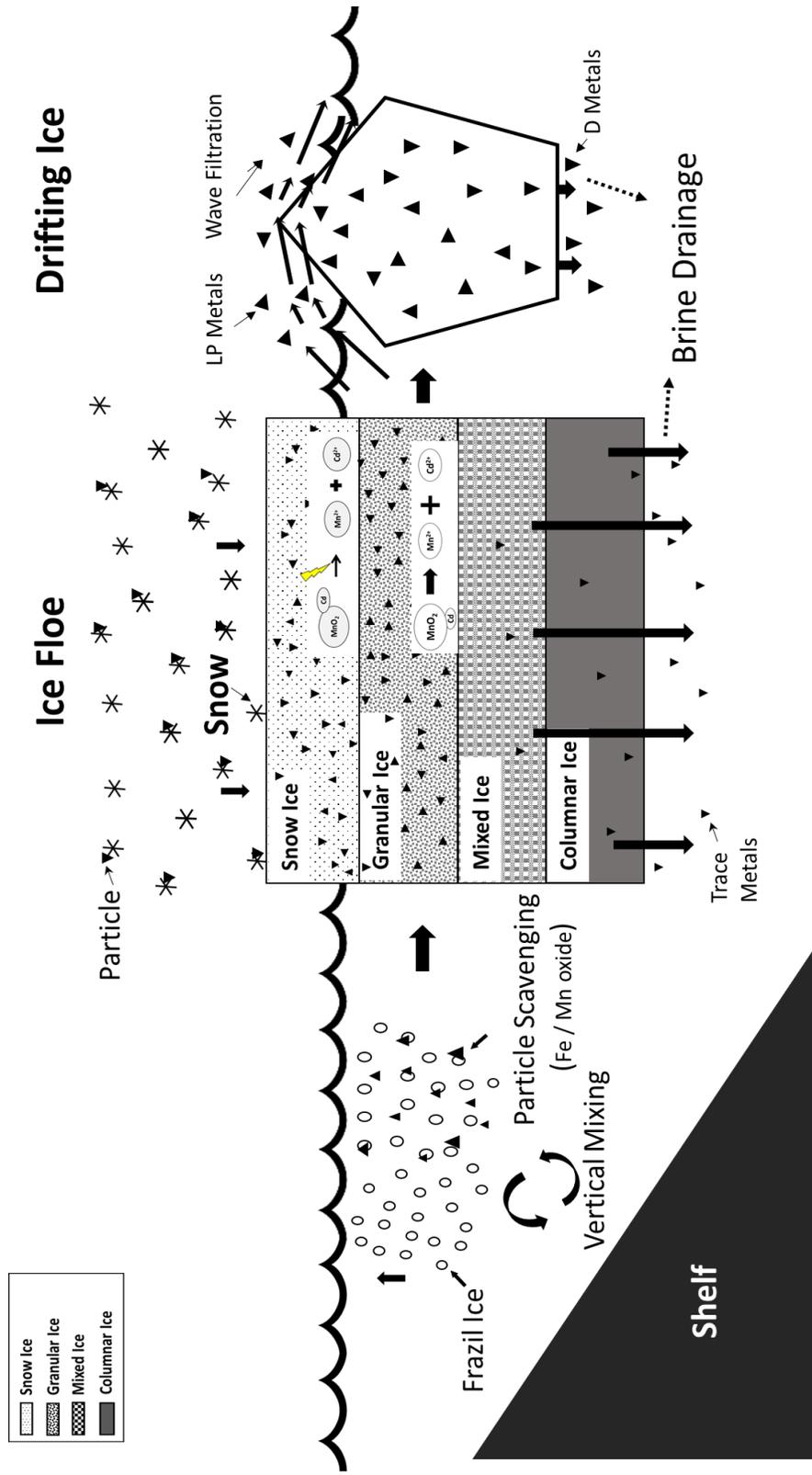
Figure 5.3. Schematic of trace metal accumulation, chemical transformation and release processes in drift ice from the shelf area and interior floe ice from the basin area. Sea ice structure of interior floe ice are represented in the schematic.

Table 5.1. Comparison of the physical characteristics between drifting ice from the Chukchi Sea and sea ice from the interior of an ice floe in the Canada Basin.

Sea Ice Form	Age of Ice	Ice Structure	Ice Condition	Mobility	Wave Influence	Oxic Condition
Drifting Ice	-	-	Permeable	High	High	High
Floe Ice	Multi-Year	Identifiable	Variable	Stable	Low to none	Low

Table 5.2. Comparison of the observed accumulation or release process between drifting ice from the Chukchi Sea and sea ice from the interior of an ice floe in the Canada Basin.

Sea Ice Form	Brine Drainage	Particle Scavenging by Frazil	Wave Filtration	High LPFe	Chemical Transformation (Reduction)	Differences within Ice Structure	Snow Ice
Drifting Ice	O	-	O	O	-	-	-
Floe Ice	O	O	-	O	O	O	O

References

Aagaard, K., Carmack, E.C., 1989. The role of sea ice and other fresh water in the Arctic circulation. J. Geophys. Res. 94, 14,485-14,498.

Ackley, S.F., Dieckmann, G., Shen, H., 1987. Algal and foram incorporation into new sea ice. Eos 68, 1736.

Ackley, S.F., Buck, K.R., Taguchi, S., 1979. Standing crop of algae in the sea ice of the Weddell Sea region. Deep-Sea Res. 26A, 269-281.

Ackley, S.F., Lange, M., Wadhams, P., 1990. Snow cover effects on Antarctic Sea ice thickness. in: Sea ice properties and processes, S. F. Ackley and W. F. Weeks, (Eds), CRREL Monograph 90-1,300 pp.

Ackley, S.F., Sullivan, C.W., 1994. Physical controls on the development and characteristics of Antarctic sea ice biological communities-a review and synthesis. Deep-Sea Res. I 41, 1583-1604.

Aguilar-Islas, A.M., Hurst, M.P., Buck, K.N., Sohst, B., Smith, J.G., Lohan, M.C., Bruland, K.W., 2007. Micro-and macronutrients in the southeastern Bering Sea: Insight into iron-replete and iron-depleted regimes. Prog. Oceanogr. 73, 99-126.

Aguilar-Islas, A.M., Rember, R.D., Mordy, C.W., Wu, J., 2008. Sea ice-derived dissolved iron and its potential influence on the spring algal bloom in the Bering Sea. Geophys. Res. Lett. 35, L24601, doi: 10.1029/2008GL035736.

Balistrieri, L.S., Murray, J.W., Paul, B., 1992. The cycling of iron and manganese in the water column of Lake Sammamish, Washington. Limn. Oceanogr. 37, 510-528.

Barrie, L.A., 1986. Arctic air pollution: An overview of current knowledge. Atmos. Environ. (1967) 20, 643-663, https://doi.org/10.1016/0004-6981(86)90180-0.

Boyle, E.A., Huested, S.S., Jones, S.P., 1981. On the distribution of copper, nickel, and cadmium in the surface waters of the North Atlantic and North Pacific Ocean. J. Geophys. Res. 86, 8048-8066.

Boyle, E.A., Sclater, F.R., Edmond, J.M., 1976. On the marine geochemistry of cadmium. Nature 263, 42-44.

Bruland, K.W., Knauer, G.A., Martin, J.H., 1978. Cadmium in northeast Pacific waters. Limnol. Oceanogr. 23, 618-625.

Bruland, K.W., Orians, K.J., Cowen, J.P., 1994. Reactive trace metals in the stratified central North Pacific. Geochim. Cosmochim. Acta 58, 3171-3182.

Bruland, K.W., Rue, E.L., 2001. Analytical methods for the determination of concentrations and speciation of iron, in: Hunter, K.A., Turner, D.R. (Eds.), The biogeochemistry of iron in seawater. Wiley and Sons Inc., Baffins Lane pp. 256-289.

Campbell, N.J., Collin, A.E., 1958. The discoloration of Foxe Basin ice. J. Fish. Res. Board Can. 15, 1175-1188.

Cid, A.P., Nakatsuka, S., Sohrin, Y., 2012. Stoichiometry among bioactive trace metals in the Chukchi and Beaufort Seas. J. Oceanogr. 68, 985-1001.

Cid, A.P., Urushihara, S., Minami, T., Norisuye, K., Sohrin, Y., 2011. Stoichiometry among bioactive trace metals in seawater on the Bering Sea shelf. J. Oceanogr. 67, 747-764.

Coachman, L.K., Aagaard, K., Tripp, R.B., 1975. Bering Strait: The Regional Physical Oceanography, Univ. of Wash. Press, Seattle.

Comiso, J. C., Meier, W.N., Gersten, R., 2017. Variability and trends in the Arctic Sea ice cover: Results from different techniques. J. Geophys. Res. Oceans 122, 6883–6900, https://doi.org/10.1002/2017JC012768.

Comiso, J.C., Parkinson, C.L., Gersten, R., Stock, L., 2008. Accelerated decline in the Arctic sea ice cover. Geophys. Res. Lett. 35, L01703, doi:10.1029/2007GL031972.

Cooper, L.W., Whitledge, T.E., Grebmeier, J.M., Weingartner, T., 1997. The nutrient, salinity, and stable oxygen isotope composition of Bering and Chukchi Seas waters in and near the Bering Strait, J. Geophys. Res. 102, 12563-12573.

Cox, G.F.N., Weeks, W.F., 1974. Salinity variations in sea ice. J. Glaciol. 13, 109–120.

Cox, G.F.N, Weeks. W.F., 1988. Numerical simulations of the profile properties of undeformed first-year sea ice during the growth season. J. Geophys. Res. 93, 12,449–12,460.

Cullen, J.T., Lane, T.W., Morel, F.M.M., Sherrell, R.M., 1999. Modulation of cadmium uptake in phytoplankton by seawater CO2 concentration. Nature 402, 165-167.

de Baar, H.J.W., Boyd, P.W., Coale, K.H., Landry, M.R., Tsuda, A., Assmy, P., Bakker, D.C.E., Bozec, Y., Barber, R.T., Brzezinski, M.A., Buesseler, K.O., Boyé, M., Croot, P.L., Gervais, F., Gorbunov, M.Y., Harrison, P.J., Hiscock, W.T., Laan, P., Lancelot, C., Law, C.S., Levasseur, M., Marchetti, A., Millero, F.J., Nishioka, J., Nojiri, Y., van Oijen, T., Riebesell, U., Rijkenberg, M.J.A., Saito, H., Takeda, S., Timmermans, K.R., Veldhuis, M.J.W., Waite, A.M., Wong, C-S., 2005. Synthesis of iron fertilization experiments: From the Iron Age in the Age of Enlightenment. J. Geophys. Res. 110, C09S16, doi:10.1029/2004JC002601.

de Baar, H.J.W., Saager, P.M., Nolting R.F., van der Meer, J., 1994. Cadmium versus phosphate in the world ocean. Mar. Chem. 46, 261-281.

de la Rosa, S., Maus, S., 2012. Laboratory study of frazil ice accumulation under wave conditions. The Cryosphere 6, 173-191.

Dethleff, D., 2005. Entrainment and export of Laptev Sea ice sediments, Siberian Arctic. J. Geophys. Res. 110, https://doi.org/10.1029/2004JC002740.

Dethleff, D, Kempema, E.W., Koch, R., Chubarenko, I., 2009. On the helical flow of Langmuir circulation – Approaching the process of suspension freezing. Cold Reg. Sci. Technol. 56, 50-57.

Dethleff, D., Loewe, P., Kleine, E., 1998. The Laptev Sea flaw lead-detailed investigation on ice formation and export during 1991/92 winter season. Cold Reg. Sci. Technol. 27, 225-243.

Deutsch, C., Gruber, N., Key, R.M., Sarmiento J.L., 2001. Denitrification and N2 fixation in the Pacific Ocean. Global Biogeochem. Cycles 15, 483-506.

Dieckmann, G.S., Hellmer, H.H., 2010. The Importance of Sea Ice: An Overview, in: T. D., G.S., (Ed.), Sea Ice 2nd ed., Blackwell Publishing Ltd., Oxford, pp. 1-22

Eicken, H., 2003. From the Microscopic, to the Macroscopic, to the Regional Scale: Growth, Microstructure and Properties of Sea Ice, in: Thomas, D.N., Dieckmann, G.S. (Eds.), Sea Ice: An Introduction to its Physics, Chemistry, Biology and Geology. Blackwell Science Ltd., Oxford, pp. 22-81.

Eicken, H., Gradinger, R., Gaylord, A., Mahoney, A., Rigor, I., Melling, H., 2005. Sediment transport by sea ice in the Chukchi and Beaufort Seas: Increasing importance due to changing ice conditions? Deep-Sea Res. II 52, 3281-3302.

Eicken, H., Lange, M.A., 1989. Development and Properties of Sea Ice in the Coastal Regime of the Southeastern Weddell Sea. J. Geophys. Res. 94, 8193-8206.

Eicken, H., Lensu, M., Lepparanta, M., Tucker, III W.B., Gow, A.J., Salmela O., 1995. Thickness, structure, and properties of level summer multiyear ice in the Eurasian sector of the Arctic Ocean. J. Geophys. Res. 100, 22,697-22,710.

Ewing, M., Donn, W.L., 1958. A theory of ice ages II. Science 127, 1159-1161.

Evans, L., Nishioka, J., 2018. Quantitative analysis of Fe, Mn and Cd from sea ice and seawater in the Chukchi Sea, Arctic Ocean. Polar Sci. 17, 50-58.

Fischer, H., Siggaard-Anderson, M-L., Ruth, U., Rothlisberger, R., Wolff, E., 2007. Glacial/Interglacial changes in mineral dust and sea-salt records in polar ice cores: sources, transport and deposition. Rev. Geophys. 45, RG1002, doi:10.1029/2005RG000192.

Fritsen, C. H., Ackley, S. F., Kremer, J. N., Sullivan, C. W., 1998. Flood-Freeze Cycles and Microalgal Dynamics in Antarctic Pack Ice, in: Lizotte, M. P., Arrigo, K. R. (Eds.), Antarctic Sea Ice: Biological Processes, Interactions and Variability. American Geophysical Union, Washington, D. C. https://doi.org/10.1029/AR073p0001.

Fritsen, C.H., Lytle, V.I., Ackley, S.F., Sullivan, C.W., 1994. Autumn Bloom of Antarctic Pack-Ice Algae. Science 226, 782-784.

Froelich, P.N., Klinkhammer, G.P., Bender, M.L., Luedtke, N.A., Heath, G.R., Cullen D., Dauphin P., Hammond, D., Harman, B., Maynard, V., 1979. Early oxidation of organic matter in pelagic sediments of the eastern equatorial Atlantic: suboxic diagenesis. Geochim. Cosmochim. Acta 43, 1075-1090.

Garrison, D.L., Ackley, S.F., Buck, K.R., 1983. A physical mechanism for establishing algal populations in frazil ice. Nature 206, 363-365.

Geider, R.J., Roche, J.L., 1994. The role of iron in phytoplankton photosynthesis, and the potential for iron-limitation of primary productivity in the sea. Photosynth. Res. 39, 275-301.

Giannelli, V., Thomas, D., Hass, C., Kattner, G., Kennedy, H., Dieckmann, G.S., 2001. Behaviour of dissolved organic matter and inorganic nutrients during experimental sea-ice formation. Ann. Glaciol. 33, 317-321.

Glud, R.N., Rysgaard, S., Kuhl, M., 2002. A laboratory study on O_2 dynamics and photosynthesis in ice algal communities: Quantification by microsensors, O_2 exchange rates, 14C incubations and PAM fluorometer. Aquat. Microb. Ecol. 27, 301-311.

Golden, K.M., Ackley, S.F., Lytle, V.I., 1998. The Percolation Phase Transition in Sea Ice. Science 282, 2238-2241.

Granskog, M.A., Kaartokallio, H., 2004. An estimation of the potential fluxes on nitrogen, phosphorus, cadmium and lead from sea ice and snow in the northern Baltic Sea. Water. Air. Soil. Pollut. 154, 331-347.

Grotti, M., Soggia, F., Ianni, C., Frache, R., 2005. Trace metals distributions in coastal sea ice of Terra Nova Bay, Ross Sea, Antarctica. Antarct. Sci. 17, 289-300.

Gruber, N., Sarmiento, J.L., 1997. Global patterns of marine nitrogen fixation and denitrification. Global Biogeochem Cycles 11, 235-266.

Guo, T., DeLaune, R.D., Patrick, W.H. Jr., 1997. The influence of sediment redox chemistry on chemically active forms of arsenic, cadmium, chromium and zinc in estuarine sediment. Environ. Int. 23, 305-316.

Häkkinen, S., 1986. Coupled ice-ocean dynamics in the Marginal Ice Zones: Upwelling/downwelling and eddy generation. J. Geophys. Res. 91, 819-832.

Hatje, V., Bruland, K.W., Flegal, A.R., 2014. Determination of rare earth elements after pre-concentration using NOBIAS-chelate PA-1 ®resin: method development and application in the San Francisco Bay plume. Mar. Chem. 160, 34-41.

Hatta, M., Measures, C.I., Selph, K.E., Zhou, M., Hiscock, W.T., 2013. Iron fluxes from the shelf regions near the South Shetland Islands in the Drake Passage during the austral - winter 2006. Deep - Sea Res. II 90, 89-101.

Hedges, J.I., 1992. Global biogeochemical cycles: progress and problems. Mar. Chem. 39, 67 – 93.

Hendry, K.R., Rickaby, R.E.M., de Hoog, J.C., Weston, K., Rehkamper, M., 2009. The cadmium-phosphate relationship in brine: biological versus physical control over micronutrients in sea ice environments. Antarct. Sci. 278, 67-77.

Hioki, N., Kuma, K., Morita, Y., Sasayama, R., Ooki, A., Kondo, Y., Obata, H., Nishioka, J., Yamashita, Y., Nishino, S., Kikuchi, T., Aoyama, M., 2014. Laterally spreading iron, humic-like dissolved organic matter and nutrients in cold, dense sub-surface water of the Arctic Ocean. Sci. Rep. 4, doi:10.1038/srep06775.

Hölemann, J.A., Schirmacher, M., Prange, A., 1999. Dissolved and particulate major and trace elements in newly formed ice from the Laptev Sea (Transdrift III, October 1995), in: Kassens H. (Eds.), Land-Ocean Systems in the Siberian Arctic: Dynamics and History, Springer, Berlin pp. 101-111.

Hölemann, J.A., Schirmacher, M., Prange, A., 1997. Dissolved and Particulate Major and Trace Elements in Newly Formed Ice from the Laptev Sea (Transdrift III, October 1995), in:

Kassens, H., Bauch, H.A., Dmitrenko, I., Eicken, H., Hubberten, H.W., Melles, M., Thiede, J., Timokhov L. (Eds.), Land-Ocean Systems in the Siberian Arctic. Springer, Berlin, pp. 101-111.

Hopkins, M. A., Tuhkuri, J., Lensu, M., 1999. Rafting and ridging of thin ice sheets. J. Geophys. Res. 104, 13,605–13,613.

Horner, R., Ackley, S.F., Dieckmann, G.S., Gulliksen, B., Hoshiai, T., Legendre, L., Melnikov, I.A., Reeburgh, W.S., Spindler, M., Sullivan, C.W., 1992. Ecology of sea ice biota. Polar Biol. 12, 417-427.

Huang, X., Chen, T., Zou, M., Chen, D., Pan, M., 2017. The adsorption of Cd(II) on manganese oxide investigated by batch and modeling techniques. Int. J. Environ. Res. Public Health 14, 1145, https://doi.org/10.3390/ijerph14101145.

Hudier, E.J-J., Ingram, R.G., Shirasawa, K., 1995. Upward flushing of sea water through first year ice. Atmos.-Ocean 33, 569-580, https://doi.org/10.1080/07055900.1995.9649545.

Hurst, M.P., Aguilar-Islas, A.M., Bruland, K.W., 2010. Iron in the southeastern Bering Sea: Elevated leachable particulate Fe in shelf bottom waters as an important source for surface waters. Cont. Shelf Res. 30, 467-480.

Hurst, M.P., Bruland, K.W., 2007. An investigation into the exchange of iron and zinc between soluble, colloidal, and particulate size-fractions in shelf waters using low-abundance isotopes as tracers in shipboard incubation experiments. Mar. Chem. 103, 211-226.

Ito, M., Ohshima, K.I., Fukamachi, Y., Mizuta, G., Kusumoto, Y., Nishioka, J., 2017. Observations of frazil ice formation and upward sediment transport in the Sea of Okhotsk: A possible mechanism of iron supply to sea ice. J. Geophys. Res. Oceans 122, 788-802, doi:10.1002/2016JC012198.

Janssens, J., Meiners, K.M., Tison, J-L., Dieckmann, G., Delille, B., Lannuzel, D., 2016. Incorporation of iron and organic matter into young Antarctic sea ice during its initial growth stages. Elementa 4, http://doi.org/10.12952/journal.elementa.000123.

Janssens, J., Meiners, K.M., Tison, J-L., Townsend, A.T., Lannuzel, D., 2018. Organic matter controls of iron incorporation in growing sea ice. Front Earth Sci. 6(22), http://doi.org/10.3389/feart.2018.00022.

Jardon, F.P., Vivieer, F., Vancoppenolle, M., Lourenco, A., Bouruet-Aubertot, P., Cuypers, Y., 2013. Full-depth desalination of warm sea ice. J. Geophys. Res.: Ocean 118, 435-447.

Jeroen, Ooms, 2018. magick: Advanced Graphics and Image-Processing in R. R package version 1.8. https://CRAN.R-project.org/package=magick.

Kanna, N., Nishioka, J., 2016. Bio-availability of iron derived from subarctic first-year sea ice. Mar. Chem. 186, 189-197.

Kanna, N., Toyota, T., Nishioka, J., 2014. Iron and macro-nutrient concentrations in sea ice and their impact on the nutritional status of surface waters in the southern Okhotsk Sea. Prog. Oceanogr. 126, 44-57.

Kempema, E.W., Reimnitz, E., Barns, P.W., 1989. Sea ice sediment entrainment and rafting in the Arctic. J. Sediment. Petrol. 59, 308-317.

Kingery, W.D., Goodnow, W.H., 1963. Brine migration in seal ice, in: Ice and Snow, W.D Kingery (Eds.), M.I.T. Press, pp. 237-247.

Klunder, M.B., Bauch, D., Laan, P., de Baar, H.J.W., van Heuven, S., Ober, S., 2012. Dissolved iron in the Arctic shelf seas and surface waters of the central Artic Ocean: Impact of Arctic river water and ice - melt. J. Geophys. Res. 117, C01027, doi:10.1029/2011JC007133.

Knauer, G.A., Martin, J.H., 1981. Phosphorus-cadmium cycling in northeast Pacific waters. J. Mar. Res. 39, 65-76.

Kondo, Y., Obata, H., Hioki, N., Ooki, A., Nishino, S., Kikuchi, T., Kuma, K., 2016. Transport of trace metals (Mn, Fe, Ni, Zn and Cd) in the western Arctic Ocean (Chukchi Sea and Canada Basin) in late summer 2012. Deep-Sea Res. I 116, 236-252.

Kovacs, A., 1996. Sea ice, part I, bulk salinity versus ice floe thickness. CRREL Report 96, 16.

Krachler, M., Zheng, J., Koerner, R., Zdanowicz, C., Fisher, D., Shotyk, W., 2005. Increasing atmospheric antimony contamination in the northern hemisphere: snow and ice evidence from Devon Island, Arctic Canada. J. Environ. Monit. 12, 1169-1176.

Krembs, C., Eicken, H., Junge, K., Deming, J.W., 2002. High concentrations of exopolymeric substances in Arctic winter sea ice: implications for the polar ocean carbon cycle and cryoprotection of diatoms. Deep-Sea Res. I 49, 2163-2181.

Kuma, K., Katsumoto, A., Nishioka, J., Matsunaga, K., 1998. Size-fractionated iron concentrations and Fe (III) hydroxide solubilities in various coastal waters. Estuar. Coast. Shelf Sci. 47, 275-283.

Lagerstrom M.E., Field M.P., Seguret M., Fischer L., Hann S., and Sherrell R.M. 2013. Automated on-line flow-injection ICP-MS determination of trace metals (Mn, Fe, Co, Ni, Cu and Zn) in open ocean seawater: Application to the GEOTRACES program. Mar. Chem. 155, 71-80.

Landing, W.M., Bruland, K., 1987. The contrasting biogeochemistry of iron and manganese in the Pacific Ocean. Geochim. Cosmochim. Acta 51, 29-43.

Lange, M. A., Ackley, S. F., Wadhams, P., Dieckmann, G. S., Eicken, H., 1989. Development of sea ice in the Weddell Sea. Ann. Glaciol. 12, 92–96.

Lange, M. A., Eicken, H., 1991. Textural characteristics of sea ice and the major mechanism of ice growth in the Weddell Sea. Ann. Glaciol. 15, 210–215.

Lange, M. A., Schlosser, P., Ackley, S.F., Wadhams, P., Dieckmann, G.S., 1990. 18O concentrations in sea ice of the Weddell Sea, Antarctica. J. Glaciol. 36, 315-323, https://doi.org/10.3189/002214390793701291.

Lannuzel, D., Bowie, A.R., Remenyi, T., Lam, P., Townsend, A., Ibisanmi, E., Butler, E., Wagener, T., Schoemann, V., 2011b. Distributions of dissolved and particulate iron in the sub-Antarctic and Polar Frontal Southern Ocean (Australian sector). Deep Sea Res. II 58, 2094-2112.

Lannuzel, D., Bowie, A.R., van der Merwe, P.C., Townsend, A.T., Schoemann, V., 2011a. Distribution of dissolved and particulate metals in Antarctic sea ice. Mar. Chem. 124, 134-146.

Lannuzel, D., Grotti, M., Abelmoschi, M.L., van der Merwe, P., 2015. Organic ligands control the concentrations of dissolved iron in Antarctic sea ice. Mar. Chem. 174, 120-130.

Lannuzel, D., Schoemann, V., de Jong, J., Chou, L., Delille, B., Becquevort, S., Tison, J-L., 2008. Iron study during a time series in the western Weddell pack ice. Mar. Chem. 108, 85-95.

Lannuzel, D., Schoemann, V., de Jong, J., Pasquer, B., van der Merwe, P., Masson, F., Tison, J-L., Bowie, A., 2010. Distribution of dissolved iron in Antarctic sea ice: Spatial, seasonal, and inter-annual variability. J. Geophys. Res. 115, G03022 https://doi.org/10.1029/2009JG001031.

Lannuzel, D., Schoemann, V., de Jong, J., Tison, J-L., Chou, L., 2007. Distribution and biogeochemical behavior of iron in the East Antarctic sea ice. Mar. Chem. 106, 18-32.

Lannuzel, D., Vancoppenolle, M., van der Merwe, P., de Jong, J., Meiners, K.M. Grotti, M., Nishioka, J., Schoemann, V., 2016. Iron in sea ice: Review and new insights. Elementa 4: 000130, doi:10.12952/journal.elementa.00130.

Lannuzel, D., van der Merwe, P.C., Townsend, A.T., Bowie, A.R., 2014. Size fractionation of iron, manganese and aluminium in Antarctic fast ice reveals a lithogenic origin and low iron solubility. Mar. Chem. 161, 47-56.

Lee, J., Boyle, E., Echegoyen-Sanz, Y., Fitzsimmons, J., Zhang, R., Kayser, R., 2011. Analysis of trace metals (Cu, Cd, Pd, and Fe) in seawater using single batch Nitrilotriacetate resin extraction and isotope dilution inductively coupled plasma mass spectrometry. Anal. Chim. Acta 686, 93-101.

Lohan, M.C., Bruland, K.W., 2008. Elevated Fe(II) and dissolved Fe in hypoxic shelf waters off Oregon and Washington: an enhanced source of iron to coastal upwelling regimes. Environ. Sci. and Tech. 42, 6462-6468.

Macdonald, R.W., Carmack, E.C., McLaughlin, F.A., 1999. Connections among ice, runoff and atmospheric forcing in the Beaufort Gyre. Geophys. Res. Lett. 26, 2223-2226.

Macdonald, R.W., Paton, D.W., Carmack, E.C., 1995. The freshwater budget and under-ice spreading of Mackenzie River water in the Canadian Beaufort Sea based on salinity and $^{18}O/^{16}O$ measurements in water and ice. J. Geophys. Res. 100, 895 - 919.

Macdonald, R.W., Solomon, S.M., Cranston, R.E., Welch, H.E., Yunker, M.B., Gobeil, C., 1998. A sediment and organic carbon budget for the Canadian Beaufort Shelf. Mar. Geol. 144, 255-273.

Maenhaut, W., Salma, I., Cafmeyer, J., 1996. Regional atmospheric aerosol composition and sources in the eastern Transvaal, South Africa and impact of biomass burning. J. Geophys. Res. 101, 23,631-23,650.

Marsay, C.M., Aguilar-Islas, A., Fitzsimmons, J.N., Hatta, M., Jensen, L.T., John, S.G., Kadko, D., Landing, W.M., Lanning, N.T., Morton, P.L., Pasqualini, A., Rauschenberg, S., Sherrell, R.M., Shiller, A.M., Twining, B.S., Whitmore, L.M., Zhang, R., Buck, C.S., 2018. Dissolved and particulate trace elements in late summer Arctic melt ponds. Mar. Chem. 204, 70-85.

Martin, J.H., 1990. Glacial-interglacial CO_2 change: The iron hypothesis. Paleoceanography 5, 1-13.

Martin, J.H., Fitzwater, S.E., Gordon, R.M., 1990. Iron deficiency limits phytoplankton growth in Antarctic waters. Global Biogeochem. Cycles 4, 5-12.

Martin, S., Kauffman, P., 1981. A field and laboratory study of wave damping by grease ice. J. Glaciol. 27, 283-313.

Massonnet, F., Fichefet, T., Goosse, H., Bitz, C.M., Philippon-Berthier, G., Holland, M.M., Barriat, P.-Y., 2012. Constraining projections of summer Arctic sea ice. Cryosphere 6, 1383-1394.

Masqué, P., Cochran, J.K., Hirschberg, D.J., Dethleff, D., Hebbeln, D., Winkler, A., Pfirman, S., 2007. Radionuclides in Arctic sea ice: Tracers of sources, fates and ice transit time scales. Deep Sea Res. Part I: Oceanogr. Res. Pap. 54, 1289-1310.

Matsunaga, K., Abe, K., 1985. Relationship between cadmium and phosphate in the Northwest Pacific Ocean. J. Oceanogr. Soc. Japan 41, 193-197.

Maykut, G.A., 1985. The ice environment, in: Horner, R.A., (Eds.), Sea Ice Biota., CRC Press Inc., Florida, pp. 21-82.

McPhee, M.G., Maykut, G.A., Morison, J.H., 1987. Dynamic and Thermodynamics of the Ice/Upper Ocean System in the Marginal Ice Zone of the Greenland Sea. J. Geophys. Res. 92, 7017-7031.

Melnikov, I.A., Kolosova, E.G., Welch, H.E., Zhitina, L.S., 2002. Sea ice biological communities and nutrient dynamics in the Canada Basin of the Arctic Ocean. Deep-Sea Res. Part 1: Oceanogr. Res. Pap. 42, pp. 1623-1649.

Miao, A-J., Wang, W-X., 2006. Cadmium toxicity to two marine phytoplankton under different nutrient conditions. Aquat. Toxicol. 78, 114-126.

Miller, L.A., Fripiat, F., Else, B.G.T., Bowman, J.S., Brown, K.A., Collins, R.E., Ewert, M., Fransson, A., Gosselin, M., Lannuzel, D., Meiners, K.M., Michel, C., Nishioka, J., Nomura, K., Papadimitriou, S., Russell, L.M, Sorensen, L.L., Thomas, D.N., Tison, J-L., van Leeuwe, M.A., Vancoppenolle, M., Wolff, E.W., Zhou, J., 2015. Methods for biogeochemical studies of sea ice: the state of the art, caveats, and recommendations. Elementa 3: 000038 doi: 10.12952/journal.elementa.000038

Milne, A., Landing, W., Bizimis, M., Morton, P., 2010. Determination of Mn, Fe, Co, Ni, Cu, Zn, Cd and Pb in seawater using high resolution magnetic sector inductively couple mass spectrometry (HR-ICP-MS). Anal. Chim. Acta 665, 200-207.

Minami, T., Konagaya, W., Zheng, L., Takano, S., Sasaki, M., Murata, R., Nakaguchi, Y., Sohrin, Y., 2015. An off-line automated preconcentration system with ethylenediaminetriacetate

chelating resin for the determination of trace metals in seawater by high-resolution inductively coupled plasma mass spectrometry. Analytica Chimica. Acta 854, 183-190.

Mizutani, A., Nagase, K., Kikuchi, A., Kanazawa, H., Akiyama, Y., Kobayashi, J., Annaka, M., Okano, T., 2010. Preparation of thermo-responsive polymer brushes on hydrophilic polymeric beads by surface-initiated atom transfer radical polymerization for a highly resolutive separation of peptides. J. Chromatogr. A, 5978-5985.

Morel, R.M.M., Rueter, J.G., Price, N.M., 1991. Iron nutrition of phytoplankton and its possible importance in the ecology of ocean regions with high nutrient and low biomass. Oceanography 4, 56 – 61.

Morel, F.M.M., 1993. Principles of Aquatic Chemistry. John Wiley & Sons, New York, pp. 446.

Morel, F.M.M., Price, N.M., 2003. The biogeochemical cycles of trace metals in the oceans. Science 300, 944-947.

Morgan, J.J., 2005. Kinetics of reaction between O2 and Mn(II) species in aqueous solutions. Geochim. Cosmochim. Acta 69, 35 – 48.

Mortimer, C.H., 1941. The exchange of dissolved substances between mud and water in lakes. J. Ecol. 29, 280-329.

Mouselimis, L., 2018. OpenImageR: An Image Processing Toolkit. R package version 1.0.8. https://CRAN.R-project.org/package=OpenImageR.

NASA National Snow and Ice Data Center Distributed Active Archive Center. https://nsidc.org/arcticseaicenews/

Nealson, K., 1978. The isolation and characterization of marine bacteria which catalyze manganese oxidation, in: Kromben, W. (Eds.), Environmental Biogeochemistry and Geomicrobiology, Ann Arbor Press, Michigan pp. 847-858.

Newyear, K., Martin, S., 1997. A comparison of theory an laboratory measurements of wave propagation and attenuation in grease ice. J. Geophys. Res. 102, 25091-25099.

Nishino, S., Shimada, K., Itoh, M., 2005. Use of ammonium and other nitrogen tracers to investigate the spreading of shelf waters in the western Arctic halocline. J. Geophys. Res. 110, C10005, doi:10.1029/2003JC002118.

Nishioka, J., Takeda, S., de Baar, H.J.W., Croot, P.L., Boyé, M., Laan, P., Timmermans, K.R., 2005. Changes in the concentrations of iron in different size fractions during an iron enrichment experiment in the open Southern Ocean. Mar. Chem. 95, 51-63.

Nishioka, J., Takeda, S., 2000. Changing in the concentrations of iron in different size fractions during growth of the oceanic diatom *Chaetoceros* sp.: importance of small colloidal iron. Mar. Biol. 137, 231-238.

Nishioka, J., Takeda, S., Wong, C.S., Johnson, W.K., 2001. Size-fractionated iron concentrations in the northeast Pacific Ocean: Distribution of soluble and small colloidal iron. Mar. Chem. 74, 157-179.

Nomura, D., Yoshikawa-Inoue, H., Toyota, T., 2006. The effect of sea-ice growth on air-sea CO_2 flux in a tank experiment. Tellus 58B, 418-426.

Nürnberg, D., Wollenburg, I., Dethleff, D., Eicken, H., Kassens, H., Letzig, T., Reimnitz, E., Thiede, J., 1994. Sediments in Arctic sea ice: Implications for entrainment, transport and release. Mar. Geol. 119, 185-214.

Obata, H., Karatani, H., Nakayama, E., 1993. Automated determination of iron in seawater by chelating resin concentration and chemiluminescence detection. Anal. Chem. 65, 1524-1528.

Obata, H., Karatani, H., Matsui, M., Nakayama, E., 1997. Fundamental studies for chemical speciation of iron in seawater with an improved analytical method. Mar. Chem. 56, 97-106.

Osterkamp, T.E., Gosink, J.P., 1984. Observations and analyses of sediment-laden sea ice, in: Barnes, P.W., Schell, D.M., Reimnitz, E., (Eds.), The Alaskan Beaufort Sea: Ecosystems and environments, Academic Press, University of California pp. 73-93.

Overland, J.E., Hanna, E., Hanssen-Bauer, I., Kim, S-J., Walsh, J.E., Wang, M., Bhatt, U.S., Thoman, R.L., 2017. Surface Air Temperature [in Arctic Report Card 2017], http://ww.arctic.noaa.gov/Report-Card.

Pardue, J.H., DeLaune, R.D., Patrick, W.H. Jr., 1992. Metal to Aluminum Correlation in Louisiana Coastal Wetlands: Identification of Elevated Metal Concentrations. J. Environ. Qual. 21, 539-545.

Peers, G, Price, N.M., 2004. A role for manganese in superoxide dismutases and growth of iron-deficient diatoms. Limnol. Oceanogr. 49, 1774 – 1783.

Perovich, D., Meier, W., Tschudi, M., Farrell, S., Hendricks, S., Gerland, S., Hass, C., Krumpen, T., Polashenski, C., Ricker, R., Webster, M., 2017. Sea Ice [in Arctic Report Card 2017], http://ww.arctic.noaa.gov/Report-Card.

Persson, P-O., Andersson, P.S., Zhang, J., Porcelli, D., 2011. Determination of Nd isotopes in water: A chemical separation technique for extracting Nd from seawater using a chelating resin. Ana. Chem. 83, 1336-1341.

Petrich, C., Eicken, H., 2010. Growth, Structure and Properties of Sea Ice. in: Thomas, D.N., Dieckmann, G.S. (Eds.) Sea Ice. 2nd ed. Blackwell Publishing Ltd., Oxford, pp. 23-77.

Pfirman, S.L., Colony, R., Nürnberg, D., Eicken, H., Rigor, I., 1997. Reconstructing the origin and trajectory of drifting Arctic sea ice. J. Geophys. Res. 102, 12,575-12,586.

Pfirman, S.L., Eicken, H., Bauch, D., Weeks, W.F., 1995. The potential transport of pollutants by Arctic sea ice. Sci. Total Environ. 159, 129-146.

Planchon, F.A.M., Gabrielli, P., Gauchard, P.A., Dommergue, A., Barbante, C., Cairns, W.R.L., Cozzi, G., Nagorski, S.A., Ferrari, C.P., Boutron, C.F., Capodaglio, G., Cescon, P., Varga, A., Wolff, E.W., 2004. Direct determination of mercury at the sub-picogram per gram level in polar snow and ice by ICP-SFMS. J. Anal. At. Spectrom. 19, 823-830, https://doi.org/10.1039/b402711f.

Przybylak, R., 2007. Recent air-temperature changes in the Arctic. Ann. Glaciol. 46, 316-324.

R Core Team (2013). R: A language and environment for statistical computing. R Foundation for statistical Computing, Vienna, Austria. URL http://www.R-project.org/.

Reimnitz, E., Clayton, J.R., Kempema, E.W., Payne, J.R., Weber, W.S., 1993. Interaction of rising frazil with suspended particles: tank experiments with applications to nature. Cold Reg. Sci. Technol. 21, 117-135.

Reimnitz, E., Dethleff, D., Nürnberg, D., 1994. Contrasts in Arctic shelf sea-ice regimes and some implications: Beaufort Sea versus Laptev Sea. Mar. Geol. 119, 215-225.

Reimnitz, E., Marincovich, Jr L., McCormick, M., Briggs, W.M., 1992. Suspension freezing of bottom sediment and biota in the Northwest Passage and implications for Arctic Ocean sedimentation. Can. J. Earth Sci. 29, 693-703.

Roach, A.T., Aagaard, K., Pease, C.H, Salo, S.A., Weingartner, T., Pavlov, V., Kulakov, M., 1995. Direct measurements of transport and water properties through Bering Strait. J. Geophys. Res. 100, 18443-18457.

Royer, T.C., 1998. Coastal Processes in the northern North Pacific, in: Robinson, A.R., Brink, K.H. (Eds.), The Sea, vol. 11., Wiley, New York, pp. 395-414.

Rysgaard, S., Glud, R.N., 2004. Anaerobic N2 production in Arctic sea ice. Limnol. Oceanogr. 49, 86-94.

Rysgaard, S., Glud, R.N., Sejr, M.K., Blicher, M.E., Stahl, H.J., 2008. Denitrification Activity and oxygen dynamics in Arctic Sea Ice. Polar Biol. 31, 527-537, https://doi.org/10.1007/s00300-007-0384-x.

Saager, P.M., de Baar, H.J.W., Burkill, P.H., 1989. Manganese and iron in Indian Ocean waters. Geochim. Cosmochim. Acta 53, 2259 – 2267.

Schlosser, C., De La Rocha, C.L., Streu, P., Croot, P.L., 2012. Solubility of iron in the Southern Ocean. Limnol. Oceanogr. 57, 684-697.

Sedwick, P.N., DiTullio, G.R., 1997. Regulation of algal blooms in Antarctic shelf waters by the release of iron form melting sea ice. Geophys. Res. Lett. 24, 2515-2518.

Shiller, A.M., 1997. Manganese in surface waters of the Atlantic Ocean. Geophys. Res. Lett. 24, 1495 – 1498.

Smedsrud, L.H., 2001. Frazil-ice entrainment of sediment: large-tank laboratory experiments. J. Glaciol. 47, 461-471.

Smeets, K., Cuypers, A., Lambrechts, A., Semane, B., Hoet, P., Laere, A.V., Vangronsveld, J., 2005. Induction of oxidative stress and antioxidative mechanisms in Phaseolus vulgaris and Cd application. Plant Physiol. Biochem. 43, 437-444.

Smith, J.D., 1978. Measurement of turbulence in ocean boundary layers. Proceedings of a Working Conference on Current measurement, Tech. Rep. EL-SG-3-78, pp. 95-128, Coll. of Mar. Stud., Univ. of Del., Newark.

Sohrin, Y., Bruland, K.W., 2011. Global status of trace elements in the ocean. Trends Anal. Chem. 30, 1291-1307.

Sohrin, Y., Urushihara, S., Nakatsuka, S., Kono, T., Higo, E., Minami, T., Norisuye, K., Umetani, S., 2008. Multielemental determination of GEOTRACES key trace metals in seawater by ICPMS after preconcentration using an ethylenediaminetriacetic acid chelating resin. Anal. Chem. 80, 6267-6273.

Spindler, M., 1994. Notes on the biology of sea ice in the Arctic and Antarctic. Polar Biol. 14, 319-324.

Stumm, J.L., Morgan, J.J., 1981. Aquatic Chemistry. Wiley and Sons, New York.

Sunda, W.G., 2001. Bioavailability and bioaccumulation of iron in the sea, in: Turner, D.R., Hunter, K.A. (Eds.), The Biogeochemisty of iron in seawater. Wiley and Sons, New York pp. 41-84.

Sunda, W.G., 1989. Trace metal interaction with marine phytoplankton. Biol. Oceanogr. 6, 411 – 442.

Sunda, W.G., Huntsman, S.A., Harvey, G.R., 1983. Photoreduction of manganese oxides in seawater and its geochemical and biological implications. Lett. Nature 301, 234-236.

Takata, H., Zheng, J., Tagami, K., Aono, T., Uchida, S., 2011. Determination of [232]Th in seawater by ICP-MS after preconcentration and separation using a chelating resin. Talanta 85, 1772-1777.

Takeda, S., Obata, H., 1995. Response of equatorial Pacific phytoplankton to subnanomolar Fe enrichment. Mar. Chem. 50, 219-227.

Templeton, D.M., Ariese, F., Cornelis, R., Danielsson, L-G., Muntau, H., van Leeuwen, H.P., Lobinski, R., 2000. Guidelines for terms related to chemical speciation and fractionation of elements. Definitions, structural aspects, and methodological approaches. Pure Apply Chem. 72(8), 1453-1470.

Thomas, D.N., Dieckmann, G.S., 2003. Sea Ice: An introduction to its physics, chemistry, biology and geology, Blackwell, Malden Mass.

Thomas, D.N., Papadimitriou, S., Michel, C., 2010. Biogeochemistry of sea ice, in: Thomas, D.N., Dickmann CS, (Eds). Sea Ice, Second ed., Wiley-Blackwell, Chichester, pp. 425-467.

Tison, J-L., Hass, C., Gowing, M.M., Sleewaegen, S., Bernard, A., 2002. Tank study of physico-chemical controls on gas content and composition during growth of young sea ice. J. Glaciol. 48(161), 177-191.

Tovar-Sanchez, A., Duarte, C.M., Alonso, J.C., Lacorte, S., Tauler, R., Galban-Malagon, C., 2010. Impacts of metals and nutrients released from melting multiyear Arctic sea ice. J. Geophys. Res. 115, C07003 doi:10.1029/2009JC005685.

Tovar-Sanchez, A., Duarte, C.M., Hernandez-Leon, S., Sanudo-Wilhelmy, S.A., 2007. Krill as a central node for iron cycling in a Southern Ocean. Geophys. Res. Lett. Ocean 115, L11601. doi:10.1029/2006GL029096.

Toyota, T., 2018. Sea ice nomenclature (cited from WMO (2014)), in: Kawano T. (Ed.), Guideline of ocean observations, vol. 7, Oceanographic Society of Japan, pp. G705ENrl-26 - G705ENrl-42.

Toyota, T., Koda, H., 2016. Tank experiments on the granular ice formation processes. IAHR.

Toyota, T., Kawamura, T., Ohshima, K.I., Shimoda, H., Wakatsuchi, M., 2004. Thickness distribution, texture and stratigraphy, and a simple probabilistic model for dynamical thickening of sea ice in the southern Sea of Okhotsk. J. Geophys. Res. 109, C06001, https://doi.org/10.1029/2003JC002090.

Toyota, T., Takatsuji, S., Tateyama, K., Naoki, K., Ohshima, K.I., 2007. Properties of sea ice and overlying snow in the southern Sea of Okhotsk. J. Oceanogr. 63, 393-411.

Tsumune, D., Nishioka, J., Shimamoto, A., Takeda, S., Tsuda, A., 2005. Physical behaviour of SEEDS iron-fertilized patch by sulphur hexafluoride tracer release. Prog. Oceanogr. 64, 111-127.

Ueda, M., Teshima, N., Sakai, T., Joichi, Y., Motomizu, S., 2010. Highly sensitive determination of Cadmium and Lead in leached solutions from ceramic ware by Graphite Furnace Atomic Absorption Spectrometry coupled with sequential injection-based solid phase extraction method. Anal. Sci. 26, 597-602.

Ukita, J., Kawamura, T., Tanaka, N., Toyota, T., Wakatsuchi, M., 2000. Physical and stable isotopic properties and growth processes of sea ice collected in the southern Sea of Okhotsk. J. Geophys. Res. 105, 22,083–22,093.

Untersteiner, N., 1968. Natural desalination and equilibrium salinity profile of perennial sea ice. J. Geophys. Res. 73, 1,251-1,257.

Vallee, B.L., Ulmer, D.D., 1972. Biochemical effects of mercury, cadmium and lead. Ann. Rev. Biochem. 41, 91-128.

Vancoppenolle, M., Goosse, H., de Montety, A., Fichefet, T., Tremblay, B., Tison, J-L., 2010. Modeling brine and nutrient dynamics in Antarctic sea ice: The case of dissolved silica. J. Geophys. Res. 115, C02005, doi:10.1029/2009JC005369.

van der Merwe, P.C., Lannuzel, D., Bowie, A.R, Mancuso Nichols, C.A., Meiners, K.M., 2011. Iron fractionation in pack and fast ice in East Antarctica: Temporal decoupling between the

release of dissolved and particulate iron during spring melt. Deep-Sea Res. Part II 58, 1222-1236.

Wadhams, P, Squire, V.A., Ewing, J.A., Pascal, R.W., 1986. The effect of the Marginal Ice Zone on the directional wave spectrum of the ocean. J. Phys. Oceanogr. 16, 358-376.

Wadhams, P, Squire, V.A., Goodman, D.J., Cowan, A.M, Moore, S.C., 1988. The Attenuation Rates of Ocean Waves in the Marginal Ice Zone. J. Geophys. Res. 93, 6799-6818.

Wagenbach, D., Ducroz, F., Mulvaney, R., Keck, L., Minikin, A., Legrand, M., Hall, J.S., Wolff, E.W., 1998. Sea-salt aerosol in coastal Antarctic Regions. J. Geophys. Res. 103, 10,961-10,974.

Wang, M-J., Wang, W-X., 2009. Cadmium in three marine phytoplankton: Accumulation, subcellular fate and thiol induction. Aquat. Toxicol. 95, 99-107.

Weeks, W.F., Ackley, S.F., 1986. The growth, structure and properties of sea ice, in: Untersteiner, N. (Eds.), The Geophysics of Sea Ice. Plenum Press, New York, pp 9-164.

Weingartner, T. J., Cavalieri, D.J., Aagaard, K., Sasaki, Y., 1998. Circulation, dense water formation, and outflow on the northeast Chukchi Shelf. J. Geophys. Res., 103, 7647–7661, https://doi.org.10.1029/98JC00374.

Weingartner, T.J., Danielson, S.L., Royer, T.C., 2005. Freshwater variability and predictability in the Alaska Coastal Current. Deep-Sea Res. II 52, 169-191.

Weissenberger, J., Dieckmann, G., Gradinger, R., Spindler, M., 1992. Sea ice: A cast technique to examine and analyze brine pockets and channel structure. Limnol. Oceangr. 37, 179-183.

Weissenberger, J., Grossmann, S., 1998. Experimental formation of sea ice: importance of water circulation and wave action for incorporation of phytoplankton and bacteria. Polar Biol. 20, 178-188.

Woodgate, R.A., Aagaard, K., 2005. Revising the Bering Strait freshwater flux into the Arctic Ocean. Geophys. Res. Lett. 32, L02602, doi:10.1029/2004GL021747.

Woodgate, R.A, Aagaard, K., Weingartner, T.J., 2005. A year in the physical oceanography of the Chukchi Sea: Moored measurements from autumn 1990-1991. Deep-Sea Res. II 52, 3116-3149.

Wu, J., Luther, G.W., 1995. Complexation of Fe (III) by natural organic ligands in the Northwest Atlantic Ocean, as determined by a competitive equilibration method and kinetic approach. Mar. Chem. 50, 159-177.

Yamamoto-Kawai, M., McLaughlin, F.A., Carmack, E.C., Nishino, S., Shimada, K., 2008. Freshwater budget of the Canada Basin, Arctic Ocean, from salinity, δ18O, and Nutrients. J. Geophys. Res. 113, C01007, https://doi.org/10.1029/2006JC003858.

Yu, K-T., Lam, M.H-W., Yen, Y-F., Leung, A.P.K., 2000. Behavior of trace metals in the sediment pore waters of intertidal mudflats of a tropical wetland. Environ. Toxicol. Chem. 19, 535-542.

Zhu, Y., Itoh, A., Umemura, T., Haraguchi, H., Inagaki, K., Chiba, K., 2010. Determination of REEs in natural water by ICP-MS with the aid of an automatic column changing system. J. Anal. At. Spectrom. 25, 1253-1258.

Zwally, H.J., Comiso, J.C., Gordon, A.L., 1985. Antarctic offshore leads and polynyas and oceanographic effects, in: S.S. Jacobs (Ed.), Oceanology of the Antarctic Continental Shelf, Antarctic Research Series 43, AGU, Washington, DC., pp. 203-226.

Acknowledgments